A&A 428, 383–399 (2004)
DOI: 10.1051/0004-6361:20040252

Astronomy & Astrophysics

Exploring the X-ray sky with the XMM-Newton bright serendipitous survey⋆,⋆⋆

R. Della Ceca[1], T. Maccacaro[1], A. Caccianiga[1], P. Severgnini[1], V. Braito[1], X. Barcons[2], F. J. Carrera[2], M. G. Watson[3], J. A. Tedds[3], H. Brunner[4], I. Lehmann[4], M. J. Page[5], G. Lamer[6], and A. Schwope[6]

[1] INAF-Osservatorio Astronomico di Brera, via Brera 28, 20121 Milano, Italy
e-mail: [rdc;tommaso;caccia;paola;braito]@brera.mi.astro.it
[2] Instituto de Fisica de Cantabria (CSIC-UC), Avenida de los Castros, 39005 Santander, Spain
e-mail: [barcons;carreraf]@ifca.unican.es
[3] X-ray Astronomy Group, Department of Physics and Astronomy, Leicester University, Leicester LE1 7RH, UK
e-mail: [mgw;jat]@star.le.ac.uk
[4] Max-Planck-Institut für Extraterrestrische Physik, Postfach 1312, 85741 Garching, Germany
e-mail: [hbrunnerl;ile]@mpe.mpg.de
[5] Mullard Space Science Laboratory, University College London, Holmbury St. Mary, Dorking, Surrey RH5 6NT, UK
e-mail: mjp@mssl.ucl.ac.uk
[6] Astrophysikalisches Institut Potsdam (AIP), An der Sternwarte 16, 14482 Potsdam, Germany
e-mail: [glamer;aschwope]@aip.de

Received 12 February 2004 / Accepted 14 July 2004

Abstract. We present here "The XMM-Newton Bright Serendipitous Survey", composed of two flux-limited samples: the XMM-Newton Bright Source Sample (BSS, hereafter) and the XMM-Newton "Hard" Bright Source Sample (HBSS, hereafter) having a flux limit of $f_x \simeq 7 \times 10^{-14}$ erg cm^{-2} s^{-1} in the 0.5−4.5 keV and 4.5−7.5 keV energy band, respectively. After discussing the main goals of this project and the survey strategy, we present the basic data on a complete sample of 400 X-ray sources (389 of them belong to the BSS, 67 to the HBSS with 56 X-ray sources in common) derived from the analysis of 237 suitable XMM-Newton fields (211 for the HBSS). At the flux limit of the survey we cover a survey area of 28.10 (25.17 for the HBSS) sq. deg. The extragalactic number-flux relationships (in the 0.5−4.5 keV and in the 4.5−7.5 keV energy bands) are in good agreement with previous and new results making us confident about the correctness of data selection and analysis. Up to now ∼71% (∼90%) of the sources have been spectroscopically identified making the BSS (HBSS) the sample with the highest number of identified XMM-Newton sources published so far. At the X-ray flux limits of the sources studied here we found that: a) the optical counterpart in the majority (∼90%) of cases has a magnitude brighter than the POSS II limit ($R \sim 21^{\rm mag}$); b) the majority of the objects identified so far are broad line AGN both in the BSS and in the HBSS. No obvious trend of the source spectra (as deduced from the Hardness Ratios analysis) as a function of the count rate is measured and the average spectra of the "extragalactic" population corresponds to a (0.5−4.5 keV) energy spectral index of ∼0.8 (∼0.64) for the BSS (HBSS) sample. Based on the hardness ratios we infer that about 13% (40%) of the sources in the BSS (HBSS) sample are described by an energy spectral index flatter than that of the cosmic X-ray background. Based on previous X-ray spectral results on a small subsample of objects we speculate that all these sources are indeed absorbed AGN with the $N_{\rm H}$ ranging from a few times 10^{21} up to few times 10^{23} cm^{-2}. We do not find strong evidence that the 4.5−7.5 keV survey is sampling a completely different source population if compared with the 0.5−4.5 keV survey; rather we find that, as expected from the CXB synthesis models, the hard survey is simply picking up a larger fraction of absorbed AGN. At the flux limit of the HBSS sample we measure surface densities of optically type 1 and type 2 AGN of 1.63 ± 0.25 deg^{-2} and 0.83 ± 0.18 deg^{-2}, respectively; optically type 2 AGN represent 34 ± 9% of the total AGN population. Finally, we have found a clear separation, in the hardness ratio diagram and in the (hardness ratio) vs. (X-ray to optical flux ratio) diagram, between Galactic "coronal emitting" stars and extragalactic sources. The information and "calibration" reported in this paper will make the existing and incoming XMM-Newton catalogs a unique resource for astrophysical studies.

Key words. X-rays: diffuse background – surveys – X-rays: active galaxies

⋆ Based on observations obtained with XMM-Newton, an ESA science mission with instruments and contributions directly funded by ESA Member States and the USA (NASA). The majority of the new optical spectroscopy data used here have been obtained using the facilities of the Italian "Telescopio Nazionale Galileo" (TNG) and of the European Southern Observatory (ESO).

⋆⋆ Tables 2–4 and Appendices are only available in electronic form at http://www.edpsciences.org

1. Introduction

Deep *Chandra* and *XMM-Newton* observations (Brandt et al. 2001; Rosati et al. 2002; Moretti et al. 2003; Hasinger et al. 2001; Alexander et al. 2003) have recently resolved >∼80% of the 2−10 keV cosmic X-ray background (CXB) into discrete sources down to $f_x \sim 3 \times 10^{-16}$ erg cm^{-2} s^{-1}.

The statistical analysis (stacked spectra and hardness ratios) performed on these faint samples provide information on the X-ray spectral properties of the sources making up most of the CXB. The X-ray data are consistent with AGN being the dominant contributors of the CXB (see Brandt et al. 2004, and reference therein) and, as inferred by the X-ray colors, a significant fraction of these sources have hard, presumably obscured, X-ray spectra, in agreement with the predictions of CXB synthesis models (see Setti & Woltjer 1989; Madau et al. 1994; Comastri et al. 1995, 2001; Gilli et al. 2001; Ueda et al. 2003).

However the majority of the sources found in these medium to deep fields are too faint to provide good X-ray spectral information. Furthermore, the extremely faint magnitude of a large number of their optical counterparts makes the spectroscopic identifications very difficult, or even impossible, with the present day ground-based optical telescopes.

Thus, notwithstanding the remarkable results obtained by reaching very faint X-ray fluxes, the broad-band physical properties (e.g. the relationship between optical absorption and X-ray obscuration and the reason why AGN with similar X-ray properties have completely different optical appearance) are not yet completely understood. A step forward toward the solution of these problems has been recently obtained by Mainieri et al. (2002); Piconcelli et al. (2002, 2003); Georgantopoulos et al. (2004); Caccianiga et al. (2004) and Perola et al. (2004) using samples of serendipitous sources for which medium/good quality XMM-Newton and optical data are available.

With the aim of complementing the results obtained by medium to deep X-ray surveys, the XMM-Newton Survey Science Centre[1] (SSC) has conceived the "XMM-Newton Bright Serendipitous Survey". This survey comprises two high galactic latitude ($|b| > 20°$), flux limited samples of serendipitous XMM-Newton sources: the XMM Bright Source Sample (hereafter BSS) and the XMM Hard Bright Source Sample (hereafter HBSS) having a flux limit of $f_x \simeq 7 \times 10^{-14}$ erg cm^{-2} s^{-1} in the 0.5−4.5 keV and 4.5−7.5 keV energy bands, respectively. In addition to the issues related to the CXB, where is now largely accepted that X-ray obscured AGNs play a significant (and perhaps major) role, the use of the 4.5−7.5 keV energy band partially reduces the strong bias against absorbed sources which occurs when selecting at softer energies (or when selecting in the optical domain), and is therefore fundamental to study the accretion history in the Universe (see e.g. Fiore et al. 2003). A similar energy selection band (i.e. 5−10 keV) was pioneered by the *Beppo*SAX-HELLAS (Fiore et al. 2001) and the ASCA-SHEEP (Nandra et al. 2003) surveys.

The well defined criteria (completeness, representativeness, etc.) of this sample will allow both a detailed study of individual sources of high interest, and statistical studies of populations. In particular, the BSS and HBSS samples will be fundamental to complement other medium and deep XMM-Newton and *Chandra* survey programs (having fluxes 10 to 100 times fainter and covering a smaller area of the sky) and will provide a larger baseline for all evolutionary studies. Moreover, the good X-ray statistics which characterize most of the sources in the "XMM-Newton Bright Serendipitous Survey", combined with the relative brightness of their optical counterparts, will allow us to investigate their physical properties in detail. Indeed this sample is already contributing to the solution of some critical open (and "hot") questions like the relationship between optical absorption and X-ray obscuration (Caccianiga et al. 2004) and the physical nature of the "X-ray bright optically normal galaxies" (Severgnini et al. 2003). Many of these issues are investigated with difficulty using the fainter X-ray samples because of their typical poor counts statistics for each source.

The spectroscopic identifications together with the X-ray (spectral, morphological and variability) parameters will be made available to the community and can be used to define statistical identification procedures to select rare and interesting classes of X-ray sources, enabling the application of these procedures to the vast amount of XMM-Newton serendipitous data that will be accumulated during the lifetime of the mission[2].

In this paper we discuss the BSS and the HBSS survey strategy, we present a complete sample of 400 sources extracted from the analysis of 237 XMM-Newton fields and we discuss some preliminary statistical results based on the spectroscopic identification done so far.

This paper is organized as follows. In Sect. 2 we discuss the survey strategy (e.g. energy selection bands, primary selection camera and criteria for field and source selection), we present basic information on the XMM-Newton fields used and on the sources belonging to the BSS and HBSS samples and we discuss the completeness of the "XMM-Newton Bright Serendipitous Survey". In Sect. 3 we discuss the number-flux relationship, the identification work done so far, the broad-band X-ray spectral properties of the sample, the position of

[1] The XMM-Newton Survey Science Centre is an international collaboration involving a consortium of 10 institutions appointed by ESA to help the SOC in developing the software analysis system, to pipeline process all the XMM-Newton data, and to exploit the XMM-Newton serendipitous detections, see http://xmmssc-www.star.le.ac.uk

[2] One of the responsibilities of the XMM-Newton SSC is the production of the XMM-Newton Source Catalogue. This catalogue will provide a rich and unique resource for generating well-defined samples for specific studies, using the fact that X-ray selection is a highly efficient way of selecting certain types of objects, like for instance AGN, clusters of galaxies and active stars. The first XMM-Newton Serendipitous Source Catalogue (1XMM), released on 2003 April 7, contains source detections drawn from 585 XMM-Newton EPIC observations and a total of ∼30 000 individual X-ray sources having a likelihood value above 8 and good quality flags. The median flux (in the total photon energy band 0.2−12 keV) of the catalogue sources is $\sim 3 \times 10^{-14}$ erg cm^{-2} s^{-1}, with ∼12% of them having fluxes below $\sim 1 \times 10^{-14}$ erg cm^{-2} s^{-1}, see http://xmmssc-www.star.le.ac.uk/

the sources in the diagram obtained using the X-ray spectral information (provided by the hardness ratio) and the X-ray to optical flux ratio as well as the surface densities ($\mathrm{Log}\,(N > S)-\mathrm{Log}\,S$) of optically type 1 and type 2 AGN in the HBSS sample. Finally, the summary and the conclusions are reported in Sect. 4. In the appendices we discuss our approach to evaluate the background quality of the data used and to deal with the X-ray sources falling close to the gaps between the CCDs or close to the edge of the CCDs. Throughout this paper $H_0 = 65$ km s^{-1} Mpc^{-1} and $\Omega_\lambda = 0.7$, $\Omega_\mathrm{M} = 0.3$ are assumed; the energy spectral index, α_E, quoted in this paper refers to a power-law spectral model having $S_\mathrm{E} \propto E^{-\alpha_\mathrm{E}}$.

2. Survey strategy and sample(s) selection

2.1. Selection energy band(s)

We have decided to survey the bright X-ray sky in two complementary energy bands: the 0.5−4.5 keV and the 4.5−7.5 keV energy bands.

The choice of the 0.5−4.5 keV energy band is mainly motivated by the desire to avoid the very soft photons (minimizing non-uniformities introduced by the different values of Galactic absorbing column densities along the line of sight) and by the need to compromise between a broad passband (to favor throughput) and a narrow passband (to minimize non-uniformities in the selection function due to different source spectra). Furthermore in the 0.5−4.5 keV band XMM-Newton has the highest throughput.

The choice of the 4.5−7.5 keV energy band (one of the energy bands used in the standard pipeline processing system of the XMM-Newton data) was instead dictated by the need to study the composition of the source population (in terms of observed and intrinsic energy distribution and absorption properties) as a function of the energy selection band, comparing the sources selected in this band with those selected in the softer 0.5−4.5 keV energy range. Moreover this energy band reduces the strong bias against absorbed sources which occurs when selecting at softer energies.

2.2. Primary selection camera

The source sample has been defined using the data from the EPIC MOS2 detector only. The main reasons for this choice are:

1. unlike the EPIC pn, the EPIC MOS cameras have a detector pattern that simplifies the analysis of the field. For example, in the case of the EPIC MOS detectors the source target, in the large majority of the observations, is fully contained in the central chip;
2. the PSF in the 2 EPIC MOSs is narrower than in the EPIC pn. In particular, the EPIC MOS2 has the "best" PSF ($FWHM \sim 4.4''$ and $HEW \sim 13.0''$ at 1.5 keV, see Ehle et al. 2003). As a comparison, the EPIC pn PSF has $FWHM \sim 6.6''$ and $HEW \sim 15.2''$, while the EPIC MOS1 PSF has $FWHM \sim 4.3''$ and $HEW \sim 13.8''$.
3. the gaps between the EPIC MOS chips are narrower than the gaps in the EPIC pn detector, simplifying source detection and analysis and maximizing the survey area;
4. unlike with the EPIC pn camera, we can still use part of the EPIC MOS2 observations in large- and small-window mode by only excluding the area occupied by the central chip. Since ∼25% of the observations have been performed in window mode, retaining these observations will maximize the searched area, speeding up the creation and definition of the source sample.

The major disadvantage of the EPIC MOS2 camera when compared to the EPIC pn camera is the reduced sensitivity, because of its smaller effective area. However, since the BSS and HBSS samples contain relatively bright sources, and considering the minimum exposure times used here (see Sect. 2.5) this lower efficiency does not affect the source selection of the samples presented here. Obviously, once a source is detected and included in the sample, additional information using data from the EPIC MOS1 and pn detectors are collected to increase the statistics for the X-ray spectra, timing and morphology analysis.

2.3. Source detection

Each EPIC MOS2 observation used here (see Table 2) has been processed through the pipeline processing system used for the production of the XMM-Newton Serendipitous Source Catalogue, based on tasks from the XMM-Newton Science Analysis Software. Full details about the processing system, the pipeline products as well as the source searching procedures, flux measurements, source likelihood parameter, corrections for vignetting and PSF, etc. can be found in `http://xmmssc-www.star.le.ac.uk`. We note that the count rate(s) reported in this paper have been already corrected for vignetting and PSF.

2.4. Criteria for source selection

Since the BSS and HBSS samples have been designed to contain relatively bright X-ray sources not all the sources detected in each individual MOS2 field are adequate to be included in these samples. We discuss here the criteria for the BSS and HBSS source selection within each EPIC MOS2 field:

1. *BSS sample*: 0.5−4.5 keV count-rate $\geq 1\times10^{-2}$ cts/s. At this count rate limit, and given the considered range of MOS2 exposure times (see Table 2 and Fig. 1), all the selected sources have a likelihood parameter in the 0.5−4.5 keV energy band greater than ∼18 (corresponding to a probability for a random Poissonian fluctuation to have caused the observed source counts of 1.5×10^{-8}). No further constraint is thus needed to ensure the source reliability.
   HBSS sample: 4.5−7.5 keV count-rate $\geq 2 \times 10^{-3}$ cts/s and likelihood parameter in the 4.5−7.5 keV energy band greater than 12 (corresponding to a probability of 6×10^{-6} for a spurious detection).

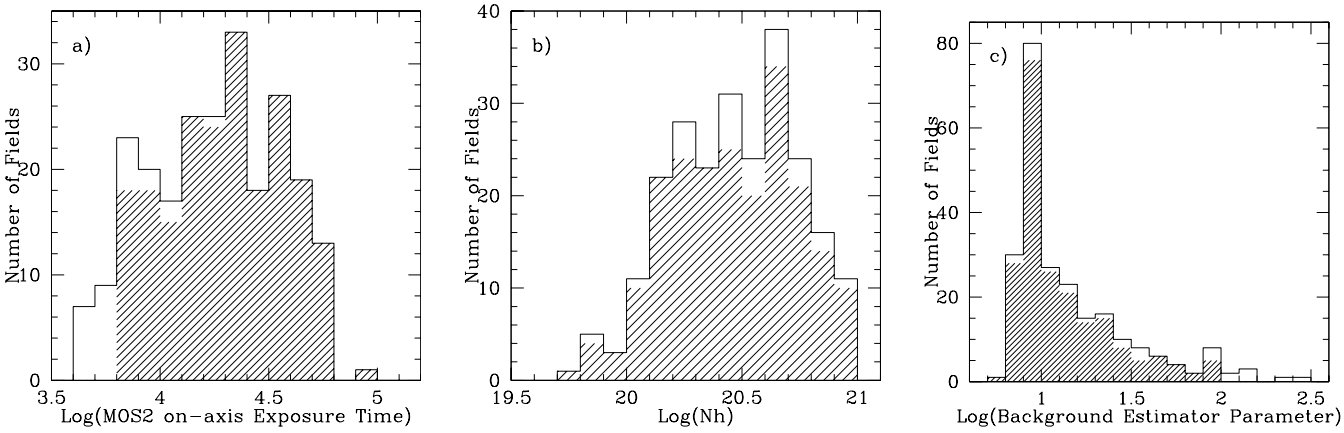

Fig. 1. Histograms of some basic properties of the XMM-Newton MOS2 fields used for the sample selection. Normal histograms refer to the XMM-Newton fields used to define the BSS sample, while shaded histograms refer to the subset of XMM-Newton fields used to define the HBSS sample. Panel **a)** histogram of the MOS2 on-axis good-time exposure; Panel **b)** histogram of the Galactic hydrogen column density along the line of sight; Panel **c)** histogram of the Background Estimator Parameter (see Appendix B for details).

The combination of count-rate limit(s) and likelihood parameter(s) of the sources in the BSS and HBSS samples is such that none of them are expected to be spurious.
The count rate to flux conversion factors (CR2F) depend on the source spectra and in Table 1 we report some CR2F as a function of the input source spectra for a fixed Galactic $N_{\rm H}$ value of 3×10^{20} cm^{-2} (corresponding to the median value for the XMM-Newton fields used here).
For a source with a power-law spectrum with energy spectral index $\alpha_{\rm E}$ between 0.7 and 0.8 the count rate limit in the two chosen bands corresponds to a flux limit of $\sim 7 \times 10^{-14}$ erg cm^{-2} s^{-1}.

2. Sources with a distance from the EPIC MOS2 center between an inner radius ($R_{\rm in}$) and an outer radius ($R_{\rm out}$).
$R_{\rm in}$ depends on the actual size and brightness of the target and on the window mode. $R_{\rm in}$ ranges between 0 (e.g. survey fields with no "target") and 8 arcmin (e.g. bright/extended X-ray sources or large- and small-window mode). In this way the area of the detector "obscured" by the presence of the target or not exposed is excluded from the analysis. To guarantee that all the sources in the catalogue are truly serendipitous, the size of $R_{\rm in}$ has been adapted in order to exclude the target and the sources physically related to the target. $R_{\rm out}$ is, for the large majority of the fields, equal to 13 arcmin. In the few overlapping fields we have excluded from the analysis the outer region of one of the overlapping fields in order to obtain a mosaic of separate and independent regions on the sky. The values of $R_{\rm in}$ and $R_{\rm out}$ used for each MOS2 image are listed in Table 2.
3. We have also excluded the sources too close to the edges of the field of view or to the gaps between the CCDs. These sources could have either the flux and/or the source centroid poorly determined (due to the proximity to the edges and/or the gaps), and therefore could degrade the quality of the data, and would require uncertainty corrections thus representing a problem in the subsequent analysis and interpretation of the data. In Appendix A we discuss the procedure used to take into account this problem in an objective way. Obviously, the excluded area has been taken into account in the computation of the sky coverage.

2.5. Criteria for field selection

Not all the available EPIC MOS2 pointings are adequate for producing the BSS and HBSS samples. We have defined a set of selection criteria to avoid problematic regions of the sky, to maximize the availability of ancillary information at other frequencies (i.e. optical and radio) and to speed up the optical identification process. The majority of the fields selection criteria are common to the BSS and HBSS; however, as discussed below, we have been more conservative on the minimum exposure time and background properties for the fields used to define the HBSS sample. The criteria adopted for field selection are:

1. availability to SSC before March 2003 (XMM-Newton fields that are public or with PI granted permission);
2. high Galactic latitude ($|b| \geq 20°$) to avoid crowded fields, to obtain a relatively "clean" extragalactic sample and to have magnitude information for the optical counterparts from the Digital Sky Survey material (the Automated Plate Machine – APM – catalogue[3] is almost complete for $|b| \geq 20°$);
3. Galactic absorbing column density along the line of sight less than 10^{21} cm^{-2}, to minimize non-uniformities introduced by large values of the Galactic $N_{\rm H}$;
4. exclusion of fields centered on bright and/or extended X-ray or optical targets and those containing very bright stars in the optical band. In the first two cases the effective area of sky covered and the actual flux limit are difficult to estimate correctly, making the derivation of the sky-coverage more uncertain; in the latter case the search for the optical counterpart of the X-ray sources could be very difficult or even impossible due to the presence of the bright star;

[3] http://www.ast.cam.ac.uk/~apmcat/

Table 1. MOS2 count rate to flux conversion factors.

α_E	*HR*2	Flux (0.5−4.5 keV) 10^{-12} erg cm^{-2} s^{-1}	Flux (4.5−7.5 keV) 10^{-11} erg cm^{-2} s^{-1}
(1)	(2)	(3)	(4)
−3.0	0.77	14.3; 14.4; 15.0	4.53; 4.54; 4.59
−2.0	0.56	12.8; 12.9; 13.6	4.24; 4.25; 4.30
−1.0	0.22	10.6; 10.8; 11.7	3.97; 3.97; 4.03
−0.5	0.01	9.47; 9.61; 10.6	3.84; 3.84; 3.90
0.0	−0.22	8.35; 8.49; 9.55	3.71; 3.72; 3.77
0.4	−0.38	7.56; 7.70; 8.82	3.62; 3.62; 3.68
0.5	−0.42	7.38; 7.53; 8.66	3.59; 3.60; 3.65
0.7	−0.49	7.06; 7.20; 8.37	3.55; 3.55; 3.61
0.9	−0.57	6.78; 6.92; 8.11	3.50; 3.51; 3.56
1.0	−0.60	6.65; 6.79; 8.00	3.48; 3.49; 3.54
1.5	−0.74	6.16; 6.31; 7.61	3.38; 3.38; 3.43
2.0	−0.83	5.89; 6.04; 7.46	3.28; 3.28; 3.33
3.0	−0.94	5.75; 5.94; 7.62	3.10; 3.10; 3.15

Columns are as follows: (1) Energy spectral index ($S_E \propto E^{-\alpha_E}$); (2) corresponding hardness ratio *HR*2 computed as discussed in Sect. 3.3; (3) Flux (corrected for Galactic absorption) in the 0.5−4.5 keV energy band corresponding to an observed count rate of 1 cts/s in the same energy band. The three numbers refer to thin, medium and thick filters; (4) Flux (corrected for Galactic absorption) in the 4.5−7.5 keV energy band corresponding to an observed count rate of 1 cts/s in the same energy band. The three numbers refer to thin, medium and thick filters. NOTE – A Galactic absorbing column density of 3×10^{20} cm^{-2}, the median value for the XMM-Newton fields used here, has been assumed. Given the range of the Galactic absorbing column density along the line of sight (from $\sim 5 \times 10^{19}$ to 10^{21} cm^{-2}) the CR2F in the 0.5−4.5 keV energy range are accurate to ±18%; the CR2F in the 4.5−7.5 keV energy range are independent of the Galactic N_H. Please note that in the case of sources having extreme *HR*2 values the observed spectra could be much more complex than a simple power law; for these sources the conversion factor reported in the table should be considered only as indicative and a proper X-ray spectral analysis is needed.

5. exclusion of fields south of Dec = −80 deg since it could be very difficult to obtain good quality spectroscopy given the location of the optical facilities available to us;
6. good-time interval[4] exposure >∼5 ks for the BSS and ≥7 ks for the HBSS. According to the results presented and discussed below, with these constraints all the sources in the two samples are detectable across the whole field of view considered, ensuring a "flat" sensitivity and therefore a flat sky coverage at the sampled fluxes.
7. finally, we have also excluded EPIC MOS2 pointings suffering from a high background rate (i.e. accumulated during particle background flares). The background restriction has been more conservative for the set of fields that have been used to define the HBSS sample since the overall background is more critical given the faintness of the sources in the 4.5−7.5 keV energy band. We have defined and computed in an automatic way a Background Estimator Parameter (see Appendix B) which is roughly proportional to the "real background" in the MOS2 images used. The set of fields that have been used to define the HBSS sample must have the Background Estimator Parameter less than 100.

Note that we have also considered the EPIC MOS2 observations in large- and small-window mode satisfying the criteria discussed above; in these cases we have excluded from the analysis a circular area of 8 arcmin radius enclosing the central chip. No restrictions on the blocking filter in front of the MOS2 camera have been applied since, as shown in Sect. 2.6, the filter used does not affect the statistical properties of the sample[5].

The complete BSS sample reported here is based on the analysis of 237 XMM-Newton fields, while the complete HBSS sample is based on a "restricted" data set of 211 XMM-Newton pointings.

In Table 2 we report basic information on the XMM-Newton MOS2 fields used for the sample selection; in particular we list the XMM-Newton observation number, the blocking filter in front of the MOS2 instrument, the Right ascension and Declination of the MOS2 image center, the on-axis good-time exposure for the MOS2 detector, the logarithm of the Galactic Hydrogen column density along the line of sight (from Dickey & Lockman 1990), the inner and outer radius of the part of the MOS2 image used in the survey, and the total number of BSS and HBSS sources found in the surveyed area of each MOS2 image. In Table 2 we have also marked the 26 MOS2 fields not used for the production of the HBSS sample.

In Fig. 1 we show the distribution of the MOS2 on-axis good-time exposure, the distribution of the Galactic hydrogen column density along the line of sight and the distribution of the Background Estimator Parameter for the XMM-Newton MOS2 data-set used.

2.6. The XMM-Newton BSS and HBSS samples

Applying the source selection criteria discussed in Sect. 2.4 to the MOS2 fields reported in Table 2 we have selected 400 XMM-Newton sources: 389 sources belong to the BSS sample and 67 sources to the HBSS sample with 56 sources in common. Basic information on the sources are reported in Table 3 (BSS) and in Table 4 (HBSS); in particular we report the source name, the XMM-Newton observation number, Right Ascension and Declination (J2000) of the X-ray source position, the angular distance (in arcmin) between the source and the MOS2 image center, the source count rate in the 0.5−4.5 keV energy band (BSS sample) or in the 4.5−7.5 keV energy band (HBSS sample), the hardness ratios computed as described in Sect. 3.3, and the optical spectroscopic classification (see Sect. 3.2 for details). In Table 4 we have also marked the 11 sources belonging to the HBSS sample but not to the BSS sample.

In Fig. 2 we show the surface density of the sources belonging to the BSS and to the HBSS as a function of: the MOS2

[4] The good-time interval is defined as the on-axis exposure time taken from the exposure map produced in the XMM-Newton pipeline processing system.

[5] The fraction of MOS2 images with a thin, medium and thick filter used here are ∼48%, ∼46% and ∼6%, respectively.

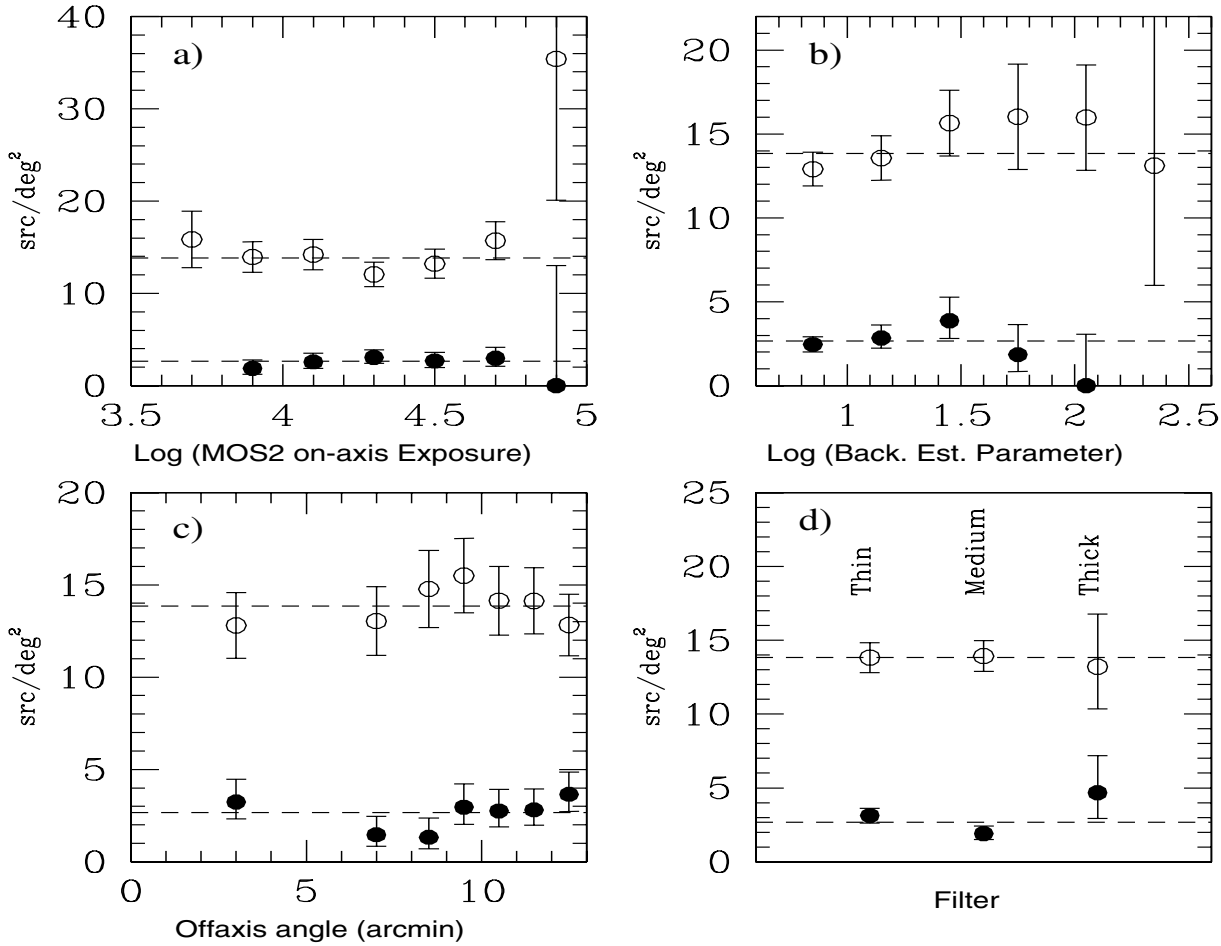

Fig. 2. Panel **a)**: source surface density as a function of the MOS2 on-axis good-time exposure for the sources belonging to the BSS (open circles) and to the HBSS (filled circles) sample. Panel **b)**: source surface density as a function of the Background Estimator Parameter; symbols as in panel **a)**. Panel **c)**: source surface density as a function of the offaxis angle; the bin size has been adapted in order to have similar areas in each bin; symbols as in panel **a)**. Panel **d)**: source surface density as a function of the blocking filter in front of the MOS2 detector; symbols as in panel **a)**. For all the panels the dashed lines correspond to the mean surface density considering the whole BSS or HBSS sample. Errors have been computed using Poisson statistic.

on-axis good-time exposure (panel a); the Background Estimator Parameter (panel b); the off-axis angle (panel c); and the blocking filter in front of the MOS2 detector (panel d). The appropriate area covered in each bin has been considered and errors have been computed using Poisson statistic. The dashed lines reported in Fig. 2 correspond to the mean surface density obtained considering the whole sample. As can be seen there is no significant trend of the source surface density with respect to the plotted parameters confirming a flat sensitivity across the field (i.e. flat sky coverage at the sampled fluxes). The only point which seems to be a factor ~2.5 above the other is the bin at the highest exposure time in the BSS sample (see panel a). This excess is due to 5 sources found in the field 0022740101 (centered on the Lockman hole), the only pointing in the bin considered; however the error bars are large and so the reported surface density is not significantly different from the mean value. The absolute source surface density as a function of the flux ($\mathrm{Log}\,N - \mathrm{Log}\,S$) is also in very good agreement with previous and new measurements (see Sect. 3.1) making us confident of the correctness of the data analysis and source selection.

3. First results

3.1. The number-counts relationship(s)

In Fig. 3 we show (filled circles) a binned representation of the extragalactic[6] number-flux relationships in the 0.5−4.5 keV energy band (panel a) and in the 4.5−7.5 keV energy band (panel b). As already shown in Sect. 2.6, the sky coverage of this survey at the flux limit used to define the BSS and the HBSS samples is flat and equal to 28.10 sq.deg and 25.17 sq.deg, respectively; given the flat sky coverage the errors in the binned representation are Poissonian errors on the total number of sources having a flux greater than any fixed flux. A conversion factor appropriate for a power-law spectral model with energy index equal to 0.8 (0.7) in the 0.5−4.5 keV (4.5−7.5 keV) energy band, filtered by an $N_{\mathrm{H_{Gal}}} \sim 3{\times}10^{20}$ cm^{-2}

[6] Since we are primarily interested in the extragalactic number-flux relationship we have excluded from the computation the sources classified as stars (see Sect. 3.2). Based on the results presented in Sect. 3.5 we are confident that the large majority of the unidentified sources are associated to extragalactic objects.

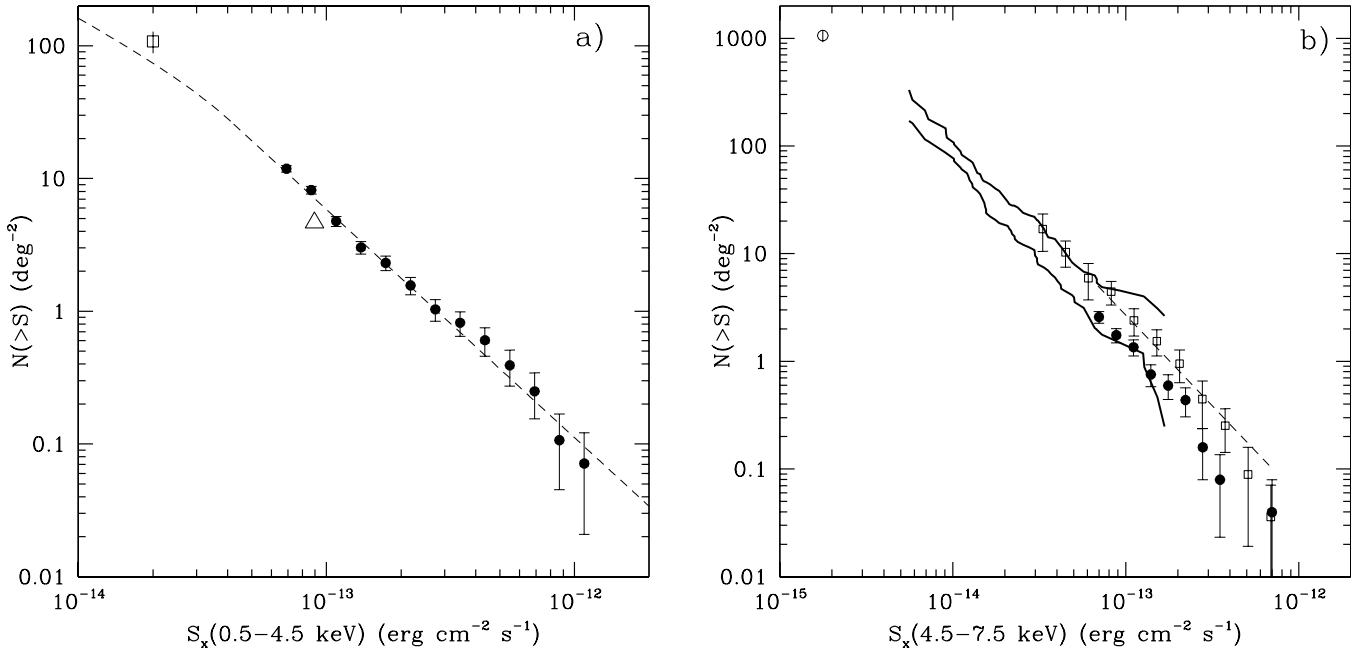

Fig. 3. The extragalactic number-flux relationship in the 0.5−4.5 keV energy band (panel **a**)) and in the 4.5−7.5 keV energy band (panel **b**)) obtained using the BSS and HBSS samples (binned representation: black filled circles). In the 0.5−4.5 keV Log $(N > S)$ − Log S (panel **a**)) we have also reported the ROSAT (0.5−2.0 keV) Log $(N > S)$ − Log S (dashed line) and the EMSS (0.3−3.5 keV) extragalactic number density at $\sim 10^{-13}$ erg cm^{-2} s^{-1} (open triangle) both converted to the 0.5−4.5 keV energy band. The open square at $S \simeq 2 \times 10^{-14}$ erg cm^{-2} s^{-1} represents the extragalactic surface density (0.5−4.5 keV) obtained by the XMM-Newton AXIS Medium Survey project. In panel **b)** (4.5−7.5 keV Log $(N > S)$ − Log S) we have also reported the HELLAS2XMM Log $(N > S)$ − Log S interval (area inside the thick solid lines), the HELLAS Log $(N > S)$ − Log S (open squares) and the SHEEP Log $(N > S)$ − Log S (dashed line). The open circle at $S \simeq 2 \times 10^{-15}$ erg cm^{-2} s^{-1} represents the extragalactic surface density (5−10 keV band) in the Lockman hole field. Both these latter number densities have been converted from their original (5−10 keV) band to the 4.5−7.5 keV band.

(the median value of the $N_{\rm H_{Gal}}$ of the survey), has been used in the conversion between the count rate and the flux. The energy spectral index used in the 0.5−4.5 keV energy band corresponds to the "average" one of the extragalactic BSS population in the same energy selection band (see Sect. 3.3). In the 4.5−7.5 keV energy band we have used $\alpha_{\rm E} = 0.7$, the same energy spectral index assumed from other recent surveys in the 5−10 keV band (e.g. the HELLAS2XMM survey, Baldi et al. 2002) and very close to the median energy spectral index in the 0.5−4.5 keV band of the extragalactic HBSS population (see below for details). We recall that, given the median $N_{\rm H_{Gal}}$ of the survey, the count rate to flux conversion factor in the 0.5−4.5 keV (4.5−7.5 keV) energy band are accurate ∼±20 (∼±8)% for an energy spectral index in the range between 0 to 2.

Both Log $N(>S)$−Log S distributions can be well described by a power-law model $N(>S) \propto S^{-\alpha}$; their best fit spectral parameters, obtained applying the maximum likelihood method to the unbinned data (see Maccacaro et al. 1982 for details), are reported in Table 5.

The fits have been performed from a flux of $\simeq 7 \times 10^{-14}$ erg cm^{-2} s^{-1} (the faintest flux) to a flux of $\simeq 1 \times 10^{-12}$ erg cm^{-2} s^{-1} (we have excluded from the fit 3 extragalactic BSS sources brighter than this flux limit). For fluxes brighter than this limit we may not be complete since "bright" X-ray sources were chosen as targets of observations and then excluded, by definition, from the survey. However we note that the surface density of sources with flux greater than $\sim 1 \times 10^{-12}$ erg cm^{-2} s^{-1} is such that about 2.7 (0.9) sources in the BSS (HBSS) sample are expected given the covered sky area; these numbers are fully consistent with what is observed.

Table 5. The extragalactic Log $(N > S)$ − Log S maximum likelihood best fit parameters: $N(> S) = K \times (S/10^{-13})^{-\alpha}$, where $N(> S)$ is the surface densities of sources having a flux greater than S in deg^{-2}.

Sample	Objects	α	K
(1)	(2)	(3)	(4)
BSS[a]	330	$1.80^{1.91}_{1.69}$	$6.1^{5.8}_{6.4}$
HBSS	65	$1.64^{1.89}_{1.41}$	$1.5^{1.4}_{1.6}$
HBSS AGN1	41	$1.72^{2.03}_{1.42}$	$0.92^{0.82}_{1.0}$
HBSS AGN2	21	$1.57^{1.99}_{1.18}$	$0.50^{0.42}_{0.58}$

Columns are as follows: (1) Sample; (2) Number of sources used in the fit; (3) Best fit power-law slope and 68% confidence intervals; (4) Log $(N > S)$ − Log S normalization and 68% confidence intervals. Note that the normalization K is not a parameter of the fit but is determined by re-scaling the model to the number of objects in the sample. The normalization K reported here corresponds to the surface densities at 1×10^{-13} erg cm^{-2} s^{-1} . NOTE – [a] As explained in Sect. 3.1 we have excluded from the fit the 3 BSS extragalactic sources having a flux greater than 1×10^{-12} erg cm^{-2} s^{-1} .

Both $\mathrm{Log}\,(N > S) - \mathrm{Log}\,S$ derived here have been compared with a number of representative $\mathrm{Log}\,(N > S) - \mathrm{Log}\,S$ reported in the literature. In particular, in Fig. 3 panel a, we have reported: a) the extragalactic ROSAT (0.5−2.0 keV) $\mathrm{Log}\,(N > S) - \mathrm{Log}\,S$ from Hasinger et al. (1998) (dashed line); b) the EMSS (0.3−3.5 keV) extragalactic number density at $\sim 10^{-13}$ erg cm^{-2} s^{-1} (open triangle; Gioia et al. 1990); and c) the extragalactic surface density obtained from the XMM-Newton AXIS Medium Survey team in the 0.5−4.5 keV energy range (Barcons et al. 2002; open square at $S \simeq 2 \times 10^{-14}$ erg cm^{-2} s^{-1}). To convert the ROSAT 0.5−2.0 keV band fluxes and the EMSS 0.3−3.5 keV band fluxes into 0.5−4.5 keV fluxes we have used a power-law spectral model having $\alpha_{\rm E} \simeq 1.0$, corresponding to the mean spectral index of the ROSAT and the EMSS sources (see Hasinger et al. 1993 and Maccacaro et al. 1988, respectively).

In panel b) we have compared our result with: a) the extragalactic XMM-Newton (5−10 keV) $\mathrm{Log}\,(N > S) - \mathrm{Log}\,S$ from the HELLAS2XMM survey (area inside the thick solid lines; Baldi et al. 2002); b) the *Beppo*SAX-HELLAS (5−10 keV) $\mathrm{Log}\,(N > S) - \mathrm{Log}\,S$ (open squares; Fiore et al. 2001); c) the ASCA-SHEEP (5−10 keV) $\mathrm{Log}\,(N > S) - \mathrm{Log}\,S$ (dashed line; Nandra et al. 2003). Finally, the open circle at $S \simeq 2 \times 10^{-15}$ erg cm^{-2} s^{-1} represents the extragalactic surface density in the (5−10 keV) energy band from the XMM-Newton observation of the Lockman hole field (Hasinger et al. 2001). For consistency with previous hard survey both these latter number densities have been converted from their original (5−10 keV) band to the 4.5−7.5 keV band using a power-law spectral model having $\alpha_{\rm E} = 0.7$. We found that our results are fully consistent with those obtained from the other XMM-Newton related survey (e.g. the HELLAS2XMM 5−10 keV survey) and, moreover, our better statistics above 7×10^{-14} erg cm^{-2} s^{-1} allow us to significantly constrain the 4.5−7.5 keV extragalactic number densities above this flux.

On the other hand the extragalactic HBSS $\mathrm{Log}\,(N > S) - \mathrm{Log}\,S$ falls below both the *Beppo*SAX-HELLAS and the ASCA-SHEEP determinations. Given the results discussed in Sect. 2.6 and the very similar slope between our $\mathrm{Log}\,(N > S) - \mathrm{Log}\,S$ and the *Beppo*SAX/ASCA $\mathrm{Log}\,(N > S) - \mathrm{Log}\,S$ we have checked if this problem could be related to an offset of the absolute flux scale in the 4.5−7.5 keV energy range between XMM-Newton and *Beppo*SAX/ASCA. To this purpose we have cross-correlated the HELLAS and the SHEEP sources with the total catalogue of XMM-Newton sources obtained from the analysis of the 237 XMM-Newton fields reported in Table 2. Using a search radius of 90″ and considering the point-like XMM-Newton sources with a 4.5−7.5 keV likelihood parameter greater than 12 and with an "Illumination Factor" (see Appendix A for details) greater than 0.8, we have found 6 "bona fide" HELLAS-XMM coincidences and 2 "bona fide" SHEEP-XMM coincidences. The ratio between the 4.5−7.5 keV XMM-Newton fluxes and the 5−10 keV *Beppo*SAX fluxes in the case of the HELLAS sources ranges between 0.09 and 0.98 with a mean value of 0.47, while in the case of the two SHEEP sources the ratio between the 4.5−7.5 keV XMM-Newton fluxes and the 5−10 keV ASCA fluxes is equal to ≃0.63 for both objects.

Table 6. The current optical breakdown of the BSS and HBSS samples.

	BSS[1]	HBSS
Objects[2]	389 (166)	67
Identified:	278 (146)	60
Identification rate	71% (88%)	90%
AGN-1	180 (100)	39
AGN-2	26 (15)	16
Galaxies[3]	7 (3)	1
Clusters of Galaxies	4 (1)	1
BL Lacs	5 (3)	1
Stars[4]	56 (24)	2

[1] In brackets we have reported the optical breakdown for the BSS sources with Right Ascension below 5$^{\rm h}$ or above 17$^{\rm h}$; [2] Note that 56 sources are in common between the BSS and HBSS samples; [3] We stress that some of the sources classified as "Optical Normal Galaxy" could indeed host an optically elusive AGN (see e.g. Severgnini et al. 2003); [4] To our knowledge all but one (XBS J014100.6−675328) of the sources classified as stars are coronal emitters.

Although these small numbers do not allow us to draw firm conclusions we note that using a conversion factor between the fluxes in the 5−10 keV energy range and the fluxes in the 4.5−7.5 keV energy range equal to 0.47 (instead of 0.69 as expected for $\alpha_{\rm E} = 0.7$ and as assumed in Fig. 3) the HBSS $\mathrm{Log}\,(N > S) - \mathrm{Log}\,S$ and the *Beppo*SAX-HELLAS $\mathrm{Log}\,(N > S) - \mathrm{Log}\,S$ turn out to be in perfect agreement. This suggests that an offset in the absolute flux scale could easily explain the disagreement in the number densities discussed above; this possible discrepancy in the flux scale has to be further investigated.

3.2. Optical identification and classification

One of the main characteristics of the X-ray sources presented here is that the majority (∼90%) of them have an optical counterpart above the POSS II limit ($R \sim 21^{\rm mag}$), thus allowing spectroscopic identification even on 2−4 meter class telescopes. Furthermore, given the good accuracy of the X-ray positions[7] and the magnitude of the optical counterparts there is no ambiguity in the optical identification for the large majority of cases.

Up to now 285 X-ray sources have been spectroscopically identified (either from the literature or from our own observations mainly at the Italian "Telescopio Nazionale Galileo" -TNG, at the ESO 3.6 m, at the Calar Alto 2.2 m or at

[7] Using the optical position of the sources classified as type 1 AGN we have evaluated that the 90% confidence level error circle has a radius equal to ∼4″; about 99% of the type 1 AGN are within 6″ from the X-ray position. This is consistent with what found in other XMM-Newton surveys (Barcons et al. 2002; Fiore et al. 2003).

the NOT 2.6 m[8] telescopes) leading to a 71% and 90% identification rate for the BSS and HBSS samples respectively.

The optical breakdown of the sources identified so far is reported in Table 6. We stress that the source detection algorithm is optimized for point-like sources, so the sample of clusters of galaxies is not statistically complete nor representative of the cluster population.

To our present knowledge all but one (XBS J014100.6−675328[9]) of the sources classified as stars are coronal emitters. If we consider the BSS sources with Right Ascension below 5^h or above 17^h (spectroscopic identification rate of ∼88%, see Table 6), the X-ray coronal emitting stars represent ∼14% of the $|b| > 20°$ (0.5−4.5 keV) population at the sampled fluxes. This fraction must be compared with ∼1.5% of coronal emitters in the HBSS sample[10]; this smaller fraction of stars in the HBSS sample, compared with that in the BSS sample, is entirely consistent with their low temperature coronal emission. Note that in the softer (0.5−2.0 keV) ROSAT Bright Survey Catalog (RBS, Schwope et al. 2000) the fraction of coronal emitting stars is around 37%.

The large majority (∼90%) of the extragalactic X-ray sources are emission line objects, i.e. sources for which at least one strong ($EW \gg 5$ Å in the source rest frame) emission line is present in the optical spectrum. As a comparison in the RBS the fraction of emission line AGN amongst the extragalactic sources is around 55% (Schwope et al. 2000). The few remaining non-emission line objects have been classified as "Normal Galaxies" or BL Lacs objects according to the measured Calcium break discontinuity at the rest frame wavelength of 4000 Å (see e.g. Landt et al. 2002). We stress that some of the sources classified as "Normal Galaxies" could indeed host an AGN. As already discussed by Severgnini et al. (2003) using X-ray and optical spectral data from this project, the lack of significant emission lines in the optical spectra can be explained by an adequate combination of the absorption associated with the AGN and of the optical faintness of the active nucleus with respect to the host galaxy. Furthermore for some of the sources classified as "Normal Galaxies" the H_α line (in some case the only spectroscopic evidence of the presence of an AGN in the optical domain) is not sampled. Although the presence of an AGN in the nucleus of some of these sources is highly probable (e.g. observed L_x well in excess of 10^{42} erg s^{-1}) we prefer to wait for a confirmation also from optical/infrared follow-ups; for the moment these objects are classified as "Normal Galaxies".

To classify the emission line objects we have used the criteria presented for instance in Veron-Cetty & Veron (2001) which are based on the line width and the line flux ratios. Type 1 AGN are those sources showing broad ($FWHM > 1000$ km s^{-1}) permitted lines, while type 2 AGN are those sources showing only narrow lines ($FWHM < 1000$ km s^{-1}) and, when detected, [OIII]λ5007/$H_\beta > 3$.

A few sources show permitted lines with 1000 km s^{-1} < $FWHM$ < 2000 km s^{-1} and [OIII]λ5007/H_β below 3. These sources are probably narrow line Seyfert 1 candidates and, according to our classification, have been included in the type 1 AGN group. For some sources classified as type 2 AGN we have indication of the presence of a broad component at the bottom of the narrow H_β and/or H_α lines. These sources should be properly classified as Seyfert 1.8 or Seyfert 1.9 objects; for the purpose of the present paper these sources have been included in type 2 AGN group. Finally for 26 objects a better *S/N* optical spectrum and/or a more appropriate set-up for the spectroscopic observations are needed to firmly classify them as type 1 or type 2 AGN. These 26 sources have been marked in Col. 8 of Tables 3 and 4.

3.3. 0.5–4.5 keV spectral properties

A "complete" spectral analysis for all the sources in the BSS and HBSS samples (using data from the two EPIC MOSs and the EPIC pn) is in progress; first results on selected subsamples of sources have been already discussed in Severgnini et al. (2003) and Caccianiga et al. (2004). In the meantime, and in order to extract first order X-ray spectral information we present here a "Hardness Ratio" analysis of the single sources using only EPIC MOS2 data; this latter method is equivalent to the "color−color" analysis largely used at optical wavelengths. The use here of the "Hardness Ratio" analysis is twofold. First of all it is much faster than a complete spectral analysis with the combined use of three different instruments. Second, a "Hardness Ratio" is often the only X-ray spectral information available for the faintest sources in the XMM-Newton catalogue, and thus, a "calibration" in the parameter space is needed to select "clean" and well-defined samples. On the other hand, in Caccianiga et al. (2004) we have already shown and discussed a tight correlation between X-ray absorption, as deduced from a complete X-ray spectral analysis, and "Hardness Ratio" properties.

We have used the hardness ratios as defined from the XMM-Newton pipeline processing[11]:

$$HR2 = \frac{C(2\text{−}4.5\ \text{keV}) - C(0.5\text{−}2\ \text{keV})}{C(2\text{−}4.5\,\text{keV}) + C(0.5\text{−}2\ \text{keV})}$$

[8] As part of the AXIS (An XMM-Newton International Survey) project, see http://www.ifca.unican.es/~xray/AXIS

[9] XBS J014100.6−675328 (BL Hyi), also belonging to the HBSS sample, is a well known AM Herculis object (a polar) i.e. a binary system composed of a magnetic white dwarf and a low-mass star (see Caccianiga et al. 2004, and references therein).

[10] On the basis of the results presented in Sect. 3.5 we are confident that the bulk of unidentified sources both in the BSS and HBSS samples are associated with extragalactic objects and we know that XBS J014100.6−675328 is an accreting binary system (see Caccianiga et al. 2004).

[11] We have not used here the "pipeline processing product" HR1 which is defined using the corrected count rate in the (0.15−0.5) keV and in the (0.5−2) keV energy band since the measured count rate in the (0.15−0.5) keV band is a strong function of the Galactic N_H along the line of sight. Note that the effect on *HR*2 and *HR*3 due to the different $N_{H_{Gal}}$ for the objects in the sample (which ranges between ∼10^{20} to 10^{21} cm^{-2}) is negligible.

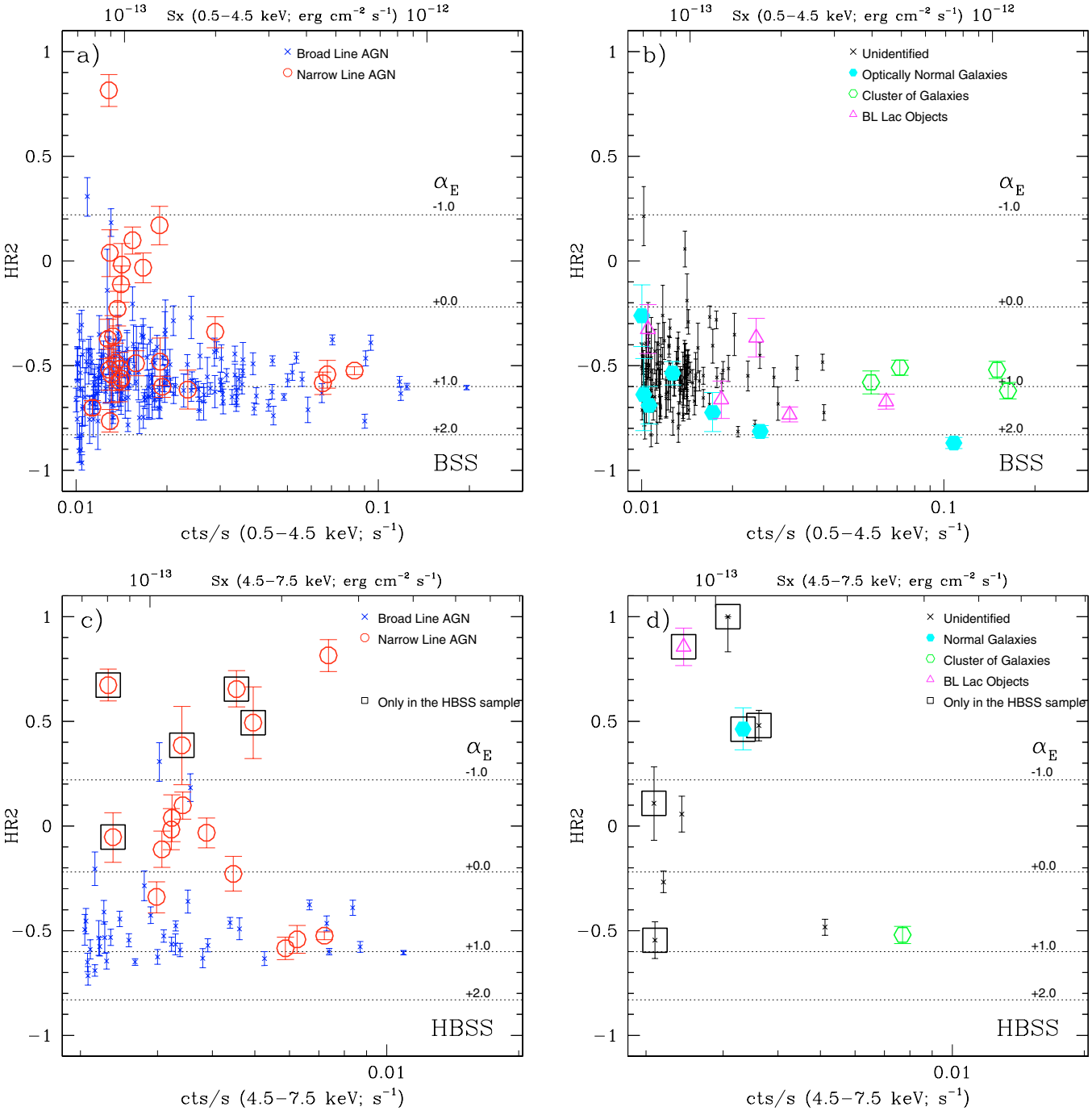

Fig. 4. *HR*2 vs. EPIC MOS2 count rate in the selection band for the sources in the BSS (panel **a)** and panel **b)**) and HBSS sample (panel **c)** and panel **d)**). We have also reported the *HR*2 expected from a unabsorbed power-law model with α_E ranging from −1 to 2 ($S_E \propto E^{-\alpha_E}$). The flux scale on the top has been computed assuming a conversion factor appropriate for $\alpha_E \sim 0.8$ (BSS sample) or $\alpha_E \sim 0.7$ (HBSS sample). We have used different symbols to mark the different kinds of objects. The eleven sources belonging only to the HBSS sample are enclosed inside empty squares in panels **c)** and **d)**.

and

$$HR3 = \frac{C(4.5{-}7.5\ \mathrm{keV}) - C(2{-}4.5\ \mathrm{keV})}{C(4.5{-}7.5\,\mathrm{keV}) + C(2{-}4.5\ \mathrm{keV})}$$

where C(0.5−2 keV), C(2−4.5 keV) and C(4.5−7.5 keV) are the "PSF and vignetting corrected" count rates in the 0.5−2, 2−4.5 and 4.5−7.5 keV energy bands, respectively.

In Fig. 4 (panel a and panel b) we plot *HR*2 as a function of the 0.5−4.5 keV count rate for the extragalactic (and unidentified) sources of the BSS sample. In particular, in panel a) we show the position of the optically classified type 1 and type 2 AGN, while in panel b) we have shown the unidentified sources, the "Optically Normal Galaxies", the Clusters of galaxies and the BL Lac objects. On the top, we have also reported the flux scale computed assuming a conversion factor

Table 7. *HR*2 statistic for some relevant BSS and HBSS sub-sample(s).

Sample	Objects	Weighted	Unweighted	Median	St.Dev.	σ intrins.
(1)	(2)	(3)	(4)	(5)	(6)	(7)
BSS Sample:						
Extragalactic	333	-0.51 ± 0.01	-0.54 ± 0.01	-0.57	0.20	0.16
ÃGN1	180	-0.54 ± 0.01	-0.56 ± 0.01	-0.58	0.15	0.12
ÃGN2	26	-0.32 ± 0.07	-0.34 ± 0.07	-0.49	0.35	0.32
Unidentified	111	-0.52 ± 0.02	-0.54 ± 0.02	-0.56	0.16	0.12
Stars	56	-0.83 ± 0.01	-0.88 ± 0.01	-0.90	0.11	0.08
HBSS Sample:						
Extragalactic	65	-0.10 ± 0.05	-0.27 ± 0.05	-0.47	0.44	0.40
ÃGN1	39	-0.44 ± 0.03	-0.49 ± 0.03	-0.53	0.21	0.18
ÃGN2	16	0.14 ± 0.11	0.05 ± 0.11	-0.02	0.45	0.44

Columns are as follows: (1) Sample; (2) Number of sources; (3) *HR*2 weighted average; (4) *HR*2 unweighted average; (5) *HR*2 median value; (6) Observed standard deviation of the *HR*2 distribution; (7) Intrinsic dispersion of the *HR*2 distribution computed using the maximum likelihood method as described in Maccacaro et al. (1988).

appropriate for $\alpha_{\rm E} \simeq 0.8$, which is the "mean" energy spectral index of the "extragalactic" sample in the 0.5−4.5 keV energy band (see below).

No obvious trend in the source spectra as a function of the count rate is measured. If we split the extragalactic BSS sample in two different bins of count rate (below or above a count rate of 1.41×10^{-2} cts/s in the 0.5−4.5 keV energy band) which includes a similar number of objects (163 and 170 sources, respectively) we found that the *HR*2 distributions of the two sub-samples are consistent with being extracted from the same distribution with a probability of 61% according to a KS test.

The weighted average of the extragalactic population is $HR2 = -0.51 \pm 0.01$ corresponding to $\alpha_{\rm E} = 0.74 \pm 0.03$ (the relation between the spectral index and *HR*2 has been tabulated for few representative spectral indices in Table 1). For comparison the weighted averages of the sources classified as type 1 AGN and unidentified objects are $HR2 = -0.54 \pm 0.01$ and $HR2 = -0.52 \pm 0.02$, respectively. The *HR*2 distribution of the sources identified as type 1 AGN appears to be "narrow" with ∼90% of the sources inside the *HR*2 range −0.75 to −0.35. On the contrary the type 2 AGN are characterized by a broader distribution with ∼42% of the objects having an observed energy spectral index apparently flatter than that of the cosmic X-ray background ($\alpha_{\rm E} = 0.4$ corresponding to $HR2 = -0.38$). For comparison only ∼10% of the unidentified X-ray sources or of the X-ray sources identified as broad line AGN seem to have spectra apparently flatter than $\alpha_{\rm E} = 0.4$.

Please note that two broad line AGN, which are clearly separated from the majority of the other broad line AGN, seem to be characterized by an extremely hard spectrum ($\alpha_{\rm E} \sim -1$). These two objects, belonging both to the BSS and HBSS samples, are XBS J091828.4+513931 ($HR2 = 0.31$) and XBS J143835.1+642928 ($HR2 = 0.18$). For the first object the optical spectra show broad H_β and H_α emission lines without any obvious sign of peculiarity, while in the case of XBS J143835.1+642928 the optical spectrum in hand is very noisy and therefore the optical classification is at the moment tentative. The X-ray spectra of both sources are described by an absorbed power-law model having an intrinsic $N_{\rm H}$ in excess of 10^{22} cm^{-2}. At the moment these two sources are the only broad line AGN displaying intrinsic absorption (as derived from a complete X-ray spectral analysis) above 10^{22} cm^{-2} but the completion of the X-ray spectral work for the total sample is needed to evaluate correctly the fraction of X-ray absorbed broad line AGN in this survey[12].

It is now worth comparing the *HR*2 properties of the extragalactic BSS and HBSS sources; in Fig. 4 (panel c and d) we plot *HR*2 as a function of the 4.5−7.5 keV count rate for the extragalactic (and unidentified) sources of the HBSS sample. As a class, the type 1 AGN in the HBSS sample seem to have the same *HR*2, and thus 0.5−4.5 keV spectral properties, of the type 1 AGN in the BSS; about 87% of them reside in the *HR*2 range between −0.75 and −0.35, with a median *HR*2 value of −0.53. On the contrary the type 2 AGN in the HBSS seem to be characterized by more extreme spectral properties if compared with the type 2 AGN in the BSS sample; ∼81% of them seem to have an energy spectral index flatter than 0.4 and ∼2/3 seem to have inverted spectra ($\alpha_{\rm E} < 0$). It is worth noting that 2 of the 3 type 2 AGNs having *HR*2 around ∼−0.55 in the HBSS sample are Seyfert 1.9 galaxies.

The *HR*2 statistic for some relevant BSS and HBSS subsample(s) have been summarized in Table 7.

We note that in the case of the extragalactic population in the BSS sample the use of the weighted average, the unweighted average or the median value of *HR*2 give consistent results on the underlying spectral index ($\alpha_{\rm E} \sim 0.74$, $\alpha_{\rm E} \sim 0.83$ and $\alpha_{\rm E} \sim 0.91$, respectively). On the contrary in the case of

[12] We note that in the HBS28 sample discussed in Caccianiga et al. (2004) none of the 19 type 1 AGN is absorbed with $N_{\rm H}$ in excess to 10^{22} cm^{-2}, implying that the fraction of X-ray absorbed type 1 AGN is less than 10% of the total type 1 AGN population. This result is also confirmed by the present HBSS sample since at most 4 (out of 39) broad line AGN are characterized by *HR*2 values typical of absorbed ($N_{\rm H} > 10^{22}$ cm^{-2}) AGN. See also Sect. 3.4.

the extragalactic population in the HBSS sample the use of the weighted average, the unweighted average or the median value of *HR*2 gives completely different results ($\alpha_{\rm E} \sim -0.27$, $\alpha_{\rm E} \sim 0.11$ and $\alpha_{\rm E} \sim 0.64$, respectively). Since the *HR*2 distribution of the extragalactic population in the HBSS sample is significantly different from a Gaussian we prefer to use as "average" spectral index of this sample that related to the median value ($\alpha_{\rm E} \sim 0.64$).

A similar result has been pointed out by Nandra et al. (2003) studying the spectral properties of the sources in the SHEEP (5−10 keV) survey. These authors prefer the use of the unweighted average over the weighted average (they did not consider median values) and reach the result that $\langle\alpha_{\rm E}\rangle \sim 0$ and the conclusion that the 5−10 keV surveys are sampling a completely different population compared with the 2−10 keV surveys. On the contrary we find strong evidence that the 0.5−4.5 spectral properties of the class of broad line AGN in the BSS and in the HBSS are very similar. Moreover, since the majority of the objects in the BSS and HBSS samples are in common we do not find compelling evidence that the surveys in the two bands are selecting completely different populations. The HBSS survey is simply more efficient than the BSS survey in selecting the hard part of the intrinsic source spectral distribution.

The eleven objects belonging only to the HBSS sample (enclosed inside empty squares in Figs. 4–6) are amongst the hardest X-ray sources in the sample; all but one (XBS J140113.4+024016, still optically unidentified) of them seem to be characterized by an apparently inverted spectrum ($\alpha_{\rm E} < 0.0$). Among these sources there are 5 type 2 AGN, one optically normal galaxy, one BLLac object and 4 unidentified objects.

3.4. Broad-band X-ray spectral properties

Combining the information on *HR*2 and *HR*3 we can now investigate in more detail the broad band spectral properties of the sample(s) as well as the selection function(s) of the BSS and HBSS.

The comparison is made in Fig. 5 where we show the position of the BSS (panels a, b and c) and HBSS (panel d) sources in the *HR*2 – *HR*3 plane. We have used different symbols and panels to mark the spectroscopically identified and unidentified objects. Useful information can be extracted by cross-comparing the position of the different optical types of sources as well as by comparing the position of the sources in the BSS and HBSS samples.

The "bulk" of the sources optically identified as broad line AGNs are strongly clustered in the region between *HR*2 = −0.75 and *HR*2 = −0.35; this is true both for the broad line AGNs belonging to the BSS sample and for those belonging to the HBSS sample (only 5 of 39 HBSS broad line AGN are outside these limits). The spread on *HR*3 is much larger than the spread on *HR*2 but note that *HR*3 is much noisier than *HR*2 since many of the sources are detected with poor statistics (or even undetected) in the 4.5−7.5 keV energy band.

All but 2 (∼96%) of the sources classified as stars[13] in the BSS sample have an *HR*2 less than −0.75. If we assume a simple Raymond-Smith thermal model, *HR*2 ≤ −0.75 corresponds to temperatures below ∼1.5 keV, in very good agreement with the identification as coronal emitting stars.

In Caccianiga et al. (2004), using a "pilot" 4.5−7.5 keV sample composed of 28 X-ray sources (26 of which in common with the current version of the HBSS sample reported in Table 4), we have already discussed the correlation between X-ray absorption, as deduced from a complete X-ray spectral analysis, and "Hardness Ratio" properties. In particular we have found that a) at the sampled fluxes, the 4.5−7.5 keV selection is picking up AGN having an intrinsic $N_{\rm H}$ up to few times 10^{23} cm^{-2}; b) all the AGN having *HR*2 > −0.35 are X-ray absorbed with $N_{\rm H}$ ranging from few times 10^{21} up to few times 10^{23} cm^{-2}. Assuming that this result is valid also for the sources presented here we can conjecture that all the sources having *HR*2 greater than −0.35 are absorbed AGN; in this part of the diagram, besides narrow line AGN, we also note a few broad line AGN and 2 sources (one in the BSS sample and one in the HBSS sample) optically identified as normal galaxies. However also in these sources their point-like X-ray emission, their X-ray spectra (a preliminary spectral analysis shows that they are described by an absorbed power-law model having $N_{\rm H} >\sim 10^{22}$ cm^{-2}) and their intrinsic luminosity (in excess of $\sim 7 \times 10^{43}$ erg s^{-1} in the 2−10 keV energy range) strongly suggest the presence of an AGN. The existence of relatively luminous X-ray sources, optically identified with "normal galaxies", has been reported since the *Einstein* Observatory era in the early eighties (Elvis et al. 1981); this kind of sources were called in a variety of names such as optically dull galaxies (Elvis et al. 1981), passive galaxies (Griffiths et al. 1995) and X-ray bright optically normal galaxies (XBONG, Comastri et al. 2002). We have already discussed in Severgnini et al. (2003) that detailed and specific optical-infrared follow-ups or higher-quality optical spectra are needed to unveil the AGN also in the optical domain. An advection-dominated accretion flow model has been recently used by Yuan & Narayan (2004) to explain their broad band properties.

Contrary to broad line AGNs and stars, narrow line (type 2) AGNs seem to be distributed over a larger area in the *HR*2 – *HR*3 plane with a well visible difference in the source position between the type 2 AGNs in BSS and those in the HBSS sample. Although many of them have the hardest spectra amongst the identified objects, highly suggestive of intrinsic absorption (see also Fig. 4), a new fact which seems to emerge from this investigation is the large number of narrow line AGN in the BSS sample occupying the locus typical of X-ray unabsorbed broad line AGN. Taking into account the still

[13] The two sources that are outside the "stellar" *HR*2 locus are XBS J014100.6−675328 and XBS J215323.7+173018. The first object, XBS J014100.6−675328, has been already discussed in footnote 9. The XMM spectrum, discussed in Caccianiga et al. (2004), is well fitted by a unabsorbed power-law model with $\Gamma \sim 1.53$ plus a thermal component having a temperature $kT \sim 55$ eV and an emission line at $E \sim 6.7$ keV. The second object (XBS J215323.7+173018) is a star having an XMM spectrum described by a thermal component with $kT \sim 1.6$ keV and a possible hard tail.

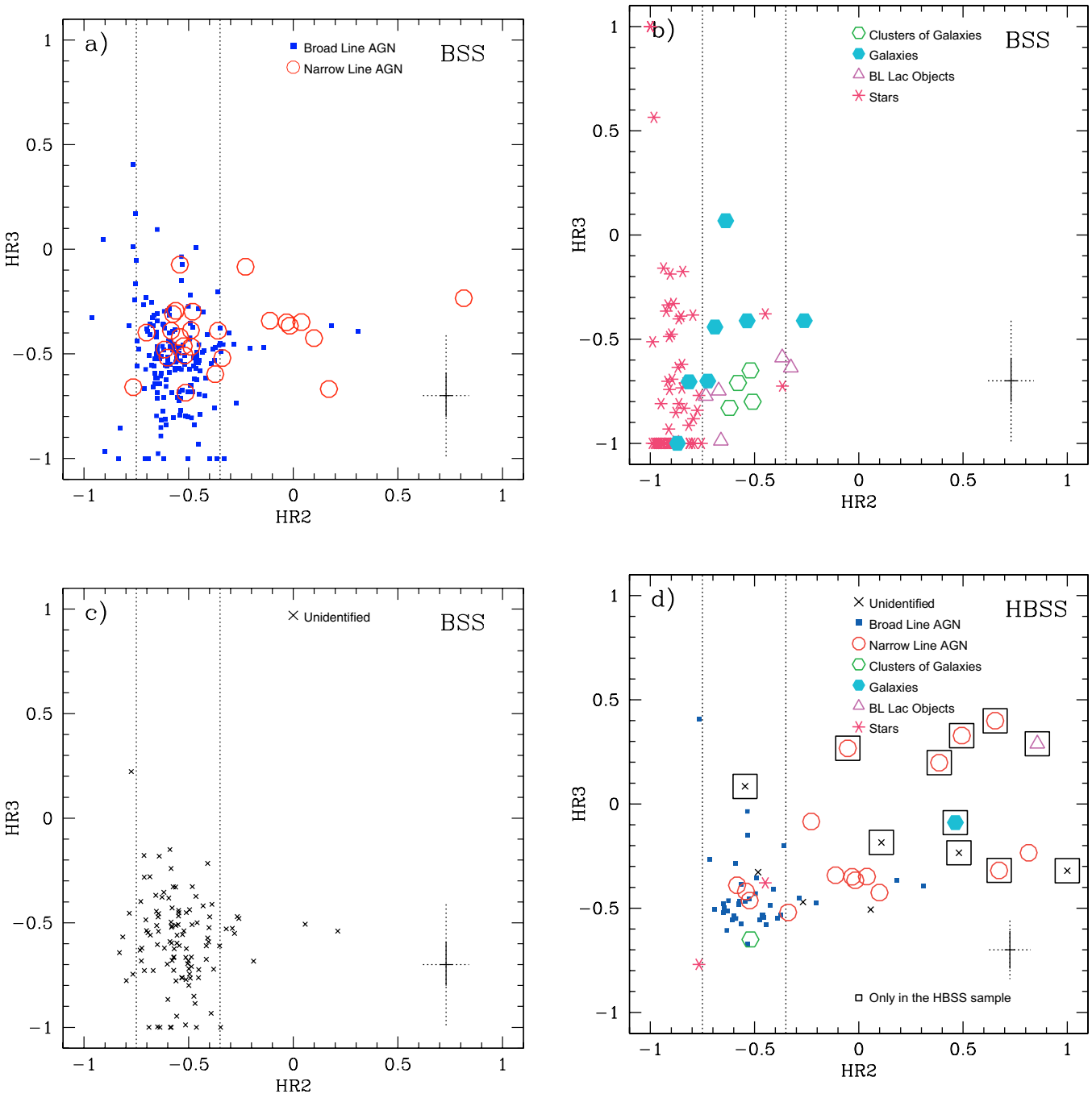

Fig. 5. *HR*2 vs. *HR*3 for the sources belonging to the BSS sample (panel **a)**, **b)** and **c)**) and to the HBSS sample (panel **d)**). The dotted lines at constant *HR*2 correspond to the locus enclosing ~90% of the type 1 AGN in the BSS sample; these lines have been reported in all panels to assist with the comparison(s). We have used different symbols to mark the spectroscopically identified and unidentified objects in the two samples. The eleven sources belonging only to the HBSS sample are enclosed inside empty squares in panel **d)**. In the lower right corner of each panel we have also reported the median error on *HR*2 and *HR*3 for the total BSS and HBSS sample (solid line) and the 90% percentile on these errors (dotted line).

incomplete spectroscopic identification work and that some sources need a better quality optical spectrum we estimate that the relative fraction of these objects over the entire type 2 AGN population may range between 50% and 75% in the case of the BSS sample and around 20% in the case of the HBSS sample[14]. It is also worth noting that 2 out of 4 of the type 2 AGN belonging to the (2−10 keV) HELLAS2XMM survey and having a good X-ray statistic (sample S1 in Perola et al. 2004) are characterized by an "observed" intrinsic $N_{\rm H}$ well below 10^{22} cm^{-2}.

To our knowledge two kinds of narrow line AGN could populate this zone, and thus could have X-ray spectral

[14] This latter estimate is consistent with the fact that in the HBS28 sample discussed in Caccianiga et al. (2004) there is only one type 2 AGN with *HR*2 between −0.75 and −0.35 out of 8 type 2 objects.

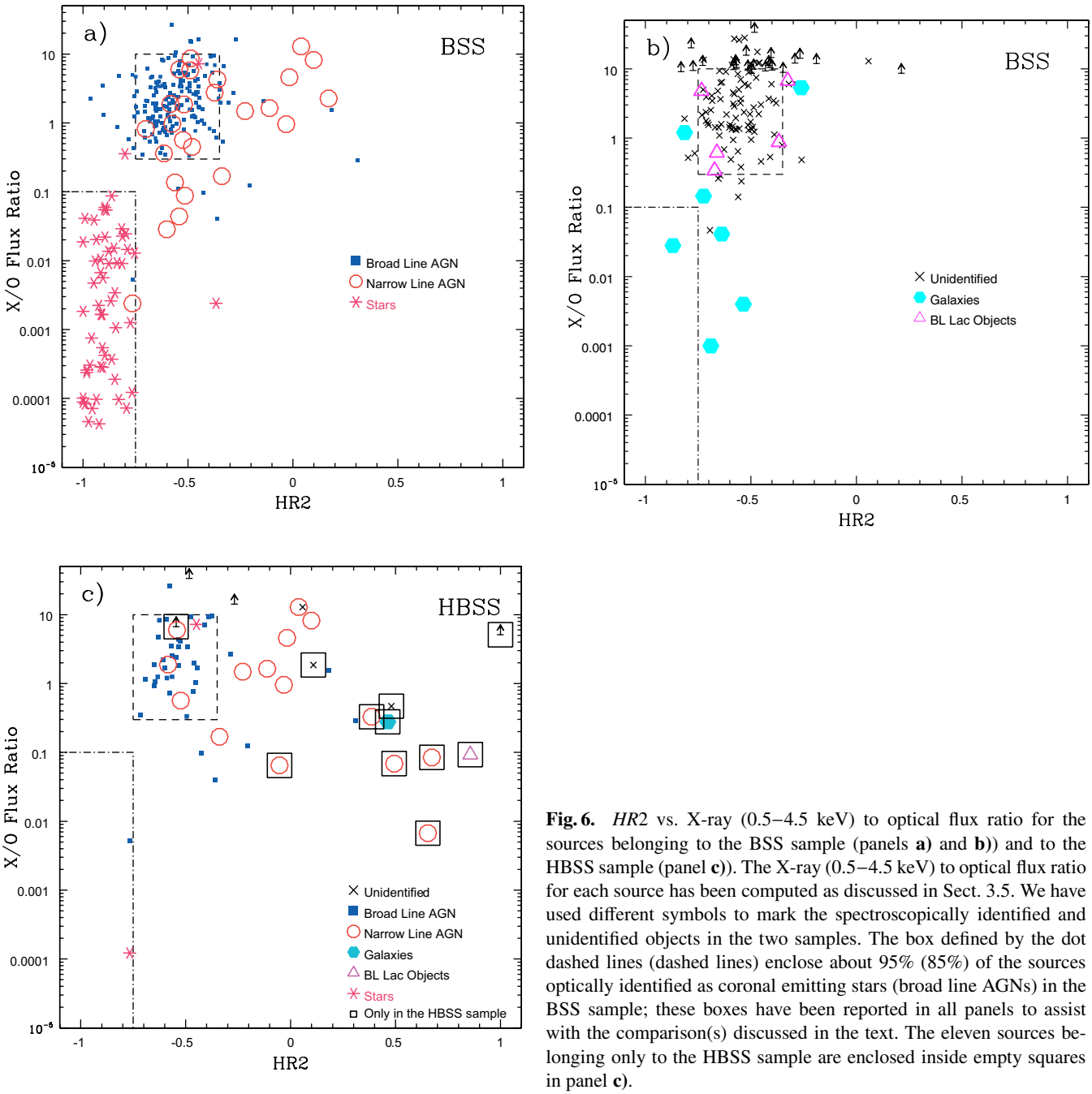

Fig. 6. *HR*2 vs. X-ray (0.5−4.5 keV) to optical flux ratio for the sources belonging to the BSS sample (panels **a)** and **b)**) and to the HBSS sample (panel **c)**). The X-ray (0.5−4.5 keV) to optical flux ratio for each source has been computed as discussed in Sect. 3.5. We have used different symbols to mark the spectroscopically identified and unidentified objects in the two samples. The box defined by the dot dashed lines (dashed lines) enclose about 95% (85%) of the sources optically identified as coronal emitting stars (broad line AGNs) in the BSS sample; these boxes have been reported in all panels to assist with the comparison(s) discussed in the text. The eleven sources belonging only to the HBSS sample are enclosed inside empty squares in panel **c)**.

properties similar to those expected from unabsorbed AGN: a) "Compton thick" absorbed AGN (see e.g. the results presented in Della Ceca et al. 1999 from ASCA data); b) objects similar to the class of unabsorbed Seyfert 2 discussed in Pappa et al. (2001); Panessa & Bassani (2002) and in Barcons et al. (2003). Also the variability could play some role if the nucleus was bright at the time of the XMM-Newton observation but was turned off at the time of the optical spectroscopy. A detailed and exhaustive analysis of these sources is beyond the scope of the present paper. A deeper investigation of their optical (e.g. finer optical classification between Seyfert 1.8, Seyfert 1.9 and Seyfert 2, analysis of the O[III] to 2−10 keV flux ratio) and X-ray (e.g. presence of Fe K_α emission lines to evaluate the Compton-thickness of the source) properties, as well as an assessment of the role played by selection effects, is in progress and will be presented elsewhere.

3.5. X-ray to optical flux ratio

A useful parameter to discriminate between different classes of X-ray sources is the X-ray to optical flux ratio (X/O flux ratio hereafter; see Maccacaro et al. 1988).

Previous investigations (see Fiore et al. 2003, and references therein) have shown that standard X-ray selected AGN (both type 1 and type 2) have typical X/O flux ratios in the range between 0.1 and 10 (for comparison standard optically selected QSOs and Seyfert 1 galaxies have X/O flux ratio ∼ 1). X/O flux ratios below 0.1 are typical of coronal

emitting stars, normal galaxies (both early type and star-forming) and nearby heavily absorbed (Compton thick) AGN. Finally at high X/O flux ratios (well above 10) we can find broad and narrow line AGN as well as high-z high-luminosity obscured AGN (type 2 QSOs), high-z clusters of galaxies and extreme BL Lac objects.

In this paper we have defined the X-ray to optical flux ratio using the observed X-ray flux in the 0.5−4.5 keV energy range and the optical red-band flux (see Fukugita et al. 1995 for the appropriate conversion factors). For the large majority (73%) of the objects we have found and used APM red magnitudes. For 19% of the objects red magnitudes have been found from the literature, measured by us during spectroscopic runs or estimated using magnitudes measured in other optical bands. Finally for the unidentified objects with optical magnitudes below the POSS II limit (30 sources) we have used an upper limit of $\mathrm{mag}_R \simeq 21.0$. We note here that, for a fixed X-ray flux, an error of ∼1 magnitude corresponds to an uncertainty of ∼60% on the X/O flux ratio; this uncertainty does not affect any of the general conclusions we discuss below.

In Fig. 6 we have plotted the X/O flux ratio versus the *HR*2 value for each source (BSS sample in panels a and b; HBSS sample in panel c). The boxes defined by the dot dashed lines (dashed line) indicate the locus of coronal emitting stars (broad line AGN) in the BSS sample and have been reported in all panels to assist with the comparisons.

As is clearly visible in Fig. 6 the bulk of coronal emitting stars is well separated from the bulk of extragalactic sources; some of the AGN (both broad and narrow line) have X/O flux ratio typical of stars but *HR*2 values typical of AGN; similarly some AGN with an *HR*2 typical of stars can be distinguished from stars thanks to their X/O flux ratio. Therefore the combined use of X/O flux ratio and *HR*2 allows us to distinguish almost unequivocally galactic sources from the extragalactic ones.

Around 10% of the extragalactic population have a X/O flux ratio greater than 10. If we consider the 2−10 keV fluxes instead of the 0.5−4.5 keV fluxes this fraction increases to ∼15%, in good agreement with the results obtained by Fiore et al. (2003) at fainter fluxes. Amongst the sources identified so far at X/O flux ratio > 10 there are some broad line and a few narrow line AGN. These results are consistent with those reported in Fiore et al. (2003) who also discuss the observational evidence that at X/O flux ratio greater than 10 is where to look for type 2 QSOs. Since the large majority of the X-ray sources at X/O flux ratio > 10 presented here is still unidentified we can not comment further on this; we can only note that many of the unidentified objects with high or very high X/O flux ratio seem to have rather standard hardness ratios.

The opposite side of the extragalactic X/O distribution (X/O flux ratio < 0.1) is populated by optically normal galaxies, type 2 AGNs and a few broad line AGN. As discussed above this part of the X/O distribution could be also populated by nearby Compton thick AGN; in this respect it is worth noting that a few of the type 2 AGN in the BSS sample populating the same *HR*2 region of the broad line AGN population have X/O flux ratios < 0.1. In the HBS sample there are also a few type 2 AGN having apparently hard spectra but low X/O flux ratios (<0.1).

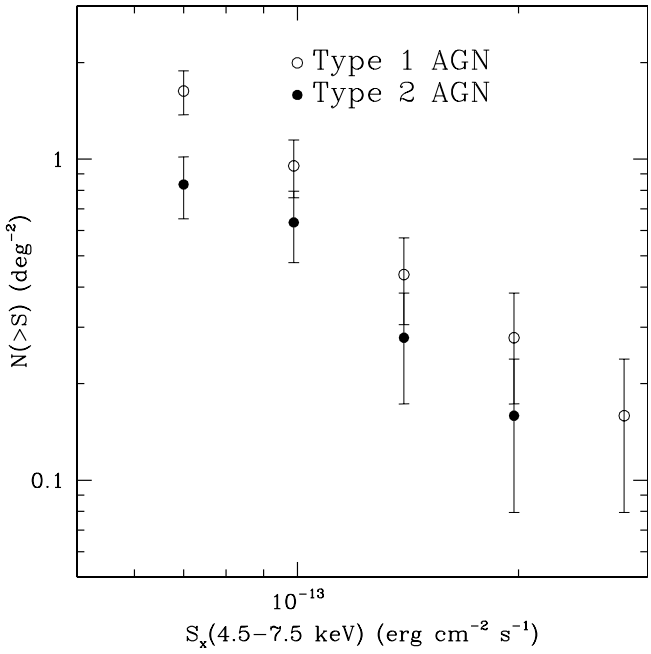

Fig. 7. The number-flux relationship in the 4.5−7.5 keV energy band for optically type 1 (open circles) and type 2 (filled circles) AGN obtained using the sources in the HBSS sample.

3.6. The number densities of optically broad and narrow line AGN

The measured X-ray $\mathrm{Log}\,(N > S) - \mathrm{Log}\,S$ of broad and narrow line AGN is a fundamental observable for cosmological investigations and, in particular, provides very strong constraints on the CXB synthesis models and on the history of the accretion in the Universe.

As discussed above the spectroscopic identification rate of the HBSS sample is ∼90%, allowing us to investigate for the first time the X-ray $\mathrm{Log}\,(N > S) - \mathrm{Log}\,S$ of optically broad and narrow line AGN in the same sample. In order to deal with the 7 unidentified HBSS sources we have made the reasonable assumption that the 5 unidentified sources having $HR2 > -0.35$ are type 2 AGN, while the 2 unidentified sources having *HR*2 in the range from −0.75 to −0.35 are type 1 AGN (see Sect. 3.3 for details).

The 4.5−7.5 keV $\mathrm{Log}\,(N > S) - \mathrm{Log}\,S$ of optically broad and narrow line AGN are reported in Fig. 7 (AGN1: open circles; AGN2: filled circles). A conversion factor appropriate for a power-law spectral model with $\alpha_{\mathrm{E}} \simeq 0.7$ has been used to obtain the fluxes. Both $\mathrm{Log}\,N(>S) - \mathrm{Log}\,S$ can be well described by a power-law model and their maximum likelihood best fit parameters have been reported in Table 5.

At the 4.5−7.5 keV flux limit of $f_x \geq \sim 7 \times 10^{-14}$ erg cm^{-2} the surface densities of optically type 1 AGN and type 2 AGN are 1.63 ± 0.25 deg^{-2} and 0.83 ± 0.18 deg^{-2}, respectively. Optically type 2 AGN represent 34 ± 9% of the AGN population shining in the 4.5−7.5 keV energy selection band at the

Table 8. Optically type 2 AGN fraction in few representative X-ray surveys.

Sample	Energy range	Flux range	Type 2 fraction	Ref./Note
(1)	(2)	(3)	(4)	(5)
ROSAT Bright Survey	0.5–2.0	$>\sim 2\times10^{-12}$	$1\pm0.5\%$	(a)
XMM BSS	0.5–4.5	$>7\times10^{-14}$	$13\pm4\%$	(b)
XMM HBSS	4.5–7.5	$>7\times10^{-14}$	$34\pm9\%$	(c)
HELLAS2XMM + Other Surveys	2–10	$10^{-15}-10^{-14}$	$57\pm12\%$	(d)
HELLAS2XMM + Other Surveys	2–10	$10^{-14}-10^{-13}$	$37\pm6\%$	(e)

Columns are as follows: (1) Sample; (2) Energy Selection Band; (3) Investigated flux range; (4) Optically type 2 AGN fraction over the total AGN density in the specific survey; (5) References and Note as follows: (a) From Schwope et al. (2000); (b) From this paper using the BSS sources with Right Ascension below 5^h or above 17^h. For this BSS subsample the spectroscopic identification rate is around 88%; (c) From this paper using the HBSS sample and taking into account the small number of sources still unidentified as discussed in Sect. 3.6; (d) Fraction of optically obscured AGN from Fiore et al. (2003). The spectroscopic ID rate of the sample in this flux range is ∼50%; (e) Fraction of optically obscured AGN from Fiore et al. (2003). The spectroscopic ID rate of the sample in this flux range is ∼81%.

flux limit of the HBSS. In Table 8 we compare the optically type 2 AGN fraction from the HBSS sample with that found in a few representative X-ray surveys. As expected from the CXB synthesis models the fraction of optically type 2 AGN decreases going to softer X-ray surveys (e.g. by a factor ∼2.6 in the XMM BSS survey and by a factor ∼34 in the ROSAT Bright Survey) while remaining almost constant (around 35%) for surveys above 2 keV down to a flux limit of 10^{-14} erg cm^{-2} s^{-1}. In the flux range between 10^{-15} and 10^{-14} erg cm^{-2} s^{-1} there is apparently an increase of the fraction of optically type 2 AGN but the spectroscopic identification rate in this flux range is still low (∼50%) preventing us from speculating further.

The optically type 2 AGN fraction from the HBSS sample is also in very good agreement with the fraction of X-ray absorbed ($N_{\rm H} > 10^{22}$ cm^{-2}) AGN found from several studies (e.g. Piconcelli et al. 2003; Perola et al. 2004) which ranges between 25% to 40% for hard X-ray fluxes spanning four orders of magnitude, from 10^{-10} to 10^{-14} erg cm^{-2} s^{-1}. While we anticipate that the "Modified Unification Scheme" for the synthesis of the CXB (Ueda et al. 2003) predicts a fraction of absorbed AGN around 41% for the fluxes (and energy band) covered by the HBSS, a proper comparison will have to wait for the completion of the X-ray spectroscopic work.

4. Summary and conclusions

In this paper we have discussed the scientific goals and the strategy of the "The XMM-Newton Bright Serendipitous Survey". This survey comprises two flux-limited samples: the BSS sample and the HBSS sample having a flux limit of $\sim7\times10^{-14}$ erg cm^{-2} in the 0.5−4.5 keV and 4.5−7.5 keV energy band, respectively.

From the analysis of 237 suitable XMM-Newton fields (211 for the HBSS), covering a useful survey area of 28.10 (25.17 for the HBSS) sq. deg of sky, we have defined (and presented here) a sample of 400 X-ray sources: 389 of them belong to the BSS, 67 to the HBSS with 56 X-ray sources in common. Up to now ∼71% (∼90%) of the sources in the BSS (HBSS) sample have been spectroscopically identified, either from the literature or from our spectroscopic observations. The main results from this study can be so summarized:

a) the extragalactic number-flux relationship in the 0.5−4.5 keV and 4.5−7.5 keV band are in good agreement with previous and new results. They are well described by a power law model, $N(>S) \propto S^{-\alpha}$, with best fit value for the slope α of 1.80 ± 0.11 and 1.64 ± 0.24 in the 0.5−4.5 keV and 4.5−7.5 keV bands, respectively;
b) at the X-ray flux limits of the survey presented here we found that the optical counterpart in the majority (∼90%) of cases has an optical magnitude brighter than the POSS II limit ($R \sim 21^{\rm mag}$). Galactic counterparts represent about 14% of the sources in the BSS sample and less than 3% of the sources in the HBSS sample. The majority of the extragalactic objects identified so far are broad line AGN both in the BSS (∼80%) and in the HBSS (∼60%);
c) we have investigated the broad-band spectral properties of the selected sources using hardness ratios. No obvious trend of the source spectra as a function of the count rate is measured. The average spectrum of the "extragalactic" population corresponds to a (0.5−4.5 keV) energy spectral index of ∼0.8 for the BSS sample and ∼0.64 for the HBSS sample. About 13% (40%) of the sources in the BSS (HBSS) sample seem to be described by an energy spectral index flatter than that of the CXB; following the results presented in Caccianiga et al. (2004) we speculate that these sources are absorbed AGN with $N_{\rm H}$ ranging from few times 10^{21} up to few times 10^{23} cm^{-2}. There are hints from this study of a significant number of narrow line AGN in the BSS sample occupying the locus typical of X-ray unabsorbed broad line AGN. A deeper investigation of their optical and X-ray properties, of the source selection function, as well as a complete X-ray spectral analysis for all the BSS and HBSS sources using data from all the EPIC instruments (a major goal of this project) is in progress and will be presented elsewhere;
d) we do not find a compelling evidence that the HBSS 4.5−7.5 keV survey is sampling a completely

different source population compared with the BSS 0.5−4.5 keV survey. Rather we find that the HBSS survey is simply picking up a larger fraction of absorbed AGN, consistent with CXB synthesis models based on the unification scheme of the AGN;

e) at the flux limit of the HBSS sample we measure surface densities of optically classified type 1 and type 2 AGN of 1.63 ± 0.25 deg^{-2} and 0.83 ± 0.18 deg^{-2}, respectively. The AGN optically classified as type 2 represent (34 ± 9)% of the total AGN population shining in the 4.5−7.5 keV energy band at the sampled fluxes. A proper comparison with X-ray absorbed/unabsorbed AGN have to wait for the completion of the ongoing X-ray spectroscopic work.

f) finally, we found a clear separation between Galactic "coronal emitting" stars and extragalactic sources in the hardness ratio diagram and in the (hardness ratio) vs. (X/O flux ratio) diagram. Since the investigated sample is a fair representation of the high Galactic latitude X-ray sky, this result will help with the selection of defined classes of sources from the XMM-Newton catalogue prior to spectroscopic observations making the existing and incoming XMM-Newton catalogs an unique resource for astrophysical studies.

Acknowledgements. This research has made use of the NASA/IPAC Extragalactic Database (NED; which is operated by the Jet Propulsion Laboratory, California Institute of Technology, under contract with the National Aeronautics and Space Administration) and of the SIMBAD database (operated at CDS, Strasbourg, France). We thank Piero Rosati for providing us some IDL routines used in the data analysis and preparation. We thank L. Maraschi, G. Trinchieri, A. Wolter, D. Worrall, N. Webb and the referee for a careful reading of the paper and for useful comments which have improved the paper. We thank Y. Ueda for having provided us with the predictions from the Modified Unification Model in tabular form. R.D.C., T.M., A.C., P.S., V.B. acknowledge partial financial support by the Italian Space Agency (ASI grants: I/R/037/01, I/R/062/02 and I/R/071/02), by the MIUR (Cofin-03-02-23) and INAF. X.B. and F.J.C. acknowledge financial support from the Spanish Ministerio de Ciencia y Tecnología, under the project ESP2003-00812. Based on observations collected at the Italian "Telescopio Nazionale Galileo" (TNG), at the German-Spanish Astronomical Center, Calar Alto (operated jointly by Max-Planck Institut für Astronomie and Instututo de Astrofisica de Andalucia, CSIC), at the European Southern Observatory (ESO) and at the Nordic Optical Telescope (NOT). We would like to thank the staff members of the TNG, ESO, Calar Alto and NOT for their support during the observations. The TNG and NOT telescopes are operated in the island of La Palma by the Nordic Optical Telescope Scientific Association and the Centro Galileo Galilei of the INAF, respectively, in the Spanish Observatorio del Roque de los Muchachos of the Instituto de Astrofísica de Canarias. We finally thank the APM team for maintaining this facility.

References

Alexander, D. M., Bauer, F. E., Brandt, W. N., et al. 2003, AJ, 126, 539
Baldi, A., Molendi, S., Comastri, A., et al. 2002, ApJ, 564, 190
Barcons, X., Carrera, F. J., & Ceballos, M. T. 2003, MNRAS, 339, 757
Barcons, X., Carrera, F. J., Watson, M. G., et al. 2002, A&A, 382, 522
Brandt, W. N., Alexander, D. M., Hornschemeier, A. E., et al. 2001, AJ, 122, 2810
Brandt, W. N., Alexander, D. M., Bauer, F. E., & Vignali, C. 2004, in Physics of Active Galactic Nuclei at All Scales, ed. D. Alloin, R. Johnson, & P. Lira (Berlin: Springer-Verlag) [arXiv:astro-ph/0403646]
Caccianiga, A., Severgnini, P., Braito, V., et al. 2004, A&A, 416, 901
Comastri, A., Setti, G., Zamorani, G., & Hasinger, G. 1995, A&A, 296, 1
Comastri, A., Fiore, F., Vignali, C., et al. 2001, MNRAS, 327, 781
Comastri, A., Mignoli, M., Ciliegi, P., et al. 2002, ApJ, 571, 771
Della Ceca, R., Castelli, G., Braito, V., Cagnoni, I., & Maccacaro, T. 1999, ApJ, 524, 674
Dickey, J. M., & Lockman, F. J. 1990, ARA&A, 28, 215
Ehle, M., Breitfellner, M., Gonzales Riestra, R., et al. 2003, XMM-Newton Users' Handbook, Issue 2.1
Elvis, M., Schreier, E. J., Tonry, J., Davis, M., & Huchra, J. P. 1981, ApJ, 246, 20
Fiore, F., Giommi, P., Vignali, C., et al. 2001, MNRAS, 327, 771
Fiore, F., Brusa, M., Cocchia, F., et al. 2003, A&A, 409, 79
Fukugita, M., Shimasaku, K., & Ichikawa, T. 1995, PASP, 107, 945
Galbiati, E., Caccianiga, A., Maccacaro, T., et al. 2004, A&A, in press
Georgantopoulos, I., Georgakakis, A., Akylas, A., et al. 2004, MNRAS, 352, 91
Gilli, R., Salvati, M., & Hasinger, G. 2001, A&A, 366, 407
Gioia, I. M., Maccacaro, T., Schild, R. E., et al. 1990, ApJS, 72, 567
Griffiths, R. E., Georgantopoulos, I., Boyle, B. J., et al. 1995, MNRAS, 275, 77
Hasinger, G., Burg, R., Giacconi, R., et al. 1993, A&A, 275, 1
Hasinger, G., Burg, R., Giacconi, R., et al. 1998, A&A, 329, 482
Hasinger, G., Altieri, B., Arnaud, M., et al. 2001, A&A, 365, L45
Landt, H., Padovani, P., & Giommi, P. 2002, MNRAS, 336, 945
Maccacaro, T., Gioia, I. M., Zamorani, G., et al. 1982, ApJ, 253, 504
Maccacaro, T., Gioia, I. M., Wolter, A., Zamorani, G., & Stocke, J. T. 1988, ApJ, 326, 680
Madau, P., Ghisellini, G., & Fabian, A. C. 1994, MNRAS, 270, 17
Mainieri, V., Bergeron, J., Hasinger, et al. 2002, A&A, 393, 425
Moretti, A., Campana, S., Lazzati, D., & Tagliaferri, G. 2003, ApJ, 588, 696
Nandra, K., Georgantopoulos, I., Ptak, A., & Turner, T. J. 2003, ApJ, 582, 615
Panessa, F., & Bassani, L. 2002, A&A, 394, 435
Pappa, A., Georgantopoulos, I., Stewart, G. C., & Zezas, A. L. 2001, MNRAS, 326, 995
Perola, G. C., Puccetti, S., Fiore, F., et al. 2004, A&A, 421, 491
Piconcelli, E., Cappi, M., Bassani, L., Di Cocco, G., & Dadina, M. 2003, A&A, 412, 689
Piconcelli, E., Cappi, M., Bassani, L., et al. 2002, A&A, 394, 835
Rosati, P., Tozzi, P., Giacconi, R., et al. 2002, ApJ, 566, 667
Schwope, A., Hasinger, G., Lehmann, I., et al. 2000, Astron. Nachr., 321, 1
Severgnini, P., Caccianiga, A., Braito, et al. 2003, A&A, 406, 483
Setti, G., & Woltjer, L. 1989, A&A, 224, 21
Ueda, Y., Akiyama, M., Ohta, K., & Miyaji, T. 2003, ApJ, 598, 886
Véron-Cetty, M.-P., & Véron, P. 2001, A&A, 374, 92
Yuan, F., & Narayan, R. 2004, ApJ, 612, 724

Online Material

Table 2. Basic information on the XMM-Newton MOS2 fields used for the sample selection.

Obs. ID	Filter	RA; Dec (J2000)	Exposure	Log Nh	$R_{\rm in}$	$R_{\rm out}$	BSS	HBSS
			s	$\rm cm^{-2}$	arcmin	arcmin	srcs	srcs
(1)	(2)	(3)	(4)	(5)	(6)	(7)	(8)	(9)
0125310101	Medium	00 00 30.4 −25 06 43.4	19 162.6	20.27	1	13	4	0
0101040101	Medium	00 06 19.7 +20 12 22.8	34 044.7	20.60	8	13	1	0
0127110201	Thin1	00 10 31.2 +10 58 40.7	7558.0	20.76	2	13	2	0
0111000101	Medium	00 18 33.0 +16 26 08.0	31 362.1	20.61	3	13	2	0
0001930101	Thin1	00 26 06.8 +10 41 12.5	18 032.3	20.71	1	13	1	1
0050140201	Thin1	00 26 35.9 +17 09 37.8	50 380.4	20.63	3	13	2	0
0112320101	Thin1	00 30 27.6 +04 51 47.4	24 577.8	20.48	1	13	1	0
0065770101	Medium	00 32 47.0 +39 34 33.3	7360.0	20.82	1	13	1	0
0125920201	Thin1	00 33 54.5 −12 07 10.8	9709.9	20.40	1	13	3	0
0125320701*	Thin1	00 50 03.0 −52 07 36.7	16 524.9	20.51	1	13	3	–
0110890401	Medium	00 57 20.0 −22 23 04.1	29 741.8	20.19	8	13	0	0
0111280301	Thin1	00 58 51.3 −27 35 47.1	7975.6	20.28	0	12	1	0
0112650401	Medium	01 04 24.0 −06 24 10.6	23 695.9	20.71	0	13	1	0
0103861601	Thick	01 05 16.4 −58 26 10.4	7127.1	20.44	8	13	1	0
0025540101	Medium	01 07 46.5 −17 30 14.0	7678.2	20.18	2	13	2	0
0113040801*	Thin1	01 20 39.7 −10 56 24.5	5692.0	20.51	1	13	4	–
0101040201	Medium	01 23 46.0 −58 48 25.8	28 994.1	20.50	8	13	0	0
0109860101	Thin1	01 25 33.4 +01 45 38.2	38 533.6	20.49	4	13	2	0
0112600601*	Medium	01 27 32.1 +19 10 32.3	3994.2	20.68	8	13	3	–
0084230301	Medium	01 31 53.7 −13 36 56.4	20 446.4	20.21	8	13	1	1
0112630201	Thin1	01 33 01.9 −40 06 23.5	31 094.2	20.28	1	13	1	0
0111430101	Medium	01 39 01.2 −17 57 06.3	33 440.3	20.16	8	13	1	0
0032140401	Medium	01 40 12.1 −67 48 40.3	7610.7	20.40	0	13	4	2
0093641001	Medium	01 43 01.7 +13 38 24.4	9329.1	20.69	4	13	2	0
0101640201	Medium	01 59 50.2 +00 23 46.8	7543.3	20.41	8	13	3	1
0084140101	Medium	02 08 38.2 +35 23 00.2	38 001.6	20.80	2	13	3	0
0112371701	Thin1	02 17 12.4 −04 39 04.2	20 001.1	20.38	0	11	2	1
0112371001	Thin1	02 18 00.3 −04 59 47.8	50 800.3	20.40	0	11	4	3
0112371501*	Thin1	02 18 48.3 −04 39 02.9	6684.2	20.40	0	11	0	–
0112370301	Thin1	02 19 36.3 −04 59 47.7	50 384.1	20.41	0	11	1	0
0111110501	Thin1	02 22 40.0 −05 09 49.0	24 185.8	20.41	0	10	0	0
0109520501	Thin1	02 23 20.0 −04 49 49.3	24 107.8	20.42	0	10	1	0
0111110401	Thin1	02 24 00.1 −05 09 53.6	28 276.2	20.42	0	10	1	0
0111110301	Thin1	02 25 20.3 −05 09 52.5	24 158.7	20.43	0	10	0	0
0111110201	Thin1	02 26 40.1 −05 09 47.1	8229.8	20.42	0	10	1	0
0111110101	Thin1	02 27 60.0 −05 09 48.4	23 809.9	20.42	0	10	0	0
0103861101	Medium	02 35 12.8 −29 36 09.9	7409.2	20.25	8	13	1	0
0098810101	Thin1	02 36 12.3 −52 19 55.6	23 450.3	20.52	2	13	2	1
0075940301	Medium	02 36 57.9 +24 38 53.7	47 426.5	20.96	8	13	0	0
0067190101	Medium	02 38 19.4 −52 11 34.1	25 627.4	20.50	3	10	1	0
0111200101	Medium	02 42 41.1 −00 00 53.7	35 485.0	20.55	8	13	4	0
0111490401	Medium	02 48 43.8 +31 06 59.2	31 028.6	20.97	8	13	0	0
0056020301	Thin1	02 56 32.8 +00 06 01.7	17 250.5	20.81	2	13	2	0
0041170101	Thin1	03 02 38.5 +00 07 31.9	47 275.7	20.85	0	13	2	1
0042340501	Thin1	03 07 03.8 −28 40 24.1	13 285.0	20.13	4	13	2	1
0122520201	Thick	03 11 59.3 −76 51 53.0	28 295.0	20.91	2	13	2	1
0110970101	Thin1	03 13 09.6 −55 03 48.4	10 239.4	20.41	0	13	2	1
0110970401	Thin1	03 14 15.9 −55 21 33.5	8457.5	20.42	0	8	0	0
0129320901	Thin1	03 16 03.7 −55 06 08.5	9948.2	20.43	0	13	1	0
0105660101	Medium	03 17 56.0 −44 14 15.1	23 150.7	20.41	6	13	2	1
0108060501	Thin1	03 32 29.1 −27 48 27.1	46 833.4	19.95	0	13	2	0
0099010101	Thin1	03 35 27.6 −25 44 54.5	18 776.9	20.01	8	13	3	0
0055140101	Thin1	03 39 35.0 −35 25 58.1	47 634.6	20.12	1	11	3	1
0111970301	Thin1	04 09 07.2 −71 17 43.9	18 740.3	20.88	8	13	3	3
0112600401	Medium	04 25 44.2 −57 13 34.4	7627.0	20.31	8	13	1	0
0103861701	Medium	04 35 17.1 −78 01 54.3	8010.5	20.88	8	13	1	0
0112880401	Thick	04 59 35.4 +01 47 16.0	18 914.3	20.89	2	13	2	0

Table 2. continued.

Obs. ID	Filter	RA; Dec (J2000)	Exposure	Log Nh	R_{in}	R_{out}	BSS	HBSS
			s	cm^{-2}	arcmin	arcmin	srcs	srcs
(1)	(2)	(3)	(4)	(5)	(6)	(7)	(8)	(9)
0111160201	Thin1	05 05 20.0 −28 48 57.6	47 984.4	20.17	2	13	4	1
0103860701*	Medium	05 16 21.3 −10 33 34.5	4740.3	20.97	8	13	1	–
0094400101	Medium	05 16 40.1 +79 40 16.7	31 727.2	20.90	2	13	4	0
0090050701	Thin1	05 19 49.4 −45 46 48.9	13 426.7	20.62	8	13	2	0
0085640101	Thin1	05 21 00.9 −25 21 52.6	9720.6	20.28	1	13	5	2
0050150101	Thin1	05 25 05.9 −33 43 13.3	13 440.2	20.35	1	13	2	0
0123720301*	Medium	05 28 44.1 −65 26 58.6	4762.6	20.73	8	13	0	–
0009220601	Medium	06 15 35.2 +71 02 12.2	11 376.9	20.92	2	13	1	0
0110930101	Medium	06 18 41.9 +78 21 25.7	19 578.2	20.86	5	13	0	0
0103860101	Medium	06 23 08.8 −64 36 15.8	8862.8	20.73	8	13	2	0
0029340101	Medium	06 41 18.4 +82 15 59.3	22 288.1	20.70	8	13	1	0
0061540101	Medium	06 52 11.4 +74 25 30.1	21 080.3	20.81	2	13	3	0
0112980201	Thin1	06 58 17.6 −55 57 30.6	41 042.1	20.81	8	13	2	0
0083000101	Medium	07 35 19.9 +43 44 27.3	13 589.8	20.77	2	13	0	0
0103862101*	Medium	07 42 32.8 +49 48 30.4	5909.3	20.75	8	13	1	–
0123100101	Thin1	07 44 03.3 +74 33 42.9	39 171.0	20.55	3	13	4	2
0111100301	Thin1	07 51 09.3 +18 07 43.0	32 111.2	20.61	1	13	1	0
0110070401	Thin1	07 55 05.0 +22 00 04.6	22 449.2	20.75	8	13	0	0
0094400301	Medium	08 04 34.3 +64 59 55.6	19 077.9	20.64	2	13	2	1
0094530401	Thin1	08 05 35.2 +24 49 56.7	8709.6	20.59	0	13	2	0
0092800101	Medium	08 31 42.4 +52 45 20.8	16 808.2	20.59	2	13	1	0
0025540301	Medium	08 38 22.8 +25 45 13.9	11 803.5	20.56	1	13	4	2
0111400101	Thick	08 39 11.6 +65 01 12.1	24 224.9	20.63	8	13	1	0
0112620101*	Medium	08 41 22.9 +70 53 37.8	4301.9	20.47	8	13	0	–
0103660201	Medium	08 47 42.4 +34 45 07.3	16 223.3	20.52	8	13	1	0
0085030101*	Thin1	08 55 35.7 +58 44 05.8	6545.6	20.62	5	13	2	–
0110660201	Medium	09 06 02.5 +62 03 02.2	8671.8	20.65	0	13	1	0
0083240201	Thin1	09 11 28.2 +05 50 57.3	19 349.7	20.56	2	13	1	0
0084230601	Medium	09 17 52.1 +51 43 33.1	16 347.4	20.16	6	13	1	1
0021740101	Medium	09 39 53.7 +35 54 06.4	10 323.5	20.16	2	13	0	0
0106460101	Thin1	09 43 01.2 +46 59 34.4	49 423.9	20.10	3	13	0	0
0017540101	Medium	09 45 25.9 −08 39 03.2	7573.9	20.56	8	13	2	0
0111290101	Thin1	09 50 48.7 +39 26 59.8	21 359.3	20.20	8	13	1	0
0065790101	Thin1	09 52 09.1 −01 48 14.6	9322.6	20.60	2	13	2	1
0070940101*	Thin1	09 53 41.5 +01 34 55.9	6021.1	20.55	5	13	2	–
0112850101	Thin1	09 54 56.3 +17 43 29.7	17 345.1	20.50	1	13	2	0
0111290201	Thin1	09 56 52.6 +41 15 24.9	12 896.7	19.90	8	13	1	0
0041170201	Medium	10 00 40.8 +25 14 24.8	46 751.9	20.44	0	13	3	0
0110930201	Medium	10 01 56.9 +55 40 41.1	7317.1	19.90	2	13	2	0
0070340201	Thin1	10 08 47.1 +53 42 00.8	21 851.2	19.87	1	13	3	0
0085170101	Thin1	10 11 13.5 +55 44 55.0	31 755.9	19.89	2	13	0	0
0086750101*	Thin1	10 16 15.4 +52 09 24.1	6574.0	19.88	2	13	3	–
0028740301	Thin1	10 18 40.5 +41 25 15.2	28 448.5	20.05	8	13	4	2
0093640301	Medium	10 19 59.8 +08 13 32.3	12 804.9	20.48	1	13	2	0
0101040301	Medium	10 23 30.7 +19 51 53.1	36 611.7	20.33	4	13	1	0
0108670101	Thin1	10 23 39.9 +04 11 25.6	50 918.8	20.48	8	13	2	0
0102040301	Thick	10 30 59.0 +31 02 51.8	26 293.5	20.29	8	13	2	0
0110950101	Thin1	10 31 54.2 −14 16 52.5	7308.6	20.82	8	13	0	0
0112810301*	Thin1	10 38 44.4 +53 30 08.4	4917.1	20.05	3	13	2	–
0059800101	Thin1	10 39 53.7 +20 50 52.2	14 293.2	20.31	2	13	5	1
0125300101	Thin1	10 44 32.4 −01 25 05.3	32 227.5	20.62	2	13	4	1
0055990201	Thin1	10 49 53.6 +32 58 58.1	19 840.1	20.30	4	13	2	1

Table 2. continued.

Obs. ID	Filter	RA; Dec (J2000)	Exposure	Log Nh	R_{in}	R_{out}	BSS	HBSS
			s	cm^{-2}	arcmin	arcmin	srcs	srcs
(1)	(2)	(3)	(4)	(5)	(6)	(7)	(8)	(9)
0022740101	Medium	10 52 44.1 +57 28 48.7	82 880.4	19.75	0	13	5	0
0094800101	Thin1	10 56 59.5 −03 37 29.8	31 924.0	20.55	2	13	1	0
0110660301*	Thin1	11 01 08.4 +86 09 59.2	6216.2	20.83	1	13	0	–
0112880201	Medium	11 01 52.3 −34 42 27.4	28 570.1	20.70	2	13	3	1
0070340301*	Medium	11 03 36.6 +35 55 11.8	8386.3	20.30	1	13	1	–
0112630101	Thin1	11 06 33.6 −18 21 35.1	12 627.6	20.66	1	13	1	0
0099030101	Thin1	11 17 18.6 +17 57 50.3	20 091.0	20.18	1	13	1	0
0111290401	Thin1	11 19 08.8 +21 19 17.4	8525.8	20.11	8	13	2	0
0107860201	Thin1	11 20 06.3 +43 17 59.9	22 162.9	20.32	1	13	0	1
0093641101	Medium	11 20 15.0 +12 59 29.1	10 566.2	20.39	5	13	3	0
0112270301	Thin1	11 22 21.7 +24 17 39.2	14 296.9	20.10	6	13	0	0
0110660401	Medium	11 26 00.6 +42 53 05.1	13 085.5	20.32	1	13	0	0
0112810101	Thin1	11 28 29.1 +58 33 43.7	20 593.3	20.00	3	13	0	0
0102040201	Thick	11 31 09.2 +31 14 08.0	23 552.4	20.31	8	13	3	3
0042341001	Thin1	11 31 56.2 −19 55 32.8	12 683.8	20.65	6	13	1	0
0112210101	Medium	11 39 02.3 −37 44 17.2	37 360.0	20.93	4	13	1	0
0094800201	Thin1	11 40 23.9 +66 08 37.6	24 709.2	20.09	1	13	0	0
0112551401*	Thin1	11 52 54.0 +36 59 06.6	6471.1	20.28	4	13	1	–
0090020101	Thin1	11 57 55.3 +55 27 07.8	10 362.7	20.09	3	13	1	0
0109141401	Medium	12 03 09.4 +44 31 52.4	62 156.3	20.12	8	13	2	0
0112310101	Medium	12 10 32.3 +39 24 19.8	30 192.1	20.30	8	13	0	0
0112610101	Medium	12 14 17.0 +14 03 16.9	51 088.9	20.44	8	13	1	0
0111840101*	Medium	12 21 22.2 +30 10 38.1	9637.0	20.24	4	13	0	–
0124110101	Medium	12 21 41.5 +75 18 38.0	17 009.1	20.46	2	13	2	0
0108860101	Thin1	12 23 07.2 +10 37 15.1	20 960.4	20.35	4	13	0	0
0070340501	Thin1	12 27 15.6 +33 32 18.9	15 390.5	20.14	1	13	4	0
0110990201	Thin1	12 27 18.4 +01 29 20.2	11 954.5	20.26	1	13	2	1
0126700301	Medium	12 29 06.6 +02 03 08.0	56 647.6	20.25	8	13	2	0
0112650101	Medium	12 31 11.4 +20 47 52.2	23 562.4	20.30	0	13	0	0
0124900101	Thin1	12 31 30.9 +64 14 20.0	33 644.1	20.30	2	13	4	0
0006220201	Thick	12 35 34.9 −39 54 55.9	42 741.5	20.86	1	13	2	1
0111550101	Thin1	12 36 48.5 +62 12 56.4	43 468.9	20.17	0	13	3	0
0109970101	Medium	12 39 39.1 −05 20 40.3	8087.8	20.36	4	13	0	0
0136950201	Thin1	12 42 37.9 −11 19 22.4	29 166.8	20.56	1	13	1	0
0111190701	Medium	12 42 48.1 +02 41 17.8	59 825.8	20.26	8	13	0	0
0051760101	Thin1	12 46 34.9 +02 22 01.1	12 244.0	20.24	2	13	4	1
0060370201	Thin1	12 49 13.5 −05 59 27.5	40 156.8	20.33	1	13	4	0
0008220201	Thick	12 51 41.5 +27 32 25.3	39 747.7	19.95	8	13	0	0
0111020101	Medium	12 53 02.9 −29 23 41.4	29 008.5	20.78	8	13	0	0
0081340201	Medium	12 56 13.6 +56 52 24.0	21 493.1	20.10	1	13	2	0
0017940101	Thin1	13 05 43.5 +18 00 59.0	50 660.2	20.32	8	13	1	0
0002940101	Medium	13 07 06.6 −23 40 27.2	7263.6	20.96	1	13	2	0
0093640401	Medium	13 20 35.4 +34 08 21.4	19 663.3	20	1	13	4	1
0100240201	Medium	13 30 47.4 +24 13 59.1	35 954.0	20.06	3	13	3	0
0061940101	Medium	13 31 52.9 +11 16 43.9	7011.7	20.29	1	13	1	0
0111160101	Thin1	13 34 19.2 +50 30 55.6	47 144.5	20.04	2	13	1	0
0111570201	Medium	13 35 53.9 −34 17 44.3	50 435.3	20.61	6	13	1	0
0096010101	Thin1	13 37 18.8 +24 23 02.3	32 367.8	20.06	8	13	1	0
0035940301	Medium	13 39 55.8 −31 38 30.3	42 378.9	20.59	5	13	1	1
0112250201	Thin1	13 47 40.0 +58 12 45.2	33 008.0	20.11	1	13	2	2
0098010101	Thin1	14 01 02.0 +02 52 44.3	32 776.7	20.37	5	13	1	2
0109910101	Thin1	14 01 34.5 −11 07 40.3	48 892.6	20.63	6	13	3	1
0092850501	Thin1	14 09 23.9 +26 18 21.4	41 167.0	20.17	2	13	2	0
0013140101	Medium	14 13 14.9 −03 12 25.5	17 838.3	20.58	8	13	1	0

Table 2. continued.

Obs. ID	Filter	RA; Dec (J2000)	Exposure	Log Nh	$R_{\rm in}$	$R_{\rm out}$	BSS	HBSS
			s	cm^{-2}	arcmin	arcmin	srcs	srcs
(1)	(2)	(3)	(4)	(5)	(6)	(7)	(8)	(9)
0112250301	Thin1	14 15 45.6 +11 29 35.7	25 593.4	20.26	2	13	2	1
0127921001	Thin1	14 17 10.3 +52 23 54.1	54 477.7	20.11	0	13	3	0
0109960101	Medium	14 17 59.2 +25 08 11.7	23 142.3	20.23	4	13	3	1
0111850201	Medium	14 28 32.5 +42 40 16.4	39 671.3	20.14	4	13	2	1
0111530101	Thick	14 38 59.9 +64 17 25.5	50 080.5	20.23	8	13	3	2
0057560301	Thin1	14 49 29.2 +08 59 51.1	38 812.8	20.31	0	13	2	0
0056030101	Medium	14 51 22.8 +19 06 02.7	58 940.0	20.39	8	13	0	0
0067750101	Thin1	14 58 21.3 −31 40 09.0	34 424.0	20.93	2	13	1	0
0070740301	Thin1	15 04 01.1 +10 26 15.0	10 625.1	20.37	8	13	1	0
0018741001	Thin1	15 18 46.4 +06 14 10.4	7406.8	20.51	4	13	2	0
0100240801	Medium	15 32 23.0 −08 32 01.3	23 738.7	20.96	3	13	2	0
0091140401	Thin1	15 32 28.6 +04 40 48.6	34 556.1	20.62	5	13	0	0
0112190401	Medium	15 35 01.4 +01 20 45.4	13 512.1	20.69	2	13	3	1
0094380801*	Medium	15 55 43.2 +11 11 16.3	5805.5	20.56	8	13	0	–
0067340601	Medium	16 07 13.8 +08 04 51.5	14 215.2	20.60	0	13	3	1
0103460801	Thin1	16 16 28.7 +12 12 22.1	13 130.2	20.66	1	13	2	0
0103461001	Thin1	16 17 36.8 +12 36 57.7	11 734.5	20.66	1	13	1	1
0061940301*	Medium	16 30 53.6 +78 10 54.5	4965.0	20.61	2	13	6	–
0112230301	Medium	16 32 45.7 +05 34 39.6	20 662.8	20.75	8	13	1	0
0049540101*	Medium	16 34 20.8 +57 09 43.1	10855.0	20.27	2	13	2	–
0067340501	Medium	16 42 17.3 +03 10 57.5	14 421.1	20.74	0	13	1	0
0101640101	Medium	16 52 58.4 +02 24 00.4	16 112.3	20.76	8	13	1	0
0113070101	Medium	16 53 59.8 +14 17 52.6	7298.1	20.74	0	13	4	2
0111060101	Medium	16 57 49.6 +35 20 35.8	9421.0	20.25	3	13	2	0
0102040101*	Thick	17 23 20.8 +34 18 00.6	6893.5	20.49	8	13	1	–
0067340101*	Medium	18 55 37.1 −46 30 57.6	10 652.7	20.72	0	11	2	–
0081341001	Thin1	19 31 21.7 −72 39 13.3	15 287.3	20.77	1	13	2	1
0081340501	Medium	20 13 30.0 −41 47 25.7	19 195.9	20.69	0	13	0	0
0111180201	Medium	20 40 10.0 −00 52 14.7	16 494.9	20.83	8	13	2	1
0111510101	Medium	20 41 50.9 −32 26 19.8	14 918.6	20.71	8	13	3	0
0130720201*	Thin1	20 44 09.0 −10 43 11.2	5311.7	20.61	8	13	0	–
0111420101	Medium	20 45 09.4 −31 20 36.6	42 956.6	20.74	8	13	0	0
0112600501	Medium	20 46 20.0 −02 48 48.4	10 549.7	20.70	8	13	1	0
0083210101	Thin1	20 54 18.8 −15 55 38.2	10 434.9	20.64	2	13	2	0
0112190601	Medium	20 56 21.6 −04 37 59.4	16 639.7	20.70	2	13	1	1
0081340401	Thin1	20 58 27.1 −42 38 56.9	15 001.6	20.59	1	13	2	1
0041150101	Medium	21 04 11.1 −11 21 40.0	38 734.2	20.67	1	13	1	0
0038540301	Thin1	21 04 40.2 −12 20 05.6	14 697.9	20.65	2	13	1	0
0088020201	Thin1	21 27 38.1 −44 48 38.5	16 093.9	20.54	1	13	2	0
0103060101	Medium	21 29 12.2 −15 38 34.7	22 041.8	20.70	3	13	1	1
0092850201	Medium	21 37 45.3 −14 32 56.4	16 014.8	20.67	2	13	1	1
0109463501	Thin1	21 37 56.5 −43 42 19.8	7577.3	20.46	2	13	3	0
0061940201*	Medium	21 38 07.9 −42 36 06.6	4867.9	20.43	1	13	5	–
0008830101	Thin1	21 40 15.5 −23 39 32.1	13 986.0	20.55	2	13	1	1
0103060401	Medium	21 51 55.9 −30 27 43.5	24 071.7	20.33	3	13	2	0
0111270101	Thin1	21 53 37.3 +17 41 57.7	13 650.1	20.83	6	13	1	0
0124930201	Medium	21 58 52.9 −30 13 28.8	36 244.5	20.23	8	13	0	0
0130920101	Thick	22 03 09.3 +18 52 27.9	16 490.5	20.78	1	13	1	0
0012440301	Thin1	22 05 10.1 −01 55 11.2	30 935.9	20.79	2	13	2	1
0106660101	Thin1	22 15 31.9 −17 44 02.6	56 908.9	20.37	1	13	1	0
0009650201	Medium	22 17 55.4 −08 20 58.0	21 026.5	20.73	8	13	4	0
0103861201	Medium	22 19 19.2 +12 08 00.1	12 172.6	20.73	8	13	1	0

Table 2. continued.

Obs. ID	Filter	RA; Dec (J2000)	Exposure	Log Nh	$R_{\rm in}$	$R_{\rm out}$	BSS	HBSS
			s	$\rm cm^{-2}$	arcmin	arcmin	srcs	srcs
(1)	(2)	(3)	(4)	(5)	(6)	(7)	(8)	(9)
0049340201	Medium	22 20 45.1 −24 40 58.1	26 840.9	20.29	6	13	0	0
0100440101	Thick	22 28 30.4 −05 18 49.5	45 013.1	20.72	2	13	1	0
0018741701	Thin1	22 34 32.9 −37 43 48.1	7080.0	20.09	4	13	0	0
0111790101	Medium	22 35 45.9 −26 03 00.4	41 302.3	20.16	4	13	2	0
0103860201	Medium	22 36 55.9 −22 13 10.1	8489.4	20.33	8	13	0	0
0103860301*	Medium	22 40 18.1 +08 03 23.2	5879.2	20.82	8	13	1	–
0006810101	Medium	22 42 39.5 +29 43 35.6	7009.1	20.81	8	13	0	0
0109070401	Medium	22 48 41.5 −51 09 57.9	14 721.9	20.13	8	13	2	0
0112240101	Medium	22 49 48.3 −64 23 11.2	30 606.8	20.47	8	13	3	0
0081340901	Medium	22 51 49.4 −17 52 17.0	22 397.4	20.43	1	13	1	0
0112910301*	Thin1	22 53 58.8 −17 33 55.8	5301.0	20.43	8	13	1	–
0009650101	Medium	22 55 18.1 −03 10 35.6	33 943.5	20.66	8	13	0	0
0112170301	Medium	23 03 15.8 +08 52 25.9	23 348.5	20.69	4	13	0	0
0109130701	Thin1	23 04 43.6 −08 41 14.5	10 615.1	20.56	8	13	1	0
0033541001	Thin1	23 04 45.0 +03 11 35.6	12 460.9	20.72	2	13	2	0
0025541001	Medium	23 04 56.8 +12 19 32.0	9954.8	20.70	3	13	5	0
0123900101	Thin1	23 13 58.9 −42 43 28.3	37 399.4	20.25	6	13	1	0
0109463601*	Thin1	23 15 18.7 −59 10 31.7	5403.3	20.46	8	13	1	–
0093640701	Medium	23 16 11.0 −42 35 01.8	14 442.9	20.27	3	13	4	0
0112880301	Thick	23 31 49.9 +19 56 28.5	14 317.3	20.63	3	13	0	0
0093550401	Medium	23 33 40.0 −15 17 12.2	22 256.9	20.30	1	13	2	0
0100241001	Thick	23 49 40.6 +36 25 30.6	8738.5	20.91	3	13	2	0

Columns are as follows: (1) XMM-Newton Observation number; (2) Filter used; (3) Right ascension and Declination (J2000) of the MOS2 image center; (4) On-Axis good-time exposure; (5) Logarithm of the Galactic hydrogen column density along the line of sight from Dickey & Lockman (1990); (6) Inner radius of the part of the MOS2 image used; (7) Outer radius of the part of the MOS2 image used; (8) total number of BSS sources found in the surveyed area of each MOS2 image; (9) total number of HBSS sources found in the surveyed area of each MOS2 image. See Sect. 2.4 for details.

NOTE – * These 26 fields have not be considered for the definition of the HBSS sample.

Table 3. Basic information on the XMM-Newton BSS sample.

Name XBS...	Obs. ID	RA; Dec (J2000)	OffAxis arcmin	Rate $\times 10^{-2}$ cts/s	*HR*2	*HR*3	Class
(1)	(2)	(3)	(4)	(5)	(6)	(7)	(8)
J000027.7−250442	0125310101	00 00 27.8 −25 04 42.6	2.10	1.13 ± 0.08	$-0.48^{+0.06}_{-0.06}$	$-0.37^{+0.11}_{-0.11}$	AGN1
J000031.7−245502	0125310101	00 00 31.8 −24 55 02.9	11.68	1.41 ± 0.13	$-0.67^{+0.07}_{-0.06}$	$-0.37^{+0.17}_{-0.17}$	AGN1
J000100.2−250501[d]	0125310101	00 01 00.2 −25 05 01.2	6.97	1.38 ± 0.10	$-0.37^{+0.07}_{-0.07}$	$-0.47^{+0.10}_{-0.10}$	AGN1
J000102.4−245850	0125310101	00 01 02.5 −24 58 50.7	10.72	1.48 ± 0.12	$-0.54^{+0.07}_{-0.07}$	$-0.71^{+0.11}_{-0.10}$	AGN1
J000532.7+200716	0101040101	00 05 32.8 +20 07 16.2	12.15	2.47 ± 0.12	$-0.81^{+0.03}_{-0.03}$	$-0.70^{+0.11}_{-0.10}$	GAL
J001002.4+110831	0127110201	00 10 02.4 +11 08 31.0	12.12	13.12 ± 0.71	$-0.79^{+0.03}_{-0.03}$	$-0.88^{+0.07}_{-0.06}$	star
J001051.6+105140	0127110201	00 10 51.6 +10 51 40.2	8.61	1.01 ± 0.15	$-0.76^{+0.09}_{-0.10}$	$-1.00^{+0.76}_{-0.00}$	star
J001749.7+161952	0111000101	00 17 49.7 +16 19 52.5	12.11	3.35 ± 0.15	$-1.00^{+0.01}_{-0.00}$	$1.00^{+0.00}_{-0.96}$	star
J001831.6+162925	0111000101	00 18 31.7 +16 29 25.6	3.31	1.82 ± 0.08	$-0.67^{+0.03}_{-0.03}$	$-0.56^{+0.08}_{-0.08}$	AGN1
J002618.5+105019[a]	0001930101	00 26 18.5 +10 50 19.3	9.56	5.19 ± 0.24	$-0.53^{+0.04}_{-0.04}$	$-0.67^{+0.06}_{-0.06}$	AGN1
J002637.4+165953	0050140201	00 26 37.4 +16 59 53.5	9.74	2.78 ± 0.10	$-0.61^{+0.03}_{-0.03}$	$-0.62^{+0.06}_{-0.05}$	AGN1
J002707.5+170748	0050140201	00 27 07.6 +17 07 48.5	7.78	1.58 ± 0.08	$-0.58^{+0.04}_{-0.04}$	$-0.39^{+0.08}_{-0.08}$	AGN1
J002953.1+044524	0112320101	00 29 53.2 +04 45 24.6	10.69	1.33 ± 0.12	$-0.91^{+0.04}_{-0.04}$	$-1.00^{+0.63}_{-0.00}$	star
J003255.9+394619[d]	0065770101	00 32 55.9 +39 46 19.9	11.90	1.11 ± 0.21	$-0.76^{+0.12}_{-0.11}$	$-0.24^{+0.32}_{-0.44}$	AGN1
J003315.5−120700	0125920201	00 33 15.6 −12 07 00.9	9.52	1.62 ± 0.20	$-0.75^{+0.08}_{-0.08}$	$-0.05^{+0.25}_{-0.26}$	AGN1
J003316.0−120456	0125920201	00 33 16.1 −12 04 56.6	9.66	1.03 ± 0.15	$-0.90^{+0.06}_{-0.06}$	$-0.97^{+1.27}_{-0.03}$	AGN1
J003418.9−115940	0125920201	00 34 19.0 −11 59 40.1	9.60	1.05 ± 0.14	$-0.69^{+0.09}_{-0.09}$	$-0.39^{+0.24}_{-0.26}$	AGN1
J005009.9−515934	0125320701	00 50 09.9 −51 59 34.7	8.10	1.38 ± 0.11	$-0.56^{+0.07}_{-0.07}$	$-0.57^{+0.13}_{-0.13}$	AGN1
J005031.1−520012	0125320701	00 50 31.1 −52 00 12.8	8.57	1.89 ± 0.14	$-0.65^{+0.05}_{-0.05}$	$-0.47^{+0.13}_{-0.13}$	AGN1
J005032.3−521543	0125320701	00 50 32.3 −52 15 43.5	9.28	1.12 ± 0.13	$-0.45^{+0.09}_{-0.09}$	$-0.53^{+0.14}_{-0.15}$	AGN1
J005822.9−274016	0111280301	00 58 22.9 −27 40 16.1	7.71	2.07 ± 0.21	$-0.91^{+0.04}_{-0.05}$	$-0.19^{+0.42}_{-0.38}$	star
J010421.4−061418	0112650401	01 04 21.4 −06 14 18.8	9.89	1.01 ± 0.09	$-0.49^{+0.08}_{-0.08}$	$-0.81^{+0.10}_{-0.11}$	AGN1
J010432.8−583712	0103861601	01 04 32.8 −58 37 12.2	12.41	1.61 ± 0.26	$-0.53^{+0.14}_{-0.13}$	$-0.07^{+0.26}_{-0.27}$	AGN1
J010701.5−172748	0025540101	01 07 01.5 −17 27 48.4	10.99	3.56 ± 0.33	$-0.47^{+0.08}_{-0.08}$	$-0.84^{+0.09}_{-0.09}$	AGN1
J010747.2−172044	0025540101	01 07 47.3 −17 20 44.6	9.49	2.27 ± 0.23	$-0.62^{+0.08}_{-0.08}$	$-0.48^{+0.19}_{-0.17}$	AGN1
J012000.0−110429	0113040801	01 20 00.1 −11 04 29.3	12.66	1.18 ± 0.25	$-0.77^{+0.14}_{-0.14}$	$0.01^{+0.50}_{-0.53}$	AGN1
J012025.2−105441	0113040801	01 20 25.3 −10 54 41.6	3.95	1.39 ± 0.18	$-0.50^{+0.11}_{-0.11}$	$-0.68^{+0.16}_{-0.18}$	
J012057.4−110444	0113040801	01 20 57.5 −11 04 44.6	9.40	2.34 ± 0.28	$-0.61^{+0.09}_{-0.09}$	$-0.48^{+0.22}_{-0.21}$	AGN2
J012119.9−110418	0113040801	01 21 20.0 −11 04 18.6	12.65	5.85 ± 0.48	$-0.71^{+0.06}_{-0.06}$	$-0.67^{+0.15}_{-0.16}$	AGN1
J012505.4+014624[d]	0109860101	01 25 05.4 +01 46 24.4	7.04	1.94 ± 0.09	$-0.46^{+0.04}_{-0.04}$	$-0.51^{+0.06}_{-0.06}$	AGN1
J012540.2+015752	0109860101	01 25 40.3 +01 57 52.1	12.35	1.41 ± 0.10	$-0.56^{+0.06}_{-0.06}$	$-0.29^{+0.11}_{-0.12}$	AGN2
J012654.3+191246[d]	0112600601	01 26 54.3 +19 12 47.0	9.20	1.02 ± 0.26	$-0.64^{+0.17}_{-0.17}$	$0.07^{+0.41}_{-0.39}$	GAL
J012757.3+185923	0112600601	01 27 57.4 +18 59 23.9	12.64	34.37 ± 1.49	$-0.92^{+0.02}_{-0.02}$	$-0.34^{+0.17}_{-0.16}$	star
J012757.2+190000	0112600601	01 27 57.2 +19 00 00.4	12.09	10.69 ± 0.81	$-0.81^{+0.04}_{-0.04}$	$-1.00^{+0.27}_{-0.00}$	star
J013204.9−400050	0112630201	01 32 04.9 −40 00 50.9	12.23	1.29 ± 0.12	$-0.67^{+0.06}_{-0.06}$	$-0.32^{+0.16}_{-0.16}$	AGN1
J013240.1−133307[a,d]	0084230301	01 32 40.1 −13 33 07.8	11.90	1.42 ± 0.14	$-0.02^{+0.10}_{-0.10}$	$-0.37^{+0.11}_{-0.11}$	AGN2
J013811.7−175416[d]	0111430101	01 38 11.8 −17 54 16.3	12.09	3.09 ± 0.17	$-0.73^{+0.04}_{-0.04}$	$-0.77^{+0.08}_{-0.08}$	BL?
J013924.8−674126	0032140401	01 39 24.8 −67 41 26.5	8.50	1.02 ± 0.14	$0.21^{+0.14}_{-0.14}$	$-0.54^{+0.13}_{-0.14}$	
J013944.0−674909[a]	0032140401	01 39 44.0 −67 49 09.4	2.69	2.04 ± 0.17	$-0.50^{+0.07}_{-0.07}$	$-0.43^{+0.13}_{-0.13}$	AGN1?
J014100.6−675328[a]	0032140401	01 41 00.7 −67 53 29.0	6.64	57.52 ± 1.03	$-0.45^{+0.02}_{-0.02}$	$-0.38^{+0.03}_{-0.03}$	star
J014109.9−675639	0032140401	01 41 09.9 −67 56 39.6	9.67	1.97 ± 0.23	$-0.35^{+0.11}_{-0.10}$	$-0.45^{+0.16}_{-0.15}$	AGN1?
J014227.0+133453	0093641001	01 42 27.1 +13 34 53.7	9.12	1.29 ± 0.14	$-0.52^{+0.10}_{-0.10}$	$-0.51^{+0.18}_{-0.18}$	AGN2?
J014251.5+133352	0093641001	01 42 51.6 +13 33 52.8	5.15	1.43 ± 0.13	$-0.46^{+0.09}_{-0.08}$	$-0.49^{+0.14}_{-0.14}$	AGN1
J015916.9+003010[c]	0101640201	01 59 17.0 +00 30 10.4	10.49	5.74 ± 0.54	$-0.58^{+0.06}_{-0.06}$	$-0.71^{+0.20}_{-0.20}$	CL+BL?
J015957.5+003309[a]	0101640201	01 59 57.5 +00 33 09.7	9.56	6.50 ± 0.39	$-0.63^{+0.05}_{-0.05}$	$-0.51^{+0.10}_{-0.10}$	AGN1
J020029.0+002846	0101640201	02 00 29.0 +00 28 46.1	10.90	3.39 ± 0.30	$-0.62^{+0.07}_{-0.07}$	$-0.36^{+0.15}_{-0.15}$	AGN1
J020757.3+351828	0084140101	02 07 57.3 +35 18 28.9	9.48	1.19 ± 0.07	$-0.52^{+0.05}_{-0.05}$	$-0.55^{+0.09}_{-0.09}$	AGN1
J020845.1+351438	0084140101	02 08 45.2 +35 14 38.0	8.49	1.80 ± 0.09	$-0.48^{+0.04}_{-0.04}$	$-0.52^{+0.07}_{-0.07}$	AGN1
J020916.4+351850	0084140101	02 09 16.5 +35 18 50.4	8.85	1.30 ± 0.08	$-0.49^{+0.06}_{-0.05}$	$-0.66^{+0.08}_{-0.08}$	
J021640.7−044404[a,d]	0112371701	02 16 40.7 −04 44 04.9	9.35	2.56 ± 0.17	$-0.72^{+0.04}_{-0.05}$	$-0.26^{+0.13}_{-0.13}$	AGN1
J021642.3−043553	0112371701	02 16 42.4 −04 35 53.0	8.14	1.32 ± 0.12	$-0.42^{+0.08}_{-0.08}$	$-0.61^{+0.11}_{-0.11}$	
J021808.3−045845[a]	0112371001	02 18 08.3 −04 58 45.7	2.26	4.87 ± 0.10	$-0.65^{+0.02}_{-0.02}$	$-0.52^{+0.04}_{-0.04}$	AGN1
J021817.4−045113[a]	0112371001	02 18 17.4 −04 51 13.3	9.58	4.47 ± 0.13	$-0.48^{+0.02}_{-0.03}$	$-0.56^{+0.04}_{-0.04}$	AGN1

Table 3. continued.

Name XBS...	Obs. ID	RA; Dec (J2000)	OffAxis arcmin	Rate $\times 10^{-2}$ cts/s	*HR*2	*HR*3	Class
(1)	(2)	(3)	(4)	(5)	(6)	(7)	(8)
J021820.6−050427	0112371001	02 18 20.7 −05 04 27.6	6.90	1.22 ± 0.06	$-0.47^{+0.04}_{-0.04}$	$-0.57^{+0.07}_{-0.07}$	AGN1
J021830.0−045514	0112371001	02 18 30.0 −04 55 14.8	8.69	3.36 ± 0.10	$-0.90^{+0.01}_{-0.01}$	$-0.69^{+0.09}_{-0.09}$	star
J021923.2−045148	0112370301	02 19 23.2 −04 51 48.1	8.63	1.40 ± 0.07	$-0.66^{+0.04}_{-0.04}$	$-0.42^{+0.09}_{-0.10}$	AGN1
J022253.0−044515	0109520501	02 22 53.0 −04 45 16.0	8.12	1.15 ± 0.09	$-0.58^{+0.06}_{-0.07}$	$-0.60^{+0.12}_{-0.13}$	
J022339.6−050728	0111110401	02 23 39.6 −05 07 28.2	5.66	1.45 ± 0.08	$-0.53^{+0.05}_{-0.05}$	$-0.76^{+0.07}_{-0.07}$	
J022707.7−050819	0111110201	02 27 07.7 −05 08 19.8	7.05	1.89 ± 0.19	$0.17^{+0.09}_{-0.09}$	$-0.67^{+0.08}_{-0.08}$	AGN2
J023459.7−294436	0103861101	02 34 59.7 −29 44 36.9	8.91	1.18 ± 0.23	$-0.26^{+0.14}_{-0.14}$	$-0.48^{+0.18}_{-0.19}$	
J023530.2−523045	0098810101	02 35 30.2 −52 30 45.2	12.59	1.88 ± 0.14	$-0.70^{+0.05}_{-0.05}$	$-0.38^{+0.14}_{-0.14}$	AGN1
J023713.5−522734[a]	0098810101	02 37 13.5 −52 27 34.4	12.07	5.60 ± 0.24	$-0.57^{+0.03}_{-0.03}$	$-0.58^{+0.07}_{-0.06}$	AGN1
J023853.2−521911	0067190101	02 38 53.3 −52 19 11.1	9.22	1.45 ± 0.11	$-0.49^{+0.06}_{-0.06}$	$-0.42^{+0.11}_{-0.11}$	AGN1
J024200.9+000020	0111200101	02 42 01.0 +00 00 20.1	10.11	2.13 ± 0.12	$-0.60^{+0.04}_{-0.04}$	$-0.52^{+0.09}_{-0.09}$	AGN1
J024204.7+000814	0111200101	02 42 04.7 +00 08 14.3	12.90	1.01 ± 0.10	$-0.57^{+0.08}_{-0.07}$	$-0.81^{+0.10}_{-0.10}$	AGN1
J024207.3+000037	0111200101	02 42 07.3 +00 00 37.6	8.59	1.26 ± 0.09	$-0.62^{+0.05}_{-0.05}$	$-0.77^{+0.09}_{-0.09}$	AGN1
J024325.6−000413	0111200101	02 43 25.6 −00 04 13.3	11.61	1.04 ± 0.08	$-0.31^{+0.07}_{-0.07}$	$-0.40^{+0.10}_{-0.10}$	AGN1
J025606.1+001635	0056020301	02 56 06.2 +00 16 35.5	12.49	1.28 ± 0.15	$-0.45^{+0.09}_{-0.09}$	$-0.93^{+0.06}_{-0.06}$	AGN1
J025645.4+000031	0056020301	02 56 45.5 +00 00 31.3	6.35	1.01 ± 0.10	$-0.49^{+0.08}_{-0.08}$	$-0.65^{+0.12}_{-0.13}$	AGN1?
J030204.2+001625	0041170101	03 02 04.2 +00 16 25.6	12.36	1.01 ± 0.07	$-0.46^{+0.06}_{-0.06}$	$-0.50^{+0.10}_{-0.10}$	
J030206.8−000121[a]	0041170101	03 02 06.9 −00 01 21.2	11.90	3.56 ± 0.13	$-0.53^{+0.03}_{-0.03}$	$-0.46^{+0.05}_{-0.06}$	AGN1
J030614.1−284019[a]	0042340501	03 06 14.2 −28 40 19.9	10.87	3.85 ± 0.23	$-0.49^{+0.05}_{-0.05}$	$-0.35^{+0.09}_{-0.09}$	AGN1
J030641.0−283559	0042340501	03 06 41.0 −28 35 59.5	6.66	1.25 ± 0.11	$-0.61^{+0.07}_{-0.07}$	$-0.81^{+0.11}_{-0.11}$	AGN1
J031015.5−765131[a]	0122520201	03 10 15.6 −76 51 31.5	5.90	5.36 ± 0.15	$-0.46^{+0.03}_{-0.03}$	$-0.53^{+0.04}_{-0.04}$	AGN1
J031146.1−550702[a]	0110970101	03 11 46.1 −55 07 02.5	12.38	6.55 ± 0.45	$-0.58^{+0.05}_{-0.05}$	$-0.39^{+0.11}_{-0.11}$	AGN2
J031311.7−765428	0122520201	03 13 11.7 −76 54 28.8	4.86	1.10 ± 0.07	$-0.43^{+0.06}_{-0.06}$	$-0.30^{+0.09}_{-0.09}$	AGN1
J031401.3−545959	0110970101	03 14 01.3 −54 59 59.5	8.34	1.29 ± 0.14	$-0.51^{+0.09}_{-0.09}$	$-0.68^{+0.14}_{-0.14}$	AGN1
J031549.4−551811	0129320901	03 15 49.4 −55 18 11.5	12.22	1.04 ± 0.16	$-0.83^{+0.09}_{-0.08}$	$-0.85^{+0.21}_{-0.13}$	AGN1
J031851.9−441815	0105660101	03 18 51.9 −44 18 15.3	10.78	1.15 ± 0.12	$-0.59^{+0.08}_{-0.07}$	$-0.40^{+0.16}_{-0.15}$	AGN1
J031859.2−441627[a,b]	0105660101	03 18 59.3 −44 16 27.6	11.55	1.54 ± 0.14	$-0.21^{+0.08}_{-0.08}$	$-0.47^{+0.10}_{-0.10}$	AGN1
J033208.7−274735	0108060501	03 32 08.7 −27 47 35.7	4.60	1.13 ± 0.06	$-0.70^{+0.03}_{-0.04}$	$-0.40^{+0.10}_{-0.09}$	AGN2?
J033226.9−274107[d]	0108060501	03 32 27.0 −27 41 07.3	7.35	1.42 ± 0.07	$-0.63^{+0.04}_{-0.04}$	$-0.59^{+0.08}_{-0.07}$	AGN1
J033435.5−254259	0099010101	03 34 35.6 −25 42 59.3	11.87	1.10 ± 0.12	$-0.50^{+0.09}_{-0.09}$	$-1.00^{+0.18}_{-0.00}$	AGN1
J033453.9−254154	0099010101	03 34 54.0 −25 41 54.6	8.14	1.89 ± 0.13	$-0.62^{+0.05}_{-0.05}$	$-0.38^{+0.12}_{-0.12}$	AGN1
J033506.0−255619	0099010101	03 35 06.1 −25 56 19.9	12.41	1.18 ± 0.12	$-0.63^{+0.08}_{-0.08}$	$-0.82^{+0.13}_{-0.16}$	AGN1
J033851.4−352646	0055140101	03 38 51.5 −35 26 46.3	8.89	1.38 ± 0.08	$-0.55^{+0.04}_{-0.04}$	$-0.68^{+0.07}_{-0.07}$	AGN1
J033912.1−352813	0055140101	03 39 12.1 −35 28 13.8	5.18	1.23 ± 0.06	$-0.40^{+0.04}_{-0.04}$	$-0.52^{+0.06}_{-0.06}$	
J033942.8−352411	0055140101	03 39 42.8 −35 24 11.3	2.40	1.33 ± 0.06	$-0.75^{+0.03}_{-0.03}$	$-0.56^{+0.09}_{-0.09}$	AGN1
J040744.6−710846	0111970301	04 07 44.6 −71 08 47.0	11.15	1.27 ± 0.15	$-0.77^{+0.07}_{-0.07}$	$-0.75^{+0.18}_{-0.22}$	
J040807.2−712702	0111970301	04 08 07.2 −71 27 02.5	10.47	6.46 ± 0.27	$-0.91^{+0.02}_{-0.02}$	$-0.74^{+0.12}_{-0.11}$	star
J041108.1−711341[a]	0111970301	04 11 08.1 −71 13 41.1	10.52	1.03 ± 0.11	$-0.53^{+0.08}_{-0.08}$	$-0.04^{+0.16}_{-0.16}$	AGN1
J042417.9−571539	0112600401	04 24 17.9 −57 15 39.2	11.86	1.04 ± 0.18	$-0.64^{+0.13}_{-0.13}$	$-0.46^{+0.32}_{-0.30}$	
J043448.3−775329	0103861701	04 34 48.4 −77 53 29.2	8.55	2.03 ± 0.22	$-0.35^{+0.10}_{-0.10}$	$-0.61^{+0.14}_{-0.13}$	
J045942.4+015843	0112880401	04 59 42.5 +01 58 43.5	11.59	1.38 ± 0.13	$-0.35^{+0.09}_{-0.08}$	$-0.49^{+0.11}_{-0.12}$	AGN1
J050011.7+013948	0112880401	05 00 11.8 +01 39 48.0	11.76	1.19 ± 0.11	$-0.35^{+0.09}_{-0.09}$	$-0.38^{+0.13}_{-0.13}$	AGN1?
J050446.3−283821	0111160201	05 04 46.3 −28 38 21.8	12.92	1.36 ± 0.10	$-0.57^{+0.06}_{-0.05}$	$-0.67^{+0.10}_{-0.10}$	
J050453.4−284532	0111160201	05 04 53.5 −28 45 32.1	6.75	1.06 ± 0.06	$-0.39^{+0.05}_{-0.05}$	$-0.41^{+0.08}_{-0.08}$	
J050501.8−284149	0111160201	05 05 01.9 −28 41 49.1	8.18	1.41 ± 0.08	$-0.65^{+0.04}_{-0.04}$	$-0.51^{+0.09}_{-0.09}$	
J050536.6−290050	0111160201	05 05 36.7 −29 00 50.8	12.43	1.68 ± 0.10	$-0.27^{+0.05}_{-0.05}$	$-0.47^{+0.07}_{-0.07}$	
J051413.5+794345	0094400101	05 14 13.6 +79 43 45.8	7.42	1.43 ± 0.09	$-0.29^{+0.06}_{-0.06}$	$-0.53^{+0.08}_{-0.08}$	
J051617.1+794408	0094400101	05 16 17.2 +79 44 08.7	4.00	4.05 ± 0.12	$-0.85^{+0.02}_{-0.02}$	$-0.73^{+0.07}_{-0.07}$	star
J051651.9+794314	0094400101	05 16 51.9 +79 43 14.6	3.01	1.77 ± 0.08	$-0.28^{+0.04}_{-0.04}$	$-0.55^{+0.06}_{-0.05}$	
J051655.3−104104	0103860701	05 16 55.3 −10 41 04.0	11.23	1.97 ± 0.31	$-0.33^{+0.14}_{-0.14}$	$-1.00^{+0.29}_{-0.00}$	AGN1
J051822.6+793208	0094400101	05 18 22.7 +79 32 08.0	9.37	1.27 ± 0.09	$-0.54^{+0.06}_{-0.06}$	$-0.41^{+0.10}_{-0.11}$	GAL
J051955.5−455727	0090050701	05 19 55.5 −45 57 27.4	10.69	3.27 ± 0.24	$-0.51^{+0.06}_{-0.06}$	$-0.77^{+0.08}_{-0.08}$	
J052022.0−252309	0085640101	05 20 22.0 −25 23 09.5	8.87	1.21 ± 0.14	$-0.66^{+0.09}_{-0.09}$	$-0.37^{+0.21}_{-0.22}$	
J052048.9−454128	0090050701	05 20 48.9 −45 41 28.5	11.67	8.35 ± 0.45	$-0.95^{+0.02}_{-0.02}$	$-0.81^{+0.17}_{-0.17}$	star
J052108.5−251913[d]	0085640101	05 21 08.5 −25 19 13.1	3.17	3.54 ± 0.20	$-0.59^{+0.05}_{-0.05}$	$-0.55^{+0.09}_{-0.09}$	AGN1
J052116.2−252957	0085640101	05 21 16.2 −25 29 57.8	8.80	1.00 ± 0.15	$-0.50^{+0.11}_{-0.12}$	$-0.70^{+0.18}_{-0.17}$	

Table 3. continued.

Name XBS...	Obs. ID	RA; Dec (J2000)	OffAxis arcmin	Rate $\times 10^{-2}$ cts/s	*HR*2	*HR*3	Class
(1)	(2)	(3)	(4)	(5)	(6)	(7)	(8)
J052144.1−251518	0085640101	05 21 44.1 −25 15 18.8	11.77	1.25 ± 0.19	$-0.60^{+0.11}_{-0.12}$	$-0.87^{+0.17}_{-0.12}$	
J052155.0−252200	0085640101	05 21 55.0 −25 22 00.7	12.24	1.82 ± 0.24	$-1.00^{+0.07}_{-0.00}$	−	star
J052509.3−333051	0050150101	05 25 09.3 −33 30 51.9	12.38	1.38 ± 0.18	$-0.56^{+0.10}_{-0.10}$	$-0.95^{+0.09}_{-0.05}$	
J052543.6−334856	0050150101	05 25 43.6 −33 48 56.4	9.70	1.01 ± 0.15	$-0.53^{+0.11}_{-0.10}$	$-0.76^{+0.15}_{-0.14}$	
J061342.7+710725[d]	0009220601	06 13 42.8 +71 07 25.9	10.51	6.44 ± 0.34	$-0.67^{+0.04}_{-0.04}$	$-0.75^{+0.08}_{-0.07}$	BL
J062134.8−643150	0103860101	06 21 34.8 −64 31 50.5	11.02	1.04 ± 0.20	$-0.41^{+0.15}_{-0.16}$	$-0.22^{+0.23}_{-0.25}$	
J062425.7−642958	0103860101	06 24 25.7 −64 29 58.3	10.39	1.99 ± 0.22	$-1.00^{+0.04}_{-0.00}$	$1.00^{+0.00}_{-1.30}$	star
J063709.1+820949	0029340101	06 37 09.2 +82 09 49.1	10.46	1.28 ± 0.11	$-0.58^{+0.06}_{-0.06}$	$-0.52^{+0.13}_{-0.13}$	
J065214.1+743230	0061540101	06 52 14.1 +74 32 30.6	7.01	2.33 ± 0.14	$-0.49^{+0.05}_{-0.05}$	$-0.58^{+0.08}_{-0.08}$	AGN1?
J065237.4+742421	0061540101	06 52 37.5 +74 24 21.9	2.09	1.08 ± 0.09	$-0.62^{+0.05}_{-0.06}$	$-0.35^{+0.12}_{-0.12}$	
J065400.0+742045	0061540101	06 54 00.1 +74 20 45.1	8.72	1.82 ± 0.15	$-0.49^{+0.06}_{-0.06}$	$-0.65^{+0.10}_{-0.10}$	AGN1
J065744.3−560817	0112980201	06 57 44.3 −56 08 17.5	11.74	1.40 ± 0.10	$-0.56^{+0.05}_{-0.05}$	$-0.78^{+0.08}_{-0.08}$	
J065839.5−560813	0112980201	06 58 39.6 −56 08 13.3	11.14	1.60 ± 0.10	$-0.65^{+0.04}_{-0.04}$	$-0.45^{+0.10}_{-0.10}$	
J074202.7+742625	0123100101	07 42 02.7 +74 26 25.8	10.86	3.02 ± 0.13	$-0.59^{+0.03}_{-0.03}$	$-0.28^{+0.07}_{-0.07}$	AGN1
J074312.1+742937	0123100101	07 43 12.1 +74 29 37.4	5.33	19.59 ± 0.25	$-0.61^{+0.01}_{-0.01}$	$-0.56^{+0.02}_{-0.02}$	AGN1
J074338.7+495431	0103862101	07 43 38.7 +49 54 31.1	12.22	1.27 ± 0.23	$-0.14^{+0.20}_{-0.20}$	$-0.47^{+0.24}_{-0.24}$	AGN1?
J074352.0+744258	0123100101	07 43 52.1 +74 42 59.0	9.30	1.99 ± 0.10	$-0.56^{+0.04}_{-0.04}$	$-0.49^{+0.08}_{-0.08}$	AGN1
J074359.7+744057	0123100101	07 43 59.7 +74 40 57.5	7.25	1.47 ± 0.08	$-0.85^{+0.03}_{-0.03}$	$-0.62^{+0.13}_{-0.14}$	star
J075117.9+180856[b]	0111100301	07 51 17.9 +18 08 56.1	2.37	1.65 ± 0.08	$-0.35^{+0.04}_{-0.04}$	$-0.46^{+0.06}_{-0.06}$	AGN1?
J080309.8+650807	0094400301	08 03 09.8 +65 08 07.6	12.10	2.91 ± 0.22	$-0.97^{+0.02}_{-0.01}$	$-1.00^{+1.30}_{-0.00}$	star
J080411.3+650906	0094400301	08 04 11.4 +65 09 06.2	9.49	1.39 ± 0.12	$0.06^{+0.09}_{-0.09}$	$-0.51^{+0.09}_{-0.09}$	
J080504.6+245156	0094530401	08 05 04.6 +24 51 56.4	7.23	1.07 ± 0.13	$-0.53^{+0.11}_{-0.11}$	$-0.56^{+0.20}_{-0.20}$	
J080608.1+244420	0094530401	08 06 08.2 +24 44 20.4	9.34	4.49 ± 0.30	$-0.74^{+0.05}_{-0.04}$	$-0.48^{+0.14}_{-0.13}$	AGN1
J083049.8+524908	0092800101	08 30 49.8 +52 49 08.2	8.81	1.40 ± 0.13	$-0.48^{+0.08}_{-0.08}$	$-0.85^{+0.09}_{-0.08}$	
J083737.1+254751	0025540301	08 37 37.2 +25 47 51.1	10.61	9.08 ± 0.37	$-0.47^{+0.04}_{-0.04}$	$-0.53^{+0.06}_{-0.06}$	AGN1
J083737.0+255151	0025540301	08 37 37.1 +25 51 51.2	12.25	2.89 ± 0.23	$-0.34^{+0.07}_{-0.08}$	$-0.52^{+0.10}_{-0.10}$	AGN2
J083838.6+253616	0025540301	08 38 38.6 +25 36 16.8	9.63	1.32 ± 0.16	$-0.57^{+0.09}_{-0.09}$	$-0.45^{+0.20}_{-0.19}$	AGN1
J083905.9+255010	0025540301	08 39 05.9 +25 50 10.5	10.89	1.02 ± 0.15	$-0.69^{+0.10}_{-0.10}$	$-1.00^{+0.54}_{-0.00}$	
J084026.2+650638[d]	0111400101	08 40 26.2 +65 06 38.5	9.56	1.21 ± 0.09	$-0.50^{+0.06}_{-0.07}$	$-0.27^{+0.12}_{-0.12}$	AGN1
J084651.7+344634	0103660201	08 46 51.7 +34 46 34.1	10.51	1.05 ± 0.15	$-0.71^{+0.08}_{-0.08}$	$-1.00^{+0.42}_{-0.00}$	AGN1
J085427.8+584158	0085030101	08 54 27.8 +58 41 58.9	9.06	2.92 ± 0.32	$-0.83^{+0.06}_{-0.06}$	$-0.71^{+0.23}_{-0.27}$	star
J085530.7+585129	0085030101	08 55 30.8 +58 51 29.1	7.42	1.21 ± 0.19	$-0.64^{+0.11}_{-0.11}$	$-1.00^{+0.47}_{-0.00}$	
J090729.1+620824	0110660201	09 07 29.2 +62 08 24.6	11.48	1.00 ± 0.17	$-0.26^{+0.15}_{-0.15}$	$-0.41^{+0.20}_{-0.20}$	GAL
J091043.4+054757	0083240201	09 10 43.4 +05 47 57.8	11.54	2.40 ± 0.19	$-0.80^{+0.04}_{-0.04}$	$-1.00^{+0.25}_{-0.00}$	star
J091828.4+513931	0084230601	09 18 28.5 +51 39 31.3	6.92	1.09 ± 0.11	$0.31^{+0.09}_{-0.10}$	$-0.39^{+0.09}_{-0.09}$	AGN1
J094526.2−085006	0017540101	09 45 26.2 −08 50 06.5	11.06	1.39 ± 0.20	$-0.50^{+0.12}_{-0.12}$	$-0.80^{+0.16}_{-0.18}$	
J094548.3−084824	0017540101	09 45 48.3 −08 48 24.6	10.87	1.02 ± 0.16	$-0.58^{+0.13}_{-0.13}$	$-0.24^{+0.30}_{-0.27}$	
J095054.5+393924	0111290101	09 50 54.5 +39 39 24.3	12.46	1.19 ± 0.13	$-0.59^{+0.08}_{-0.09}$	$-0.32^{+0.19}_{-0.18}$	AGN1
J095134.6−015451	0065790101	09 51 34.6 −01 54 51.6	10.87	1.05 ± 0.16	$-0.50^{+0.13}_{-0.13}$	$-0.72^{+0.19}_{-0.25}$	
J095218.9−013643	0065790101	09 52 19.0 −01 36 43.1	11.78	9.02 ± 0.51	$-0.77^{+0.03}_{-0.03}$	$0.41^{+0.09}_{-0.09}$	AGN1
J095309.7+013558	0070940101	09 53 09.8 +01 35 58.6	8.00	1.15 ± 0.19	$-0.64^{+0.12}_{-0.13}$	$-0.54^{+0.30}_{-0.43}$	
J095341.1+014204[c]	0070940101	09 53 41.2 +01 42 04.4	7.14	16.29 ± 0.72	$-0.62^{+0.04}_{-0.04}$	$-0.83^{+0.09}_{-0.10}$	CL
J095416.9+173627	0112850101	09 54 16.9 +17 36 27.8	11.71	4.01 ± 0.23	$-0.72^{+0.04}_{-0.04}$	$-0.62^{+0.10}_{-0.11}$	
J095509.6+174124	0112850101	09 55 09.6 +17 41 24.5	3.80	1.41 ± 0.10	$-0.55^{+0.06}_{-0.06}$	$-0.51^{+0.11}_{-0.11}$	
J095606.4+411814	0111290201	09 56 06.5 +41 18 14.7	9.12	1.23 ± 0.15	$-0.57^{+0.09}_{-0.10}$	$-0.62^{+0.18}_{-0.17}$	
J095955.2+251549	0041170201	09 59 55.3 +25 15 49.1	10.40	1.62 ± 0.10	$-0.77^{+0.04}_{-0.04}$	$-0.84^{+0.09}_{-0.09}$	star
J100020.6+252046	0041170201	10 00 20.6 +25 20 46.7	7.83	2.37 ± 0.10	$-0.78^{+0.02}_{-0.03}$	$-0.45^{+0.09}_{-0.09}$	
J100032.5+553626	0110930201	10 00 32.5 +55 36 26.4	12.64	1.90 ± 0.27	$-0.48^{+0.11}_{-0.11}$	$-0.30^{+0.21}_{-0.21}$	AGN2
J100100.0+252103	0041170201	10 01 00.1 +25 21 03.4	7.94	1.37 ± 0.07	$-0.65^{+0.04}_{-0.04}$	$-0.60^{+0.08}_{-0.09}$	
J100309.4+554135	0110930201	10 03 09.5 +55 41 35.3	10.26	1.48 ± 0.22	$-0.47^{+0.13}_{-0.13}$	$-0.62^{+0.20}_{-0.20}$	AGN1
J100828.8+535408	0070340201	10 08 28.8 +53 54 08.3	12.42	1.09 ± 0.11	$-0.60^{+0.08}_{-0.08}$	$-0.38^{+0.17}_{-0.17}$	
J100921.7+534926	0070340201	10 09 21.8 +53 49 26.7	9.03	1.82 ± 0.13	$-0.66^{+0.05}_{-0.05}$	$-0.59^{+0.11}_{-0.12}$	AGN1

Table 3. continued.

Name XBS...	Obs. ID	RA; Dec (J2000)	OffAxis arcmin	Rate $\times 10^{-2}$ cts/s	*HR*2	*HR*3	Class
(1)	(2)	(3)	(4)	(5)	(6)	(7)	(8)
J100926.5+533426	0070340201	10 09 26.6 +53 34 26.1	9.57	1.36 ± 0.12	$-0.45^{+0.08}_{-0.08}$	$-0.46^{+0.12}_{-0.13}$	AGN1
J101506.0+520157	0086750101	10 15 06.0 +52 01 57.9	13.00	1.41 ± 0.27	$-0.59^{+0.14}_{-0.14}$	$-1.00^{+0.63}_{-0.00}$	
J101511.8+520708[d]	0086750101	10 15 11.8 +52 07 08.0	10.02	1.72 ± 0.27	$-0.65^{+0.10}_{-0.10}$	$-0.71^{+0.20}_{-0.26}$	AGN1
J101706.5+520245[d]	0086750101	10 17 06.5 +52 02 45.6	10.28	1.83 ± 0.24	$-0.66^{+0.09}_{-0.09}$	$-0.99^{+0.36}_{-0.01}$	BL
J101838.0+411635	0028740301	10 18 38.0 +41 16 35.6	8.67	1.43 ± 0.10	$-0.71^{+0.04}_{-0.04}$	$-0.73^{+0.11}_{-0.11}$	
J101843.0+413515	0028740301	10 18 43.1 +41 35 15.5	10.02	1.93 ± 0.13	$-0.60^{+0.05}_{-0.05}$	$-0.52^{+0.10}_{-0.11}$	AGN2?
J101850.5+411506	0028740301	10 18 50.6 +41 15 06.6	10.32	4.33 ± 0.18	$-0.69^{+0.03}_{-0.03}$	$-0.51^{+0.07}_{-0.08}$	AGN1
J101922.6+412049	0028740301	10 19 22.6 +41 20 49.7	9.06	3.36 ± 0.14	$-0.44^{+0.04}_{-0.04}$	$-0.58^{+0.06}_{-0.05}$	AGN1
J102016.1+082143[d]	0093640301	10 20 16.1 +08 21 43.9	9.13	1.14 ± 0.14	$-0.40^{+0.10}_{-0.10}$	$-0.47^{+0.15}_{-0.15}$	
J102044.1+081424	0093640301	10 20 44.1 +08 14 24.7	10.99	3.35 ± 0.26	$-0.94^{+0.03}_{-0.03}$	$-1.00^{+0.76}_{-0.00}$	star
J102252.0+194837	0101040301	10 22 52.1 +19 48 37.9	9.65	1.42 ± 0.10	$-0.48^{+0.06}_{-0.06}$	$-0.51^{+0.09}_{-0.09}$	
J102412.3+042023	0108670101	10 24 12.3 +04 20 23.9	12.07	1.08 ± 0.07	$-0.48^{+0.06}_{-0.06}$	$-0.68^{+0.08}_{-0.08}$	AGN1?
J102417.5+041656	0108670101	10 24 17.5 +04 16 56.4	10.88	1.60 ± 0.08	$-0.55^{+0.04}_{-0.04}$	$-0.44^{+0.08}_{-0.08}$	
J103120.0+311404	0102040301	10 31 20.0 +31 14 04.1	12.08	1.68 ± 0.13	$-0.69^{+0.05}_{-0.05}$	$-0.28^{+0.14}_{-0.14}$	
J103154.1+310732	0102040301	10 31 54.1 +31 07 32.2	12.70	1.03 ± 0.10	$-0.34^{+0.08}_{-0.08}$	$-0.46^{+0.12}_{-0.12}$	AGN1
J103745.7+532353	0112810301	10 37 45.8 +53 23 53.8	10.73	1.03 ± 0.18	$-0.71^{+0.14}_{-0.14}$	$-0.18^{+0.44}_{-0.43}$	
J103909.4+205222	0059800101	10 39 09.4 +20 52 22.0	10.44	2.25 ± 0.20	$-0.55^{+0.07}_{-0.07}$	$-0.47^{+0.14}_{-0.14}$	
J103932.7+205426	0059800101	10 39 32.8 +20 54 26.0	6.04	1.94 ± 0.15	$-0.51^{+0.06}_{-0.06}$	$-0.67^{+0.10}_{-0.10}$	
J103935.8+533036	0112810301	10 39 35.9 +53 30 36.9	7.67	2.72 ± 0.31	$-0.55^{+0.09}_{-0.09}$	$-0.71^{+0.16}_{-0.16}$	AGN1
J103958.3+203848	0059800101	10 39 58.3 +20 38 48.2	12.11	1.11 ± 0.14	$-0.43^{+0.10}_{-0.11}$	$-0.42^{+0.17}_{-0.17}$	
J104026.9+204542	0059800101	10 40 26.9 +20 45 43.0	9.32	11.76 ± 0.37	$-0.58^{+0.03}_{-0.03}$	$-0.48^{+0.05}_{-0.05}$	AGN1
J104034.3+205110	0059800101	10 40 34.4 +20 51 10.4	9.51	1.16 ± 0.12	$-0.45^{+0.09}_{-0.09}$	$-0.76^{+0.11}_{-0.12}$	
J104425.0−013521	0125300101	10 44 25.0 −01 35 21.2	10.43	1.19 ± 0.09	$-0.56^{+0.06}_{-0.06}$	$-0.52^{+0.12}_{-0.12}$	AGN1
J104451.5−012227	0125300101	10 44 51.5 −01 22 27.7	5.45	1.23 ± 0.07	$-0.41^{+0.05}_{-0.05}$	$-0.57^{+0.08}_{-0.08}$	
J104509.3−012442	0125300101	10 45 09.3 −01 24 42.3	9.23	1.02 ± 0.08	$-0.73^{+0.05}_{-0.05}$	$-0.68^{+0.14}_{-0.14}$	
J104522.1−012843	0125300101	10 45 22.1 −01 28 43.3	12.94	4.45 ± 0.22	$-0.63^{+0.04}_{-0.04}$	$-0.46^{+0.08}_{-0.08}$	AGN1
J104912.8+330459	0055990201	10 49 12.8 +33 04 59.8	10.46	2.57 ± 0.18	$-0.45^{+0.06}_{-0.06}$	$-0.54^{+0.09}_{-0.10}$	AGN1?
J105014.9+331013	0055990201	10 50 14.9 +33 10 13.2	12.11	1.51 ± 0.15	$-0.55^{+0.08}_{-0.08}$	$-0.61^{+0.14}_{-0.14}$	
J105131.1+573439	0022740101	10 51 31.1 +57 34 39.1	11.41	2.06 ± 0.10	$-0.89^{+0.02}_{-0.02}$	$-0.33^{+0.13}_{-0.13}$	star
J105239.7+572431	0022740101	10 52 39.8 +57 24 31.1	4.33	1.68 ± 0.06	$-0.65^{+0.02}_{-0.02}$	$-0.62^{+0.05}_{-0.05}$	AGN1
J105316.9+573551	0022740101	10 53 17.0 +57 35 51.6	8.31	2.48 ± 0.09	$-0.59^{+0.02}_{-0.02}$	$-0.44^{+0.05}_{-0.05}$	AGN1
J105335.0+572540	0022740101	10 53 35.1 +57 25 40.7	7.53	1.77 ± 0.07	$-0.56^{+0.03}_{-0.03}$	$-0.54^{+0.05}_{-0.05}$	AGN1
J105339.7+573104	0022740101	10 53 39.7 +57 31 04.3	7.80	1.11 ± 0.06	$-0.68^{+0.03}_{-0.03}$	$-0.26^{+0.08}_{-0.08}$	AGN1
J105624.2−033522	0094800101	10 56 24.3 −03 35 22.9	9.05	1.34 ± 0.09	$-0.57^{+0.05}_{-0.05}$	$-0.73^{+0.08}_{-0.08}$	
J110050.6−344331	0112880201	11 00 50.6 −34 43 32.0	12.71	3.97 ± 0.18	$-0.48^{+0.04}_{-0.04}$	$-0.33^{+0.07}_{-0.07}$	
J110119.0−345303	0112880201	11 01 19.1 −34 53 03.8	12.61	1.33 ± 0.13	$-0.73^{+0.06}_{-0.06}$	$-0.40^{+0.17}_{-0.18}$	
J110244.1−344604	0112880201	11 02 44.2 −34 46 04.7	11.26	1.17 ± 0.11	$-0.49^{+0.08}_{-0.08}$	$-0.71^{+0.11}_{-0.11}$	
J110320.1+355803	0070340301	11 03 20.1 +35 58 03.7	4.40	7.76 ± 0.32	$-0.98^{+0.01}_{-0.01}$	$-1.00^{+0.76}_{-0.00}$	star
J110652.0−182738	0112630101	11 06 52.0 −18 27 38.9	7.47	1.14 ± 0.12	$-0.52^{+0.09}_{-0.09}$	$-0.99^{+0.20}_{-0.01}$	
J111654.8+180304	0099030101	11 16 54.8 +18 03 04.6	7.71	1.29 ± 0.13	$-0.76^{+0.06}_{-0.05}$	$-0.66^{+0.16}_{-0.17}$	AGN2
J111928.5+130250[d]	0093641101	11 19 28.6 +13 02 50.7	11.81	1.74 ± 0.18	$-0.60^{+0.08}_{-0.08}$	$-0.29^{+0.19}_{-0.18}$	AGN1
J111933.0+212756	0111290401	11 19 33.0 +21 27 56.7	10.33	1.59 ± 0.18	$-0.42^{+0.11}_{-0.11}$	$-0.70^{+0.15}_{-0.15}$	AGN1
J111942.1+211516	0111290401	11 19 42.2 +21 15 16.2	8.75	1.01 ± 0.14	$-0.76^{+0.09}_{-0.09}$	$0.17^{+0.26}_{-0.27}$	AGN1
J112022.3+125252	0093641101	11 20 22.3 +12 52 52.7	6.84	2.56 ± 0.19	$-0.66^{+0.06}_{-0.06}$	$-0.61^{+0.13}_{-0.13}$	AGN1
J112046.7+125429	0093641101	11 20 46.8 +12 54 30.0	9.21	3.07 ± 0.24	$-0.67^{+0.06}_{-0.06}$	$-0.66^{+0.13}_{-0.14}$	AGN1
J113106.9+312518	0102040201	11 31 07.0 +31 25 18.2	11.18	1.33 ± 0.12	$-0.53^{+0.08}_{-0.08}$	$-0.15^{+0.14}_{-0.14}$	AGN1
J113121.8+310252	0102040201	11 31 21.8 +31 02 52.6	11.58	1.67 ± 0.12	$-0.03^{+0.07}_{-0.07}$	$-0.35^{+0.08}_{-0.08}$	AGN2
J113128.6−195903	0042341001	11 31 28.7 −19 59 03.4	7.35	1.50 ± 0.13	$-0.67^{+0.07}_{-0.07}$	$-0.73^{+0.14}_{-0.14}$	
J113148.7+311358	0102040201	11 31 48.7 +31 13 58.8	8.45	1.54 ± 0.10	$0.10^{+0.06}_{-0.07}$	$-0.43^{+0.07}_{-0.07}$	AGN2
J113837.9−373402	0112210101	11 38 37.9 −37 34 02.0	11.33	1.79 ± 0.12	$-0.60^{+0.05}_{-0.05}$	$-0.44^{+0.11}_{-0.10}$	AGN1?
J115317.9+364712	0112551401	11 53 17.9 +36 47 12.5	12.82	1.08 ± 0.21	$-0.46^{+0.19}_{-0.19}$	$-1.00^{+0.76}_{-0.00}$	
J115846.9+551625	0090020101	11 58 46.9 +55 16 25.4	12.98	1.74 ± 0.25	$-0.65^{+0.10}_{-0.10}$	$-0.98^{+0.45}_{-0.02}$	AGN1
J120359.1+443715	0109141401	12 03 59.2 +44 37 15.1	10.37	1.37 ± 0.07	$-0.73^{+0.03}_{-0.03}$	$-0.63^{+0.09}_{-0.09}$	
J120413.7+443149	0109141401	12 04 13.8 +44 31 49.7	11.47	1.28 ± 0.08	$-0.60^{+0.05}_{-0.04}$	$-0.70^{+0.08}_{-0.08}$	

Table 3. continued.

Name XBS...	Obs. ID	RA; Dec (J2000)	OffAxis arcmin	Rate $\times 10^{-2}$ cts/s	*HR*2	*HR*3	Class
(1)	(2)	(3)	(4)	(5)	(6)	(7)	(8)
J121501.7+140113	0112610101	12 15 01.8 +14 01 13.7	11.06	1.84 ± 0.10	$-0.58^{+0.04}_{-0.04}$	$-0.68^{+0.07}_{-0.08}$	
J122017.5+752217[c]	0124110101	12 20 17.5 +75 22 17.8	6.45	10.78 ± 0.35	$-0.87^{+0.03}_{-0.03}$	$-1.0^{+0.0}_{-0.12}$	GAL
J122350.4+752231	0124110101	12 23 50.5 +75 22 31.7	9.04	1.49 ± 0.13	$-0.55^{+0.07}_{-0.07}$	$-0.72^{+0.11}_{-0.11}$	AGN1
J122628.9+333626	0070340501	12 26 28.9 +33 36 26.6	10.57	1.08 ± 0.13	$-0.83^{+0.06}_{-0.06}$	$-0.64^{+0.25}_{-0.32}$	
J122655.1+012002	0110990201	12 26 55.1 +01 20 02.8	10.96	1.32 ± 0.16	$-0.80^{+0.07}_{-0.07}$	$-0.78^{+0.20}_{-0.20}$	
J122656.5+013126	0110990201	12 26 56.6 +01 31 26.2	5.85	1.41 ± 0.12	$-0.11^{+0.09}_{-0.09}$	$-0.34^{+0.10}_{-0.10}$	AGN2?
J122658.1+333246[c,d]	0070340501	12 26 58.1 +33 32 46.5	3.68	7.15 ± 0.25	$-0.51^{+0.04}_{-0.04}$	$-0.80^{+0.04}_{-0.04}$	CL
J122751.2+333842	0070340501	12 27 51.3 +33 38 43.0	9.80	1.87 ± 0.17	$-0.85^{+0.04}_{-0.04}$	$-0.39^{+0.23}_{-0.23}$	star
J122803.7+333957	0070340501	12 28 03.7 +33 39 57.1	12.60	1.15 ± 0.16	$-0.58^{+0.10}_{-0.10}$	$-1.00^{+0.31}_{-0.00}$	
J122837.3+015720	0126700301	12 28 37.3 +01 57 20.6	9.33	2.16 ± 0.09	$-0.88^{+0.02}_{-0.02}$	$-0.99^{+0.03}_{-0.01}$	star
J122942.3+015525	0126700301	12 29 42.4 +01 55 25.4	11.80	2.06 ± 0.11	$-0.84^{+0.03}_{-0.03}$	$-0.83^{+0.09}_{-0.09}$	star
J123036.2+642531	0124900101	12 30 36.3 +64 25 31.8	12.66	1.09 ± 0.09	$-0.70^{+0.05}_{-0.06}$	$-0.49^{+0.15}_{-0.16}$	
J123116.5+641115	0124900101	12 31 16.5 +64 11 15.1	3.46	1.06 ± 0.06	$-0.51^{+0.05}_{-0.05}$	$-0.45^{+0.09}_{-0.09}$	
J123208.7+640304	0124900101	12 32 08.8 +64 03 04.3	12.00	1.16 ± 0.11	$-0.82^{+0.05}_{-0.05}$	$-0.91^{+0.11}_{-0.07}$	star
J123218.5+640311	0124900101	12 32 18.6 +64 03 11.3	12.30	1.48 ± 0.12	$-0.58^{+0.06}_{-0.06}$	$-0.52^{+0.13}_{-0.12}$	
J123538.6+621644[d]	0111550101	12 35 38.6 +62 16 44.7	8.98	2.06 ± 0.09	$-0.59^{+0.03}_{-0.03}$	$-0.59^{+0.07}_{-0.07}$	AGN1
J123549.1−395026	0006220201	12 35 49.1 −39 50 26.8	5.25	3.23 ± 0.10	$-0.94^{+0.01}_{-0.01}$	$-1.00^{+0.14}_{-0.00}$	star
J123600.7−395217	0006220201	12 36 00.7 −39 52 18.0	5.62	17.71 ± 0.22	$-0.77^{+0.01}_{-0.01}$	$-0.77^{+0.02}_{-0.02}$	star
J123759.6+621102	0111550101	12 37 59.7 +62 11 02.9	8.51	1.95 ± 0.10	$-0.59^{+0.04}_{-0.04}$	$-0.55^{+0.08}_{-0.08}$	AGN1
J123800.9+621338	0111550101	12 38 00.9 +62 13 38.5	8.47	1.48 ± 0.08	$-0.78^{+0.03}_{-0.03}$	$-0.36^{+0.13}_{-0.12}$	AGN1
J124214.1−112512	0136950201	12 42 14.1 −11 25 12.3	8.24	1.55 ± 0.09	$-0.57^{+0.05}_{-0.05}$	$-0.33^{+0.10}_{-0.10}$	
J124557.6+022659	0051760101	12 45 57.7 +02 26 60.0	10.56	1.34 ± 0.17	$-0.59^{+0.09}_{-0.09}$	$-0.59^{+0.16}_{-0.17}$	
J124607.6+022153	0051760101	12 46 07.7 +02 21 53.6	6.81	2.41 ± 0.17	$-0.62^{+0.05}_{-0.05}$	$-1.00^{+0.10}_{-0.00}$	AGN1
J124641.8+022412	0051760101	12 46 41.8 +02 24 12.1	2.78	3.00 ± 0.17	$-0.58^{+0.05}_{-0.05}$	$-0.48^{+0.09}_{-0.09}$	AGN1
J124647.9+020955	0051760101	12 46 48.0 +02 09 55.8	12.52	1.03 ± 0.19	$-0.39^{+0.14}_{-0.14}$	$-0.93^{+0.10}_{-0.06}$	
J124903.6−061049[d]	0060370201	12 49 03.6 −06 10 49.2	11.63	2.54 ± 0.13	$-0.61^{+0.04}_{-0.04}$	$-0.55^{+0.08}_{-0.08}$	AGN1
J124914.6−060910	0060370201	12 49 14.7 −06 09 11.0	9.73	1.06 ± 0.08	$-0.50^{+0.06}_{-0.06}$	$-0.75^{+0.08}_{-0.08}$	
J124938.7−060444	0060370201	12 49 38.7 −06 04 44.9	8.20	35.88 ± 0.41	$-0.88^{+0.01}_{-0.01}$	$-0.85^{+0.02}_{-0.02}$	star
J124949.4−060722	0060370201	12 49 49.5 −06 07 22.0	11.93	1.35 ± 0.11	$-0.58^{+0.06}_{-0.06}$	$-0.43^{+0.12}_{-0.12}$	
J125457.2+564940	0081340201	12 54 57.2 +56 49 40.7	10.79	1.72 ± 0.13	$-0.46^{+0.06}_{-0.06}$	$-0.63^{+0.09}_{-0.10}$	AGN1
J125648.4+570349	0081340201	12 56 48.5 +57 03 49.1	12.37	1.19 ± 0.12	$-0.38^{+0.09}_{-0.09}$	$-0.72^{+0.11}_{-0.11}$	
J130616.8+175923	0017940101	13 06 16.9 +17 59 23.7	8.09	1.01 ± 0.06	$-0.50^{+0.05}_{-0.05}$	$-0.44^{+0.08}_{-0.08}$	
J130619.7−233857	0002940101	13 06 19.7 −23 38 57.9	10.84	2.83 ± 0.32	$-0.68^{+0.08}_{-0.08}$	$-0.56^{+0.21}_{-0.21}$	
J130658.1−234849	0002940101	13 06 58.2 −23 48 49.7	8.60	1.39 ± 0.19	$-0.52^{+0.11}_{-0.11}$	$-0.51^{+0.21}_{-0.19}$	AGN1
J132038.0+341124	0093640401	13 20 38.1 +34 11 24.3	3.10	2.91 ± 0.13	$-0.43^{+0.04}_{-0.04}$	$-0.48^{+0.06}_{-0.06}$	AGN1
J132052.5+341742	0093640401	13 20 52.5 +34 17 42.9	10.01	1.50 ± 0.12	$-0.53^{+0.07}_{-0.07}$	$-0.58^{+0.12}_{-0.12}$	AGN1
J132101.6+340656	0093640401	13 21 01.6 +34 06 56.6	5.61	3.88 ± 0.15	$-0.71^{+0.03}_{-0.03}$	$-0.57^{+0.08}_{-0.07}$	AGN1
J132105.5+341459[d]	0093640401	13 21 05.5 +34 14 59.4	9.10	2.74 ± 0.15	$-0.56^{+0.05}_{-0.05}$	$-0.56^{+0.09}_{-0.09}$	
J133023.8+241707	0100240201	13 30 23.8 +24 17 07.3	6.22	1.15 ± 0.07	$-0.68^{+0.04}_{-0.05}$	$-0.41^{+0.12}_{-0.11}$	AGN1
J133026.6+241520[d]	0100240201	13 30 26.7 +24 15 20.5	4.91	2.08 ± 0.09	$-0.82^{+0.02}_{-0.03}$	$-0.57^{+0.10}_{-0.10}$	
J133120.2+242305	0100240201	13 31 20.2 +24 23 05.1	11.78	1.77 ± 0.11	$-0.56^{+0.05}_{-0.05}$	$-0.60^{+0.09}_{-0.09}$	
J133232.6+111220[d]	0061940101	13 32 32.7 +11 12 20.7	10.70	1.05 ± 0.18	$-0.35^{+0.15}_{-0.15}$	$-1.00^{+0.31}_{-0.00}$	
J133321.2+503102	0111160101	13 33 21.3 +50 31 02.2	9.21	1.79 ± 0.08	$-0.91^{+0.02}_{-0.02}$	$-0.49^{+0.16}_{-0.16}$	star
J133626.9−342636	0111570201	13 36 26.9 −34 26 36.7	11.19	1.00 ± 0.08	$-0.90^{+0.03}_{-0.03}$	$-1.00^{+0.42}_{-0.00}$	star
J133807.5+242411	0096010101	13 38 07.6 +24 24 11.8	11.17	1.69 ± 0.11	$-0.66^{+0.05}_{-0.05}$	$-0.65^{+0.10}_{-0.10}$	AGN1
J133942.6−315004	0035940301	13 39 42.6 −31 50 04.8	11.91	1.67 ± 0.11	$-0.36^{+0.05}_{-0.06}$	$-0.20^{+0.08}_{-0.08}$	AGN1?
J134732.0+582103	0112250201	13 47 32.0 +58 21 03.8	8.38	3.43 ± 0.13	$-0.86^{+0.02}_{-0.02}$	$-0.81^{+0.07}_{-0.08}$	star
J134749.9+582111	0112250201	13 47 49.9 +58 21 11.0	8.53	12.44 ± 0.24	$-0.60^{+0.02}_{-0.02}$	$-0.54^{+0.03}_{-0.03}$	AGN1
J140100.0−110942	0109910101	14 01 00.0 −11 09 42.2	8.70	1.12 ± 0.07	$-0.57^{+0.05}_{-0.05}$	$-0.66^{+0.09}_{-0.09}$	
J140102.0−111224	0109910101	14 01 02.0 −11 12 24.3	9.27	8.34 ± 0.18	$-0.52^{+0.02}_{-0.02}$	$-0.46^{+0.03}_{-0.03}$	AGN2?
J140127.7+025605	0098010101	14 01 27.7 +02 56 05.4	7.25	7.04 ± 0.19	$-0.38^{+0.02}_{-0.02}$	$-0.53^{+0.04}_{-0.04}$	AGN1

Table 3. continued.

Name XBS...	Obs. ID	RA; Dec (J2000)	OffAxis arcmin	Rate $\times 10^{-2}$ cts/s	*HR*2	*HR*3	Class
(1)	(2)	(3)	(4)	(5)	(6)	(7)	(8)
J140219.6−110458	0109910101	14 02 19.7 −11 04 58.8	11.40	1.16 ± 0.08	$-0.94^{+0.02}_{-0.02}$	$-0.16^{+0.29}_{-0.27}$	star
J140921.1+261336	0092850501	14 09 21.2 +26 13 36.8	4.78	1.24 ± 0.06	$-0.32^{+0.04}_{-0.05}$	$-0.53^{+0.06}_{-0.06}$	
J140936.9+261632	0092850501	14 09 36.9 +26 16 32.1	3.44	1.11 ± 0.06	$-0.92^{+0.02}_{-0.02}$	$-0.70^{+0.16}_{-0.17}$	star
J141235.8−030909	0013140101	14 12 35.8 −03 09 09.3	10.29	1.72 ± 0.15	$-0.40^{+0.08}_{-0.08}$	$-0.59^{+0.11}_{-0.11}$	
J141523.8+113737	0112250301	14 15 23.8 +11 37 37.3	9.64	1.16 ± 0.09	$-0.70^{+0.05}_{-0.05}$	$-0.54^{+0.15}_{-0.15}$	
J141531.5+113156	0112250301	14 15 31.6 +11 31 56.2	4.15	3.15 ± 0.12	$-0.55^{+0.03}_{-0.03}$	$-0.47^{+0.06}_{-0.06}$	AGN1
J141643.8+521434	0127921001	14 16 43.8 +52 14 34.2	10.17	1.41 ± 0.07	$-0.58^{+0.04}_{-0.04}$	$-0.50^{+0.08}_{-0.08}$	
J141658.8+521202	0127921001	14 16 58.8 +52 12 02.8	11.98	1.01 ± 0.08	$-0.71^{+0.05}_{-0.05}$	$-0.28^{+0.14}_{-0.14}$	
J141722.6+251335	0109960101	14 17 22.7 +25 13 35.2	9.86	1.33 ± 0.12	$-0.69^{+0.06}_{-0.06}$	$-1.00^{+0.21}_{-0.00}$	AGN1
J141736.3+523028	0127921001	14 17 36.3 +52 30 28.5	7.67	1.15 ± 0.06	$-0.65^{+0.04}_{-0.04}$	$-0.40^{+0.09}_{-0.09}$	AGN1
J141809.1+250040	0109960101	14 18 09.1 +25 00 40.3	7.85	1.31 ± 0.09	$-0.59^{+0.06}_{-0.05}$	$-0.47^{+0.12}_{-0.12}$	AGN1
J141830.5+251052[c]	0109960101	14 18 30.5 +25 10 52.6	7.58	14.99 ± 0.37	$-0.52^{+0.04}_{-0.04}$	$-0.65^{+0.07}_{-0.07}$	CL
J142800.1+424409	0111850201	14 28 00.1 +42 44 09.5	7.10	1.53 ± 0.07	$-0.90^{+0.02}_{-0.02}$	$-0.48^{+0.17}_{-0.16}$	star
J142901.2+423048	0111850201	14 29 01.2 +42 30 48.8	10.84	1.70 ± 0.11	$-0.98^{+0.01}_{-0.01}$	$0.56^{+0.28}_{-0.30}$	star
J143835.1+642928	0111530101	14 38 35.1 +64 29 28.3	12.34	1.31 ± 0.09	$0.18^{+0.07}_{-0.07}$	$-0.37^{+0.07}_{-0.06}$	AGN1?
J143923.1+640912	0111530101	14 39 23.2 +64 09 12.4	8.60	2.36 ± 0.09	$-0.99^{+0.01}_{-0.01}$	$-0.51^{+0.40}_{-0.46}$	star
J144021.0+642144	0111530101	14 40 21.0 +64 21 44.1	9.79	1.42 ± 0.07	$-0.47^{+0.04}_{-0.04}$	$-0.37^{+0.07}_{-0.08}$	
J144937.5+090826	0057560301	14 49 37.6 +09 08 26.0	8.83	1.86 ± 0.10	$-0.52^{+0.04}_{-0.04}$	$-0.54^{+0.07}_{-0.07}$	
J144945.8+085921	0057560301	14 49 45.9 +08 59 21.8	4.14	1.04 ± 0.06	$-0.56^{+0.05}_{-0.04}$	$-0.51^{+0.09}_{-0.09}$	
J145857.1−313535	0067750101	14 58 57.1 −31 35 36.0	8.89	1.03 ± 0.08	$-0.55^{+0.06}_{-0.06}$	$-0.45^{+0.12}_{-0.12}$	
J150428.3+101856	0070740301	15 04 28.4 +10 18 57.0	9.91	1.67 ± 0.17	$-0.37^{+0.09}_{-0.09}$	$-1.00^{+0.13}_{-0.00}$	AGN1
J151815.0+060851	0018741001	15 18 15.1 +06 08 51.5	9.43	1.12 ± 0.19	$-0.77^{+0.10}_{-0.10}$	$0.22^{+0.33}_{-0.32}$	
J151832.3+062357	0018741001	15 18 32.4 +06 23 57.6	10.39	1.72 ± 0.27	$-0.72^{+0.10}_{-0.09}$	$-0.70^{+0.23}_{-0.27}$	GAL
J153156.6−082610	0100240801	15 31 56.6 −08 26 11.0	8.75	1.32 ± 0.11	$-0.96^{+0.02}_{-0.02}$	$-1.00^{+0.96}_{-0.00}$	star
J153205.7−082952	0100240801	15 32 05.8 −08 29 52.6	4.77	1.05 ± 0.08	$-0.45^{+0.07}_{-0.06}$	$-0.79^{+0.08}_{-0.08}$	AGN1
J153419.0+011808	0112190401	15 34 19.1 +01 18 08.2	10.91	1.37 ± 0.15	$-0.62^{+0.08}_{-0.08}$	$-0.30^{+0.18}_{-0.18}$	AGN1
J153452.3+013104[d]	0112190401	15 34 52.4 +01 31 04.6	10.57	9.44 ± 0.38	$-0.39^{+0.04}_{-0.04}$	$-0.55^{+0.05}_{-0.05}$	AGN1
J153456.1+013033	0112190401	15 34 56.2 +01 30 33.4	9.89	3.05 ± 0.23	$-0.64^{+0.05}_{-0.05}$	$-0.64^{+0.11}_{-0.11}$	AGN1
J160645.9+081525	0067340601	16 06 46.0 +08 15 25.1	12.61	1.28 ± 0.17	$0.81^{+0.08}_{-0.08}$	$-0.23^{+0.10}_{-0.10}$	AGN2?
J160706.6+075709	0067340601	16 07 06.7 +07 57 09.5	7.90	1.49 ± 0.14	$-0.65^{+0.07}_{-0.06}$	$-0.34^{+0.16}_{-0.16}$	AGN1
J160731.5+081202	0067340601	16 07 31.6 +08 12 02.9	8.43	1.67 ± 0.14	$-0.75^{+0.05}_{-0.05}$	$-0.44^{+0.17}_{-0.18}$	AGN1?
J161544.2+121708	0103460801	16 15 44.2 +12 17 08.3	11.87	1.41 ± 0.18	$-0.64^{+0.09}_{-0.09}$	$-0.18^{+0.22}_{-0.24}$	
J161615.1+121353	0103460801	16 16 15.1 +12 13 53.2	3.65	1.11 ± 0.10	$-0.65^{+0.07}_{-0.07}$	$-1.00^{+0.19}_{-0.00}$	
J161825.4+124145	0103461001	16 18 25.5 +12 41 45.5	12.82	1.14 ± 0.15	$-0.76^{+0.08}_{-0.09}$	$-0.17^{+0.31}_{-0.31}$	AGN1
J162813.9+780342	0061940301	16 28 14.0 +78 03 42.7	10.92	2.64 ± 0.34	$-0.67^{+0.09}_{-0.09}$	$-0.33^{+0.24}_{-0.24}$	AGN1
J162911.1+780442	0061940301	16 29 11.2 +78 04 42.7	8.13	1.66 ± 0.22	$-0.81^{+0.08}_{-0.08}$	$-1.00^{+0.76}_{-0.00}$	star
J162923.3+781306	0061940301	16 29 23.4 +78 13 06.6	5.11	1.41 ± 0.18	$-0.19^{+0.13}_{-0.13}$	$-0.68^{+0.14}_{-0.14}$	
J162944.8+781128	0061940301	16 29 44.8 +78 11 28.5	3.57	1.77 ± 0.20	$-0.99^{+0.02}_{-0.01}$	$-1.00^{+2.00}_{-0.00}$	star
J163141.1+781239	0061940301	16 31 41.2 +78 12 39.3	2.99	1.39 ± 0.17	$-0.61^{+0.10}_{-0.11}$	$-0.84^{+0.15}_{-0.16}$	AGN1
J163223.6+052547	0112230301	16 32 23.6 +05 25 47.1	10.44	1.89 ± 0.14	$-0.71^{+0.05}_{-0.05}$	$-0.23^{+0.14}_{-0.15}$	AGN1
J163309.8+571039	0049540101	16 33 09.8 +57 10 39.3	9.67	2.87 ± 0.27	$-0.43^{+0.07}_{-0.07}$	$-0.49^{+0.10}_{-0.11}$	AGN1
J163332.3+570520	0049540101	16 33 32.4 +57 05 20.2	7.90	1.03 ± 0.16	$-0.84^{+0.06}_{-0.06}$	$-1.00^{+0.63}_{-0.00}$	AGN1?
J163427.5+781002	0061940301	16 34 27.6 +78 10 02.5	11.00	1.79 ± 0.30	$-0.62^{+0.13}_{-0.14}$	$-0.71^{+0.24}_{-0.26}$	AGN1
J164237.9+030014[d]	0067340501	16 42 38.0 +03 00 14.3	11.90	1.22 ± 0.14	$-0.63^{+0.09}_{-0.08}$	$-0.38^{+0.20}_{-0.20}$	
J165313.3+021645	0101640101	16 53 13.3 +02 16 45.6	8.16	1.36 ± 0.13	$-0.96^{+0.03}_{-0.02}$	$-1.00^{+1.30}_{-0.00}$	star
J165314.4+141943	0113070101	16 53 14.5 +14 19 43.6	11.13	1.54 ± 0.21	$-0.42^{+0.12}_{-0.12}$	$-0.67^{+0.17}_{-0.16}$	
J165406.6+142123	0113070101	16 54 06.6 +14 21 23.6	3.89	1.12 ± 0.13	$-0.49^{+0.11}_{-0.10}$	$-0.76^{+0.14}_{-0.14}$	
J165425.3+142159	0113070101	16 54 25.4 +14 21 59.3	7.44	11.86 ± 0.53	$-0.63^{+0.03}_{-0.03}$	$-0.61^{+0.07}_{-0.07}$	AGN1
J165448.5+141311	0113070101	16 54 48.5 +14 13 11.6	12.71	6.78 ± 0.56	$-0.54^{+0.07}_{-0.07}$	$-0.42^{+0.13}_{-0.13}$	AGN2
J165710.5+352024	0111060101	16 57 10.5 +35 20 24.0	7.98	1.93 ± 0.20	$-0.90^{+0.04}_{-0.04}$	$-1.00^{+0.76}_{-0.00}$	star
J165800.7+352333	0111060101	16 58 00.7 +35 23 33.5	3.73	1.40 ± 0.13	$-0.51^{+0.08}_{-0.08}$	$-0.69^{+0.12}_{-0.13}$	AGN2?
J172230.6+341344	0102040101	17 22 30.7 +34 13 44.0	11.20	1.74 ± 0.25	$-0.65^{+0.10}_{-0.11}$	$-0.31^{+0.28}_{-0.27}$	AGN1
J185518.7−462504	0067340101	18 55 18.8 −46 25 04.0	6.69	1.55 ± 0.20	$-0.40^{+0.09}_{-0.09}$	$-1.00^{+0.13}_{-0.00}$	AGN1
J185613.7−462239[a]	0067340101	18 56 13.8 −46 22 39.2	10.44	3.02 ± 0.30	$-0.47^{+0.07}_{-0.07}$	$0.01^{+0.11}_{-0.10}$	AGN1
J193138.9−725115	0081341001	19 31 39.0 −72 51 15.0	12.10	1.48 ± 0.16	$-0.42^{+0.09}_{-0.09}$	$-0.62^{+0.13}_{-0.14}$	AGN1

Table 3. continued.

Name XBS...	Obs. ID	RA; Dec (J2000)	OffAxis arcmin	Rate $\times 10^{-2}$ cts/s	*HR*2	*HR*3	Class
(1)	(2)	(3)	(4)	(5)	(6)	(7)	(8)
J193248.8−723355[a]	0081341001	19 32 48.8 −72 33 55.2	8.39	1.37 ± 0.12	$-0.23^{+0.08}_{-0.08}$	$-0.08^{+0.10}_{-0.10}$	AGN2?
J204043.4−004548[a]	0111180201	20 40 43.5 −00 45 48.2	10.55	1.29 ± 0.15	$0.04^{+0.11}_{-0.11}$	$-0.35^{+0.12}_{-0.12}$	AGN2
J204047.5−005853	0111180201	20 40 47.6 −00 58 53.8	11.50	1.05 ± 0.14	$-0.33^{+0.12}_{-0.12}$	$-0.64^{+0.14}_{-0.15}$	BL?
J204159.2−321439	0111510101	20 41 59.3 −32 14 40.0	11.80	3.36 ± 0.23	$-0.54^{+0.05}_{-0.05}$	$-0.79^{+0.08}_{-0.07}$	AGN1
J204204.1−321601	0111510101	20 42 04.1 −32 16 01.5	10.68	1.39 ± 0.14	$-0.52^{+0.08}_{-0.08}$	$-0.80^{+0.10}_{-0.11}$	AGN1
J204208.2−323523	0111510101	20 42 08.3 −32 35 23.6	9.78	1.16 ± 0.12	$-0.63^{+0.08}_{-0.08}$	$-0.89^{+0.09}_{-0.10}$	AGN1
J204548.4−025234	0112600501	20 45 48.4 −02 52 34.4	8.74	1.29 ± 0.14	$-0.38^{+0.10}_{-0.10}$	$-0.76^{+0.12}_{-0.11}$	AGN1
J205411.9−160804	0083210101	20 54 11.9 −16 08 04.8	12.55	1.97 ± 0.23	$-0.58^{+0.09}_{-0.09}$	$-0.69^{+0.16}_{-0.16}$	AGN1
J205429.9−154937	0083210101	20 54 30.0 −15 49 37.8	6.59	1.14 ± 0.13	$-0.65^{+0.08}_{-0.08}$	$-0.80^{+0.14}_{-0.19}$	AGN1
J205635.7−044717[a]	0112190601	20 56 35.8 −04 47 17.9	9.96	3.41 ± 0.21	$-0.65^{+0.04}_{-0.05}$	$-0.48^{+0.11}_{-0.11}$	AGN1
J205829.9−423634[a]	0081340401	20 58 30.0 −42 36 35.0	2.42	5.01 ± 0.19	$-0.57^{+0.03}_{-0.03}$	$-0.47^{+0.06}_{-0.06}$	AGN1
J205847.0−423704	0081340401	20 58 47.0 −42 37 04.7	4.11	1.71 ± 0.12	$-0.93^{+0.03}_{-0.03}$	$-1.00^{+0.54}_{-0.00}$	star
J210325.4−112011	0041150101	21 03 25.4 −11 20 11.5	11.29	1.01 ± 0.09	$-0.49^{+0.07}_{-0.07}$	$-0.22^{+0.12}_{-0.13}$	AGN1
J210355.3−121858	0038540301	21 03 55.3 −12 18 58.2	11.02	1.56 ± 0.17	$-0.50^{+0.09}_{-0.09}$	$-0.80^{+0.12}_{-0.10}$	AGN1
J212635.8−445046	0088020201	21 26 35.8 −44 50 46.1	11.25	3.03 ± 0.25	$-0.92^{+0.03}_{-0.03}$	$-0.37^{+0.32}_{-0.32}$	star
J212759.5−443924	0088020201	21 27 59.6 −44 39 24.7	9.99	1.08 ± 0.12	$-0.65^{+0.08}_{-0.08}$	$-0.47^{+0.18}_{-0.19}$	
J213002.3−153414[a]	0103060101	21 30 02.3 −15 34 14.1	12.83	3.95 ± 0.21	$-0.65^{+0.04}_{-0.04}$	$-0.50^{+0.09}_{-0.09}$	AGN1
J213719.6−433347	0109463501	21 37 19.6 −43 33 47.0	10.85	2.41 ± 0.27	$-0.27^{+0.10}_{-0.10}$	$-0.74^{+0.11}_{-0.11}$	AGN1
J213729.7−423601	0061940201	21 37 29.8 −42 36 01.6	7.02	1.51 ± 0.23	$-0.56^{+0.12}_{-0.13}$	$-0.33^{+0.25}_{-0.27}$	
J213733.2−434800	0109463501	21 37 33.2 −43 48 00.9	7.07	1.03 ± 0.14	$-0.91^{+0.06}_{-0.06}$	$0.05^{+0.48}_{-0.52}$	AGN1
J213757.6−422334	0061940201	21 37 57.6 −42 23 34.2	12.68	1.37 ± 0.27	$-0.59^{+0.15}_{-0.16}$	$-0.15^{+0.36}_{-0.34}$	
J213820.2−142536	0092850201	21 38 20.2 −14 25 37.0	11.17	2.10 ± 0.17	$-0.29^{+0.07}_{-0.07}$	$-0.45^{+0.10}_{-0.10}$	AGN1
J213824.0−423019[a]	0061940201	21 38 24.0 −42 30 19.2	6.50	2.88 ± 0.27	$-0.62^{+0.08}_{-0.08}$	$-0.36^{+0.18}_{-0.18}$	AGN1
J213829.8−423958	0061940201	21 38 29.9 −42 39 58.9	5.59	1.45 ± 0.19	$-0.66^{+0.10}_{-0.10}$	$-0.50^{+0.24}_{-0.24}$	AGN1
J213840.5−424241	0061940201	21 38 40.6 −42 42 41.3	8.91	1.89 ± 0.26	$-1.00^{+0.07}_{-0.00}$	–	star
J213852.2−434714	0109463501	21 38 52.3 −43 47 14.9	11.21	1.32 ± 0.23	$-0.68^{+0.11}_{-0.12}$	$-0.36^{+0.31}_{-0.33}$	AGN1
J214041.4−234720[a]	0008830101	21 40 41.5 −23 47 20.1	9.80	3.46 ± 0.22	$-0.57^{+0.05}_{-0.05}$	$-0.39^{+0.10}_{-0.10}$	AGN1
J215218.0−302721	0103060401	21 52 18.1 −30 27 21.6	4.80	1.15 ± 0.08	$-0.69^{+0.05}_{-0.05}$	$-0.55^{+0.12}_{-0.12}$	
J215244.2−302407	0103060401	21 52 44.3 −30 24 07.4	11.03	3.28 ± 0.16	$-0.65^{+0.04}_{-0.04}$	$-0.68^{+0.08}_{-0.07}$	AGN1
J215323.7+173018	0111270101	21 53 23.7 +17 30 18.6	12.09	1.08 ± 0.16	$-0.37^{+0.12}_{-0.13}$	$-0.73^{+0.16}_{-0.14}$	star
J220320.8+184930	0130920101	22 03 20.9 +18 49 30.3	4.03	1.58 ± 0.11	$-0.49^{+0.06}_{-0.06}$	$-0.39^{+0.10}_{-0.10}$	AGN2?
J220446.8−014535	0012440301	22 04 46.8 −01 45 35.6	11.22	1.23 ± 0.10	$-0.45^{+0.07}_{-0.07}$	$-0.69^{+0.10}_{-0.09}$	AGN1
J220601.5−015346[a]	0012440301	22 06 01.5 −01 53 47.0	12.92	1.85 ± 0.12	$-0.41^{+0.06}_{-0.06}$	$-0.41^{+0.09}_{-0.09}$	AGN1
J221623.3−174317	0106660101	22 16 23.4 −17 43 17.9	12.29	1.15 ± 0.08	$-0.55^{+0.05}_{-0.06}$	$-0.57^{+0.10}_{-0.10}$	AGN1
J221722.4−082018	0009650201	22 17 22.5 −08 20 18.2	8.18	1.76 ± 0.13	$-0.38^{+0.07}_{-0.07}$	$-0.48^{+0.10}_{-0.10}$	AGN1
J221729.3−081154	0009650201	22 17 29.4 −08 11 54.2	11.12	2.00 ± 0.16	$-0.54^{+0.06}_{-0.06}$	$-0.53^{+0.12}_{-0.11}$	AGN1
J221750.4−083210	0009650201	22 17 50.4 −08 32 10.8	11.28	1.32 ± 0.12	$-0.79^{+0.06}_{-0.06}$	$-1.00^{+0.37}_{-0.00}$	star
J221821.9−081332	0009650201	22 18 22.0 −08 13 33.0	9.91	2.10 ± 0.13	$-0.63^{+0.05}_{-0.05}$	$-0.85^{+0.07}_{-0.07}$	AGN1
J221951.6+120123[d]	0103861201	22 19 51.6 +12 01 23.1	10.33	1.33 ± 0.15	$-0.36^{+0.10}_{-0.10}$	$-0.39^{+0.15}_{-0.15}$	AGN2
J222852.2−050915	0100440101	22 28 52.3 −05 09 15.4	11.01	1.33 ± 0.08	$-0.97^{+0.01}_{-0.01}$	$-1.00^{+0.76}_{-0.00}$	star
J223547.9−255836	0111790101	22 35 48.0 −25 58 37.0	4.41	1.21 ± 0.06	$-0.55^{+0.04}_{-0.04}$	$-0.50^{+0.08}_{-0.08}$	AGN1
J223555.0−255833	0111790101	22 35 55.0 −25 58 33.9	4.89	1.03 ± 0.06	$-0.61^{+0.04}_{-0.04}$	$-0.66^{+0.08}_{-0.09}$	AGN1
J223949.8+080926	0103860301	22 39 49.9 +08 09 26.4	9.24	1.07 ± 0.21	$-0.65^{+0.14}_{-0.14}$	$0.09^{+0.29}_{-0.31}$	AGN1
J224756.6−642721	0112240101	22 47 56.6 −64 27 21.8	12.76	1.43 ± 0.11	$-0.51^{+0.06}_{-0.06}$	$-0.62^{+0.10}_{-0.10}$	
J224833.3−511900	0109070401	22 48 33.4 −51 19 00.2	9.13	1.18 ± 0.12	$-0.91^{+0.04}_{-0.04}$	$-0.93^{+0.90}_{-0.06}$	star
J224846.6−505929	0109070401	22 48 46.7 −50 59 29.6	10.50	1.03 ± 0.14	$-0.91^{+0.05}_{-0.05}$	$-1.00^{+1.30}_{-0.00}$	star
J225025.1−643225	0112240101	22 50 25.2 −64 32 25.3	10.05	1.00 ± 0.09	$-0.66^{+0.06}_{-0.06}$	$-0.52^{+0.14}_{-0.14}$	AGN1
J225050.2−642900	0112240101	22 50 50.3 −64 29 00.4	8.87	2.42 ± 0.13	$-0.57^{+0.04}_{-0.04}$	$-0.45^{+0.08}_{-0.08}$	AGN1
J225118.0−175951	0081340901	22 51 18.1 −17 59 51.3	10.63	3.39 ± 0.20	$-0.68^{+0.04}_{-0.04}$	$-0.56^{+0.10}_{-0.10}$	AGN1?
J225349.6−172137	0112910301	22 53 49.6 −17 21 37.2	12.50	1.83 ± 0.28	$-0.95^{+0.05}_{-0.05}$	$-1.00^{+2.00}_{-0.00}$	star
J230400.4−083755	0109130701	23 04 00.4 −08 37 55.5	11.19	1.05 ± 0.14	$-0.96^{+0.04}_{-0.04}$	$-0.33^{+0.39}_{-0.61}$	AGN1
J230401.0+031519	0033541001	23 04 01.0 +03 15 19.2	11.59	1.06 ± 0.14	$-0.69^{+0.09}_{-0.09}$	$-0.44^{+0.25}_{-0.25}$	GAL
J230408.2+031820	0033541001	23 04 08.3 +03 18 20.7	11.38	5.66 ± 0.31	$-0.92^{+0.02}_{-0.02}$	$-1.00^{+0.31}_{-0.00}$	star

Table 3. continued.

Name XBS...	Obs. ID	RA; Dec (J2000)	OffAxis arcmin	Rate $\times 10^{-2}$ cts/s	*HR*2	*HR*3	Class
(1)	(2)	(3)	(4)	(5)	(6)	(7)	(8)
J230434.1+122728	0025541001	23 04 34.1 +12 27 28.3	9.68	1.39 ± 0.17	$-0.57^{+0.10}_{-0.10}$	$-0.31^{+0.21}_{-0.21}$	AGN2?
J230443.8+121636	0025541001	23 04 43.9 +12 16 36.8	4.30	1.22 ± 0.13	$-0.54^{+0.09}_{-0.09}$	$-0.77^{+0.12}_{-0.14}$	AGN1
J230459.6+121205	0025541001	23 04 59.7 +12 12 05.4	7.48	1.35 ± 0.15	$-0.49^{+0.10}_{-0.09}$	$-0.47^{+0.16}_{-0.16}$	AGN2?
J230522.1+122121	0025541001	23 05 22.1 +12 21 21.1	6.45	1.28 ± 0.14	$-0.37^{+0.09}_{-0.09}$	$-0.60^{+0.14}_{-0.13}$	AGN2
J230523.0+121325	0025541001	23 05 23.0 +12 13 25.4	8.85	1.31 ± 0.15	$-0.47^{+0.10}_{-0.10}$	$-0.89^{+0.10}_{-0.11}$	
J231342.5−423210	0123900101	23 13 42.5 −42 32 10.7	11.69	2.65 ± 0.13	$-0.64^{+0.04}_{-0.04}$	$-0.53^{+0.08}_{-0.08}$	AGN1
J231541.2−424125	0093640701	23 15 41.3 −42 41 25.6	8.42	1.19 ± 0.14	$-0.86^{+0.05}_{-0.05}$	$-0.40^{+0.33}_{-0.31}$	star
J231546.5−590313	0109463601	23 15 46.5 −59 03 13.6	8.13	1.31 ± 0.22	$-0.54^{+0.14}_{-0.14}$	$-0.07^{+0.26}_{-0.26}$	AGN2
J231553.0−423800	0093640701	23 15 53.0 −42 38 00.4	4.46	1.17 ± 0.11	$-0.84^{+0.05}_{-0.05}$	$-0.18^{+0.25}_{-0.23}$	star
J231601.7−424038	0093640701	23 16 01.7 −42 40 38.9	5.87	1.34 ± 0.12	$-0.62^{+0.07}_{-0.07}$	$-0.62^{+0.13}_{-0.14}$	
J231658.8−423853	0093640701	23 16 58.9 −42 38 53.6	9.61	2.46 ± 0.18	$-0.45^{+0.06}_{-0.06}$	$-0.72^{+0.08}_{-0.08}$	
J233325.7−152240	0093550401	23 33 25.8 −15 22 40.2	6.45	2.87 ± 0.13	$-0.87^{+0.02}_{-0.02}$	$-0.64^{+0.12}_{-0.13}$	star
J233421.9−151219	0093550401	23 34 21.9 −15 12 19.0	11.23	1.33 ± 0.12	$-0.46^{+0.08}_{-0.08}$	$-0.29^{+0.14}_{-0.15}$	AGN1
J235032.3+363156	0100241001	23 50 32.4 +36 31 56.9	12.23	2.05 ± 0.22	$-0.80^{+0.06}_{-0.07}$	$-0.38^{+0.28}_{-0.26}$	star
J235036.9+362204[d]	0100241001	23 50 37.0 +36 22 05.0	11.84	2.39 ± 0.24	$-0.37^{+0.09}_{-0.09}$	$-0.59^{+0.12}_{-0.13}$	BL

Columns are as follows: (1) Source name; (2) XMM-Newton Observation number; (3) Right Ascension and Declination (J2000) of the source (X-ray position); (4) Angular distance (in arcmin) between the source and the MOS2 image center; (5) Source count rate, and 1σ error, in the 0.5−4.5 keV energy band (units of 10^{-2} cts/s). In Table 1 we have reported the MOS2 conversion factors between the 0.5−4.5 keV count rate and the flux as a function of the energy spectral index, the hardness ratio *HR*2 and the blocking filter; (6) and (7) Hardness ratios computed as described in Sect. 3.3. The errors on the hardness ratios have been evaluated using simulations and correspond to 1σ; (8) Optical spectroscopic classification (AGN1: broad line AGN; AGN2: narrow line AGN; GAL: Optically Normal Galaxy; CL: Cluster of Galaxies; BL: BL Lac Object; star: star; ?: Tentative classification; see Sect. 3.2 for details).

NOTE – For two sources (XBS J052155.0−252220 and XBS J213840.5−424241) the hardness ratio *HR*3 is undefined since these sources are undetected above 2 keV.

[a] A detailed X-ray and optical spectral analysis of these sources have been reported in Caccianiga et al. (2004).

[b] A detailed X-ray and optical spectral analysis of these sources have been reported in Severgnini et al. (2003).

[c] These sources are more extended than the XMM-Newton EPIC MOS2 Point Spread Function at their off-axis angle. Count rates have been evaluated using aperture photometry.

[d] A detailed X-ray spectral analysis of these sources have been reported in Galbiati et al. (2004).

Table 4. Basic information on the XMM-Newton HBSS sample.

Name XBS...	Obs. ID	RA; Dec (J2000)	OffAxis arcmin	Rate $\times 10^{-3}$ cts/s	*HR*2	*HR*3	Class
(1)	(2)	(3)	(4)	(5)	(6)	(7)	(8)
J002618.5+105019[b]	0001930101	00 26 18.5 +10 50 19.3	9.56	2.35 ± 0.55	$-0.53^{+0.04}_{-0.04}$	$-0.67^{+0.06}_{-0.06}$	AGN1
J013240.1−133307[b,e]	0084230301	01 32 40.1 −13 33 07.8	11.90	3.23 ± 0.71	$-0.02^{+0.10}_{-0.10}$	$-0.37^{+0.11}_{-0.11}$	AGN2
J013944.0−674909[b]	0032140401	01 39 44.0 −67 49 09.4	2.69	2.05 ± 0.46	$-0.50^{+0.07}_{-0.07}$	$-0.43^{+0.13}_{-0.13}$	AGN1?
J014100.6−675328[b]	0032140401	01 41 00.7 −67 53 29.0	6.64	70.95 ± 3.84	$-0.45^{+0.02}_{-0.02}$	$-0.38^{+0.03}_{-0.03}$	star
J015957.5+003309[b]	0101640201	01 59 57.5 +00 33 09.7	9.56	3.80 ± 0.92	$-0.63^{+0.05}_{-0.05}$	$-0.51^{+0.10}_{-0.10}$	AGN1
J021640.7−044404[b,e]	0112371701	02 16 40.7 −04 44 04.9	9.35	2.08 ± 0.49	$-0.72^{+0.04}_{-0.05}$	$-0.26^{+0.13}_{-0.13}$	AGN1
J021808.3−045845[b]	0112371001	02 18 08.3 −04 58 45.7	2.26	2.67 ± 0.25	$-0.65^{+0.02}_{-0.02}$	$-0.52^{+0.04}_{-0.04}$	AGN1
J021817.4−045113[b]	0112371001	02 18 17.4 −04 51 13.3	9.58	3.30 ± 0.40	$-0.48^{+0.02}_{-0.03}$	$-0.56^{+0.04}_{-0.04}$	AGN1
J021822.2−050615[a,b,d]	0112371001	02 18 22.3 −05 06 15.7	8.48	4.54 ± 0.43	$0.65^{+0.09}_{-0.09}$	$0.40^{+0.07}_{-0.07}$	AGN2
J023713.5−522734[b]	0098810101	02 37 13.5 −52 27 34.4	12.07	3.23 ± 0.61	$-0.57^{+0.03}_{-0.03}$	$-0.58^{+0.07}_{-0.06}$	AGN1
J030206.8−000121[b]	0041170101	03 02 06.9 −00 01 21.2	11.90	3.10 ± 0.42	$-0.53^{+0.03}_{-0.03}$	$-0.46^{+0.05}_{-0.06}$	AGN1
J030614.1−284019[b]	0042340501	03 06 14.2 −28 40 19.9	10.87	4.61 ± 0.92	$-0.49^{+0.05}_{-0.05}$	$-0.35^{+0.09}_{-0.09}$	AGN1
J031015.5−765131[b]	0122520201	03 10 15.6 −76 51 31.5	5.90	4.39 ± 0.46	$-0.46^{+0.03}_{-0.03}$	$-0.53^{+0.04}_{-0.04}$	AGN1
J031146.1−550702[b]	0110970101	03 11 46.1 −55 07 02.5	12.38	5.87 ± 1.12	$-0.58^{+0.05}_{-0.05}$	$-0.39^{+0.11}_{-0.11}$	AGN2
J031859.2−441627[b,d]	0105660101	03 18 59.3 −44 16 27.6	11.55	2.16 ± 0.49	$-0.21^{+0.08}_{-0.08}$	$-0.47^{+0.10}_{-0.10}$	AGN1
J033845.7−352253[a,b]	0055140101	03 38 45.8 −35 22 53.4	10.49	2.37 ± 0.36	$-0.05^{+0.12}_{-0.12}$	$0.27^{+0.11}_{-0.11}$	AGN2
J040658.8−712457[a,b]	0111970301	04 06 58.9 −71 24 57.7	12.55	3.41 ± 0.68	$0.39^{+0.19}_{-0.19}$	$0.20^{+0.16}_{-0.16}$	AGN2
J040758.9−712833[a,b]	0111970301	04 07 59.0 −71 28 33.5	12.12	4.96 ± 0.91	$0.49^{+0.17}_{-0.17}$	$0.33^{+0.13}_{-0.13}$	AGN2
J041108.1−711341[b]	0111970301	04 11 08.1 −71 13 41.1	10.52	2.20 ± 0.42	$-0.53^{+0.08}_{-0.08}$	$-0.04^{+0.16}_{-0.16}$	AGN1
J050536.6−290050	0111160201	05 05 36.7 −29 00 50.8	12.43	2.19 ± 0.44	$-0.27^{+0.05}_{-0.05}$	$-0.47^{+0.07}_{-0.07}$	
J052108.5−251913[e]	0085640101	05 21 08.5 −25 19 13.1	3.17	2.11 ± 0.55	$-0.59^{+0.05}_{-0.05}$	$-0.55^{+0.09}_{-0.09}$	AGN1
J052128.9−253032[a]	0085640101	05 21 28.9 −25 30 32.4	10.73	3.08 ± 0.88	$1.00^{+0.00}_{-0.17}$	$-0.32^{+0.15}_{-0.15}$	
J074202.7+742625	0123100101	07 42 02.7 +74 26 25.8	10.86	3.38 ± 0.49	$-0.59^{+0.03}_{-0.03}$	$-0.28^{+0.07}_{-0.07}$	AGN1
J074312.1+742937	0123100101	07 43 12.1 +74 29 37.4	5.33	10.92 ± 0.64	$-0.61^{+0.01}_{-0.01}$	$-0.56^{+0.02}_{-0.02}$	AGN1
J080411.3+650906	0094400301	08 04 11.4 +65 09 06.2	9.49	2.41 ± 0.50	$0.06^{+0.09}_{-0.09}$	$-0.51^{+0.09}_{-0.09}$	
J083737.1+254751	0025540301	08 37 37.2 +25 47 51.1	10.61	7.30 ± 1.12	$-0.47^{+0.04}_{-0.04}$	$-0.53^{+0.06}_{-0.06}$	AGN1
J083737.0+255151	0025540301	08 37 37.1 +25 51 51.2	12.25	2.98 ± 0.71	$-0.34^{+0.07}_{-0.08}$	$-0.52^{+0.10}_{-0.10}$	AGN2
J091828.4+513931	0084230601	09 18 28.5 +51 39 31.3	6.92	3.03 ± 0.54	$0.31^{+0.09}_{-0.10}$	$-0.39^{+0.09}_{-0.09}$	AGN1
J095218.9−013643	0065790101	09 52 19.0 −01 36 43.1	11.78	24.50 ± 2.98	$-0.77^{+0.03}_{-0.03}$	$0.41^{+0.09}_{-0.09}$	AGN1
J101850.5+411506	0028740301	10 18 50.6 +41 15 06.6	10.32	2.16 ± 0.49	$-0.69^{+0.03}_{-0.03}$	$-0.51^{+0.07}_{-0.08}$	AGN1
J101922.6+412049	0028740301	10 19 22.6 +41 20 49.7	9.06	2.46 ± 0.47	$-0.44^{+0.04}_{-0.04}$	$-0.58^{+0.06}_{-0.05}$	AGN1
J104026.9+204542	0059800101	10 40 26.9 +20 45 43.0	9.32	8.70 ± 1.15	$-0.58^{+0.03}_{-0.03}$	$-0.48^{+0.05}_{-0.05}$	AGN1
J104522.1−012843	0125300101	10 45 22.1 −01 28 43.3	12.94	3.00 ± 0.67	$-0.63^{+0.04}_{-0.04}$	$-0.46^{+0.08}_{-0.08}$	AGN1
J104912.8+330459	0055990201	10 49 12.8 +33 04 59.8	10.46	2.06 ± 0.51	$-0.45^{+0.06}_{-0.06}$	$-0.54^{+0.09}_{-0.10}$	AGN1?
J110050.6−344331	0112880201	11 00 50.6 −34 43 32.0	12.71	5.12 ± 0.69	$-0.48^{+0.04}_{-0.04}$	$-0.33^{+0.07}_{-0.07}$	
J112026.7+431520[a]	0107860201	11 20 26.7 +43 15 20.3	4.58	2.32 ± 0.37	$0.67^{+0.08}_{-0.08}$	$-0.32^{+0.09}_{-0.09}$	AGN2
J113106.9+312518	0102040201	11 31 07.0 +31 25 18.2	11.18	2.27 ± 0.44	$-0.53^{+0.08}_{-0.08}$	$-0.15^{+0.14}_{-0.14}$	AGN1
J113121.8+310252	0102040201	11 31 21.8 +31 02 52.6	11.58	3.88 ± 0.69	$-0.03^{+0.07}_{-0.07}$	$-0.35^{+0.08}_{-0.08}$	AGN2
J113148.7+311358	0102040201	11 31 48.7 +31 13 58.8	8.45	3.43 ± 0.48	$0.10^{+0.06}_{-0.07}$	$-0.43^{+0.07}_{-0.07}$	AGN2
J122656.5+013126	0110990201	12 26 56.6 +01 31 26.2	5.85	3.07 ± 0.54	$-0.11^{+0.09}_{-0.09}$	$-0.34^{+0.10}_{-0.10}$	AGN2?
J123600.7−395217	0006220201	12 36 00.7 −39 52 18.0	5.62	2.66 ± 0.29	$-0.77^{+0.01}_{-0.01}$	$-0.77^{+0.02}_{-0.02}$	star
J124641.8+022412	0051760101	12 46 41.8 +02 24 12.1	2.78	2.22 ± 0.49	$-0.58^{+0.05}_{-0.05}$	$-0.48^{+0.09}_{-0.09}$	AGN1
J132038.0+341124	0093640401	13 20 38.1 +34 11 24.3	3.10	2.89 ± 0.40	$-0.43^{+0.04}_{-0.04}$	$-0.48^{+0.06}_{-0.06}$	AGN1
J133942.6−315004	0035940301	13 39 42.6 −31 50 04.8	11.91	3.52 ± 0.51	$-0.36^{+0.05}_{-0.06}$	$-0.20^{+0.08}_{-0.08}$	AGN1?
J134656.7+580315[a]	0112250201	13 46 56.7 +58 03 15.4	11.08	3.33 ± 0.56	$0.46^{+0.10}_{-0.10}$	$-0.09^{+0.10}_{-0.10}$	GAL
J134749.9+582111	0112250201	13 47 49.9 +58 21 11.0	8.53	7.39 ± 0.66	$-0.60^{+0.02}_{-0.02}$	$-0.54^{+0.03}_{-0.03}$	AGN1
J140102.0−111224	0109910101	14 01 02.0 −11 12 24.3	9.27	7.21 ± 0.59	$-0.52^{+0.02}_{-0.02}$	$-0.46^{+0.03}_{-0.03}$	AGN2?
J140113.4+024016[a]	0098010101	14 01 13.4 +02 40 17.0	12.78	2.10 ± 0.52	$-0.55^{+0.09}_{-0.09}$	$0.08^{+0.16}_{-0.16}$	
J140127.7+025605	0098010101	14 01 27.7 +02 56 05.4	7.25	6.66 ± 0.62	$-0.38^{+0.02}_{-0.02}$	$-0.53^{+0.04}_{-0.04}$	AGN1
J141531.5+113156	0112250301	14 15 31.6 +11 31 56.2	4.15	2.58 ± 0.34	$-0.55^{+0.03}_{-0.03}$	$-0.47^{+0.06}_{-0.06}$	AGN1
J141830.5+251052[c]	0109960101	14 18 30.5 +25 10 52.6	7.58	7.70 ± 1.20	$-0.52^{+0.04}_{-0.04}$	$-0.65^{+0.07}_{-0.07}$	CL
J142741.8+423335[a]	0111850201	14 27 41.9 +42 33 35.8	11.45	3.62 ± 0.53	$0.48^{+0.07}_{-0.07}$	$-0.23^{+0.07}_{-0.07}$	
J143835.1+642928	0111530101	14 38 35.1 +64 29 28.3	12.34	3.57 ± 0.54	$0.18^{+0.07}_{-0.07}$	$-0.37^{+0.07}_{-0.06}$	AGN1?

Table 4. continued.

Name XBS...	Obs. ID	RA; Dec (J2000)	OffAxis arcmin	Rate $\times 10^{-3}$ cts/s	*HR*2	*HR*3	Class
(1)	(2)	(3)	(4)	(5)	(6)	(7)	(8)
J143911.2+640526[a]	0111530101	14 39 11.2 +64 05 26.8	12.04	2.44 ± 0.39	$0.86^{+0.09}_{-0.09}$	$0.29^{+0.11}_{-0.11}$	BL?
J153452.3+013104[e]	0112190401	15 34 52.4 +01 31 04.6	10.57	8.36 ± 1.30	$-0.39^{+0.04}_{-0.04}$	$-0.55^{+0.05}_{-0.05}$	AGN1
J160645.9+081525	0067340601	16 06 46.0 +08 15 25.1	12.61	7.36 ± 1.37	$0.81^{+0.08}_{-0.08}$	$-0.23^{+0.10}_{-0.10}$	AGN2?
J161820.7+124116[a]	0103461001	16 18 20.7 +12 41 16.3	11.56	2.09 ± 0.61	$0.11^{+0.18}_{-0.18}$	$-0.18^{+0.18}_{-0.19}$	
J165425.3+142159	0113070101	16 54 25.4 +14 21 59.3	7.44	5.26 ± 1.08	$-0.63^{+0.03}_{-0.03}$	$-0.61^{+0.07}_{-0.07}$	AGN1
J165448.5+141311	0113070101	16 54 48.5 +14 13 11.6	12.71	6.25 ± 1.79	$-0.54^{+0.07}_{-0.07}$	$-0.42^{+0.13}_{-0.13}$	AGN2
J193248.8−723355[b]	0081341001	19 32 48.8 −72 33 55.2	8.39	4.47 ± 0.73	$-0.23^{+0.08}_{-0.08}$	$-0.08^{+0.10}_{-0.10}$	AGN2?
J204043.4−004548[b]	0111180201	20 40 43.5 −00 45 48.2	10.55	3.24 ± 0.80	$0.04^{+0.11}_{-0.11}$	$-0.35^{+0.12}_{-0.12}$	AGN2
J205635.7−044717[b]	0112190601	20 56 35.8 −04 47 17.9	9.96	2.08 ± 0.50	$-0.65^{+0.04}_{-0.05}$	$-0.48^{+0.11}_{-0.11}$	AGN1
J205829.9−423634[b]	0081340401	20 58 30.0 −42 36 35.0	2.42	3.91 ± 0.56	$-0.57^{+0.03}_{-0.03}$	$-0.47^{+0.06}_{-0.06}$	AGN1
J213002.3−153414[b]	0103060101	21 30 02.3 −15 34 14.1	12.83	2.30 ± 0.47	$-0.65^{+0.04}_{-0.04}$	$-0.50^{+0.09}_{-0.09}$	AGN1
J213820.2−142536	0092850201	21 38 20.2 −14 25 37.0	11.17	2.80 ± 0.59	$-0.29^{+0.07}_{-0.07}$	$-0.45^{+0.10}_{-0.10}$	AGN1
J214041.4−234720[b]	0008830101	21 40 41.5 −23 47 20.1	9.80	3.30 ± 0.68	$-0.57^{+0.05}_{-0.05}$	$-0.39^{+0.10}_{-0.10}$	AGN1
J220601.5−015346[b]	0012440301	22 06 01.5 −01 53 47.0	12.92	2.26 ± 0.55	$-0.41^{+0.06}_{-0.06}$	$-0.41^{+0.09}_{-0.09}$	AGN1

Columns are as follows: (1) Source name; (2) XMM-Newton Observation number; (3) Right Ascension and Declination (J2000) of the source (X-ray position); (4) Angular distance (in arcmin) between the source and the MOS2 image center; (5) Source count rate, and 1σ error, in the 4.5−7.5 keV energy band (units of 10^{-3} cts/s). In Table 1 we have reported the MOS2 conversion factors between the 4.5−7.5 keV count rate and the flux as a function of the energy spectral index, the hardness ratio *HR*2 and the blocking filter; (6) and (7) Hardness ratios computed as described in Sect. 3.3. The errors on the hardness ratios have been evaluated using simulations and correspond to 1σ; (8) Optical spectroscopic classification (AGN1: broad line AGN; AGN2: narrow line AGN; GAL: Optically Normal Galaxy; CL: Cluster of Galaxies; BL: BL Lac Object; star: star; ?: Tentative classification; see Sect. 3.2 for details).

NOTE – [a] These 11 sources belong to the HBSS sample but not to the BSS sample, while the remaining 56 HBSS sources are present also in the BSS sample.

[b] A detailed X-ray and optical spectral analysis of these sources have been reported in Caccianiga et al. (2004).

[c] These sources are more extended than the XMM-Newton EPIC MOS2 Point Spread Function at their off-axis angle. Count rates have been evaluated using aperture photometry.

[d] A detailed X-ray and optical spectral analysis of these sources have been reported in Severgnini et al. (2003).

[e] A detailed X-ray spectral analysis of these sources have been reported in Galbiati et al. (2004).

Appendix A: Illumination Factor

The MOS2 cameras consist of a mosaic of 7 identical, front-illuminated CCDs with a dead space between the different chips. It is clear that serendipitous X-ray sources falling close to the gaps between the CCDs (or to their edges) could have either the flux and/or the source centroid poorly determined. The poor understanding of the corrections to be applied to these sources could represent a problem in the subsequent analysis and/or interpretation of the data. It order to take into account this problem in a objective way we have used the procedure detailed below.

From the exposure map produced from the pipeline processing system we have built a mask image representing the area on the sky which is "effectively" imaged by the CCDs. To produce this mask we have used the SAS task *emask* with *threshold1* = 0.25 and *threshold2* = 0.20 (see `http://xmm.vilspa.esa.es/external/xmm_sw_cal/sas_frame.shtml` for specific details).

Using this mask image we have thus defined the "Illumination Factor" of each source as the fraction of sky "effectively" imaged by the CCDs in a circle of 20 arcsec around the source.

The "Illumination Factor" so defined ranges between 0.3 and 1 and the lower the "Illumination Factor" the closer is the source to gaps and/or edges in the CCDs. In the BSS and/or HBSS catalogues we have retained only sources with "Illumination Factor" $\gtrsim$ 0.8. Given the PSF of the MOS2 detector and its energy and off-axis dependence we have evaluated that less than 10% of the flux is lost in the case of a source with an "Illumination Factor" equal to the lower limit of 0.8. In Table B.1 we report the complete list of sources which meet the selection criteria for the BSS and/or HBSS samples (e.g., inside the selected area between the inner and outer radius of each MOS2 image, count rate and likelihood limits, etc.) but that have been excluded from the sample because their "Illumination Factor" is below 0.8.

Finally the produced mask has been also used, in the computation of the sky coverage, to take into account the excluded area because of edges and gaps.

Appendix B: Cleaning procedure

XMM-Newton observations are subject to "flares" in the background rate, probably due to soft protons which are collimated by the X-ray mirrors toward the EPIC cameras and interact with the structure of the detectors and the detectors itself. The current understanding is that soft protons are probably organized in clouds populating the Earth's magnetosphere.

In order to check the background quality of the dataset used we have defined a "Background Estimator Parameter" which is roughly proportional to the "real background" accumulated in the MOS2 images.

To set this "Background Estimator Parameter" for each image we have produced an histogram of the total accumulated MOS2 counts in the 10−12 keV energy range as a function of time; the histogram bin size has been set to 100 seconds.

Thus, using this histogram we have:

a) evaluated the mean count rate ($\langle bck \rangle$) and its standard deviation (σ_{bck})

b) eliminated the time intervals which have a count rate greater than $\langle bck \rangle + 2 \times \sigma_{bck}$

c) repeated points a) and b) 10 times

The mean count rate at the end of the loop described above is the "Background Estimator Parameter".

Table B.1. Basic information on the sources excluded from the sample(s) since their "Illumination Factor" is less than 0.8.

Obs. ID	RA; Dec (J2000)	OffAxis arcmin	Illum.
(1)	(2)	(3)	(4)
0111000101	00 18 41.6 +16 20 33.4	5.94	0.69
0001930101	00 26 24.9 +10 31 23.7	10.77	0.68
0112320101	00 30 08.3 +05 03 40.9	12.83	0.70
0065770101	00 32 41.0 +39 40 08.2	5.70	0.42
0112600601	01 26 40.3 +19 12 13.0	12.36	0.60
0112630201	01 34 03.1 −40 02 22.8	12.38	0.68
0112371501	02 18 21.9 −04 34 51.2	7.80	0.48
0111110501	02 22 49.4 −05 14 53.0	5.58	0.27
0098810101	02 36 30.3 −52 27 04.3	7.66	0.77
0098810101	02 37 02.1 −52 23 48.0	8.53	0.62
0122520201	03 13 14.6 −76 55 55.4	5.88	0.71
0110970401	03 13 34.3 −55 26 43.6	7.85	0.76
0111970301	04 09 02.1 −71 07 54.6	9.83	0.63
0085640101	05 21 00.2 −25 28 52.5	7.00	0.49
0050150101	05 25 57.1 −33 44 35.7	10.72	0.74
0110930101	06 17 56.8 +78 16 05.3	5.81	0.66
0103860101	06 24 46.8 −64 33 46.0	10.80	0.78
0112980201	06 57 26.2 −55 49 53.9	10.49	0.78
0025540301	08 38 27.2 +25 50 53.7	5.75	0.65
0025540301	08 38 52.5 +25 37 25.3	10.27	0.58
0110660201	09 07 51.1 +62 01 58.3	12.77	0.65
0084230601	09 16 45.2 +51 41 45.0	10.53	0.57
0110930201	10 00 56.7 +55 41 01.2	8.50	0.69
0101040301	10 23 13.3 +19 56 50.5	6.43	0.62
0055990201	10 50 29.0 +33 00 42.8	7.63	0.70
0110660401	11 26 11.9 +42 52 45.9	2.09	0.78[a]
0124110101	12 21 34.3 +75 09 18.1	9.34	0.60
0124110101	12 22 07.3 +75 26 20.7	7.88	0.53
0092360601	12 52 14.1 −83 46 42.6	9.48	0.66
0002940101	13 06 32.8 −23 31 13.1	12.05	0.62
0111160101	13 34 16.9 +50 23 09.6	7.78	0.64
0111160101	13 35 09.6 +50 39 17.8	11.58	0.73
0111570201	13 35 18.7 −34 21 45.5	8.30	0.62
0112250301	14 15 39.9 +11 24 04.4	5.69	0.37
0109960101	14 18 42.7 +25 07 09.5	9.90	0.79
0070740301	15 03 39.6 +10 16 04.9	11.46	0.66
0018741001	15 18 59.7 +06 18 39.4	5.57	0.73
0061940301	16 32 39.0 +78 11 54.3	5.48	0.56
0102040101	17 22 54.3 +34 27 25.3	10.89	0.58
0061940201	21 37 47.7 −42 26 14.5	10.55	0.68
0008830101	21 39 57.9 −23 45 35.1	7.27	0.76
0111790101	22 36 06.1 −26 08 04.6	6.80	0.55
0109070401	22 47 48.1 −51 10 18.1	8.38	0.73
0025541001	23 04 43.5 +12 12 10.2	8.04	0.53
0123900101	23 14 32.2 −42 33 01.5	12.11	0.72

Columns are as follows: (1) XMM-Newton Observation number; (2) Right Ascension and Declination (J2000) of the source (X-ray position); (3) Angular distance (in arcmin) between the source and the MOS2 image center; (4) "Illumination factor".

NOTE – [a] Although this source is well contained inside the MOS2 central CCD it fall above a bad column; for this reason its "Illumination factor" is below 0.8.